INFLUENCE OF FOOD MATRIX PHYSICO-CHEMICAL PROPERTIES

ON THE BIOPHYSICS OF DIGESTION AND *IN SITU* LUMINAL VISCOSITY

By

FATEMAH M. ALHASAWI

A Dissertation submitted to the

School of Graduate Studies

Rutgers, The State University of New Jersey

In partial fulfillment of the requirements

For the degree of

Doctor of Philosophy

Graduate Program in Food Science

Written under the direction of

Dr. Michael A. Rogers

And approved by

_____

_____

_____

_____

New Brunswick, New Jersey

January 2018

ABSTRACT OF THE DISSERTATION

Influence of Food Matrix Physico-Chemical Properties on

the Biophysics of Digestion and *In Situ* Luminal Viscosity

by FATEMAH M. ALHASAWI

Dissertation Director:

Dr. Michael A. Rogers

Designing foods by modifying their form is becoming a plausible strategy to control how foods behave and are digested in the gastrointestinal (GI) tract. Given the global persistence of the type II diabetes and obesity, there is a great need for dietary interventions that target postprandial glucose levels and rate of lipolysis. A well-established structure-function relationship is found between increased viscosity and rate and extent of macronutrient hydrolysis. Nonetheless, the mechanisms underlying such relationships within specific food commodities as a function of GI viscosity are not yet well identified, especially in light of the confinements in the currently available methods for monitoring GI luminal viscosity.

A critical review was compiled to summarize the main characteristics of molecular rotors (MR)s, a class of optical probes that are sensitive to microviscosity, their current applications in biological research and their current and potential applications as sensors of physical properties in food science and engineering. MRs were

integrated with TNO Intestinal Model-1 (TIM-1) in a novel method to facilitate detection of *in situ* changes in luminal viscosity during *in vitro* GI digestion, respectively. This method was verified using maize starch samples that varied in their amylose-to-amylopectin ratio, and is applicable when microviscosity is representative of bulk viscosity.

We were able to correlate food form, and digestion kinetics in several food matrices. Carbohydrate digestion kinetics and *in vitro* gastric viscosity of three commercially available oat products, instant oats (IO), steel cut oats (SC), and oat bran (OB), were assessed. Findings included: rate of starch digestion in IO > OB > SC; IO and OB viscosities were highest at the onset of digestion and decreased with time, whereas SC onset viscosity was lowest and increased with time. IO- and SC-based meals were modified by addition of a thickening agent, milk protein concentrate (MPC), at concentrations: 0 g, 5 g, and 10 g. Oat-based meals containing 5 g or 10 g MPC yielded significantly less total bioaccessible sugar, a more rapid rate of starch digestion, and higher gastric viscosity compared with those containing 0 g MPC. Physico-chemical properties of human breast milk were compared to four Similac^{TM} infant formulas, and correlated with *in vitro* free fatty acid bioaccessibility. Breast milk samples were distinctly unique from the infant formulas: having lower viscosities as a function of pH (pH 6.5 to 3.0), a lag period during lipid digestion, and a higher rate of lipolysis. These findings suggest that modification of food form and formulation alters macronutrient bioaccessibility and luminal viscosity.

DEDICATION

This dissertation is dedicated to:

My parents

Suad N. AlHouti and Mohammad J. AlHassawi

and

My beloved small family

My husband, my son, and my daughter

Mishari, Mohammad, and Shaikha AlJassim

ACKNOWLEDGMENTS

always sticking by my side even at my lowest points, and for shielding our family in your own protective way. Mishari is the behind-the-scenes soldier that kept our family afloat; he was the silent force that pushed me to getting this degree. To Mohammad (my Hamoodi and '*Flash*') and Shaikha (my Shayookha and '*Princess*'); thank you for your tolerance of my long working hours, for being my companions throughout this very long journey, and especially for all the serenity your hugs gave me during the moments when my mind was racing with data, doubts, graphs, worry, models, and fatigue. I love you both so much!!

I will always recall when I told Mohammad that I submitted my final manuscript to Dr. Rogers, he asked me with enthusiasm, "Mama, does this mean you are a doctor now?!!" Today I can answer Mohammad and say "Yes, Hamoodi, finally!" For this I would like to say… "Hatha min fadhl Raby… AlHamd-le-Allah, wa AlShokr-le-Allah".

PREFACE

The work presented in this dissertation was conducted in its entirety in the Department of Food Science, School of Environmental and Biological Sciences, Rutgers, The State University of New Jersey, during the period of September 2013 and September 2017.

Section 2.3 of Chapter Two (2) of this dissertation, entitled "Potential applications of luminescent molecular rotors in food science and engineering" has been published in *Critical Reviews in Food Science and Nutrition*: (DOI 10.1080/10408398.2017.1278583, Published on-line June 2017), and co-authored with Dr. Maria G. Corradini, Dr. Michael A. Rogers and Dr. Richard D. Ludescher.

Chapter Five (5) of this dissertation, entitled "*In vitro* measurements of luminal viscosity and glucose/maltose bioaccessibility for oat bran, instant oats, and steel cut oats" has been published in *Food Hydrocolloids*: (DOI 10.1016/j.foodhyd.2017.04.015, September 2017, Volume 70, Pages 293-303), and co-authored with Derrick Fondaco, Karen Ben-Elazar, Shirley Ben-Elazar, Yim Yan Fan, Maria G. Corradini, Richard D. Ludescher, Douglas Bolster, Gary Carder, Yi Fang Chu, Yongsoo Chung, Prabhakar Kasturi, Jodee Johnson, and Michael A. Rogers.

Chapter Seven (7) of this dissertation, entitled "Biophysical Aspects of Lipid Digestion in Human Breast Milk and Similac™ Infant Formulas" has been published in *Food Biophysics*: (10.1007/s11483-014-9388-6, September 2015, Volume 10, Issue 3, pages 282–291), and co-authored with Derrick Fondaco, Yaqi Lan, Shirley Ben-Elazar, Karen Connolly, and Michael A. Rogers.

TABLE OF CONTENTS

LIST OF FIGURES

LIST OF TABLES

1

1 INTRODUCTION

Diet-related non-communicable chronic diseases are forecasted to make up two-thirds of the total global burden of disease in 2020 [1], with a greater incidence in younger aged groups [1]. Such statistics have generated current scientific and industrial emphasis towards dietary mediation of chronic diseases. While traditional measures assess nutrient composition of a meal to determine its physiological contribution; significant amounts of scientific evidence suggest the substantial role of the nutrient physicochemical properties on its total physiological impact. Such circumstances may lead to inadvertent physiological responses, which may prove harmful in foods designed for specific consumers, such as diabetic and/or obese.

One vivid example of such a phenomenon is the commercially available oat-based products, which are generally perceived to be glycemia-decreasing meals despite their wide range of glycemic indices, ranging between 40 and 88, for various processed whole oat grains [2]. This inconsistency is due to oats being commercially available in several forms, ranging from raw grain to ready-to-eat cereals and cooked oat porridge [2]. The diverse processing techniques to which the oat grains are exposed has been shown to modify the major physiologically-functional component of oats, which is soluble fiber β-glucan; as a result, β-glucan quality (e.g., solubility and molecular weight) [3-5], quantity [6], and starch integrity (e.g., gelatinization) are all modified [7-10]. Such physico-chemical changes affect the ability of β-glucan in oats to bind water and form a water-entrapping non-starch polysaccharide viscous network in the gastrointestinal (GI) tract [11, 12], which has been associated with a decrease in postprandial glucose response. The inverse relationship between meal viscosity and postprandial plasma levels is now widely

accepted [13]. Measurements of changes in luminal viscosity during GI transit time for different oat products are very scarce, with the majority of studies using static *in vitro* digestion methods. Such modifications are critical, given the estimated 366 million diabetics accounted for worldwide in 2011 and the alarming prediction of a 50.7% increase by the year 2030 [14]. Manifestation of a large and rapid spike in blood glucose is a well-known risk-factor of type II diabetes [15]. The metabolic response to dietary starch is a function of the rate of its hydrolysis/digestion [16, 17]. Therefore, slowing starch digestion in the small intestine offers opportunities for lowering of the postprandial glycemic response [18], critical for the management of type II diabetes.

Equivalent to the magnitude of the global type II diabetes pandemic, exists the pervasive occurrence of obesity amongst type II diabetics. An alarming one-third of the United States adult population has been categorized as obese by The Center of Disease Control and Prevention [19]. Worthy of special concern is the childhood obesity epidemic, which has been identified to contribute to an earlier onset of type II diabetes amongst adolescents [20]. Interestingly, the prevalence of childhood obesity is lower in breast-fed infants compared to formula fed infants [21-23]. Numerous hypotheses have associated the method of feeding (bottle versus at the breast) [24, 25], the hormones and adipokines in breast milk [26-32], amongst many others to this mechanism. Regrettably, the mechanism responsible for this correlation is not understood [24].

In an attempt to facilitate investigations of the effect of food physico-chemical properties on macronutrient digestibility, we integrated TNO Intestinal Model-1 (TIM-1), spectrophotometry, and molecular rotors (MR) to facilitate simultaneous measurements of real-time luminal viscosity changes and digestion kinetics, *in vitro.* The TIM-1 is an

advanced artificial digestive system that mimics the human stomach and small intestine, and is unique for its dynamic computer controlled system. "Molecular rotor" refers to molecules consisting of two or more segments that easily rotate relative to each other [33]. We exploited the sensitivity of MRs to increased molecular crowding within the TIM-1 apparatus to achieve continuous monitoring of *in vitro* luminal chyme viscosity. The digestate samples collected from TIM-1 facilitated estimation of digestion kinetics, which included total bioaccessibility and rate of hydrolysis (α-amylase or lipase). The investigated physico-chemical properties were determined using fluorescence spectra and MR, in addition to other techniques, and included: GI viscosity, available starch and β-glucan, extent of starch gelatinization, and particle size distribution. The major findings presented in this dissertation were a product of correlations between the attained parameters of digestion kinetics and physico-chemical properties, as a function of (A) changes in amylose-to-amylopectin ratio in maize starch; (B) changes in the integrity and quantity of both β-glucan and starch, due to differences in the production methods involved in oat processing; (C) addition of a thickening agent, milk protein concentrate (MPC) to oat-based meals; and (E) differences in droplet size and distribution of fat globules in Similac^TM infant formulas as compared to human breast milk. These findings provide a better understanding of relationships between food form and formulation, which may be useful in the design of food products with pre-determined physiological impact, intended for patients with specific diet-related chronic diseases.

2 LITERATURE REVIEW

2.1 Dietary Carbohydrates

2.1.1 Introduction

Carbohydrates exist in numerous forms, varying in their chemical properties: type of sugars, type of bonds linking the sugar monomers, and degree of polymerization [34]. Such differences determine whether or not carbohydrates are glycemic, in other words whether or not they are available for absorption in the small intestine [34, 35]. Consequently, physico-chemical properties of carbohydrates influence their contribution to postprandial glycemic response. While the glucose molecule is an available carbohydrate, dietary starch must first be hydrolyzed via the action of α-amylase to generate smaller units that are then available for absorption by the intestinal epithelium. Non-glycemic carbohydrates include non-starch polysaccharides, i.e. dietary fiber (DF) [34, 35], which can resist small intestinal digestion, and are fermented in the colon. Non-glycemic carbohydrates are unique in their ability to modify the physical and chemical properties of the luminal chyme [34, 35], ultimately altering macronutrient digestibility.

Postprandial glycemic response is a topic that gained great momentum in the fields of nutrition, medicine and food science, especially in light of the predicted rapid (~50%) increase in the number of diabetics worldwide between years 2011 and 2030 [14]. Postprandial glycemia refers to the concentration of glucose in the blood after consumption of a meal, which is largely affected by the rate at which glucose is absorbed [36]. A lower glycemic response is considered healthy for both diabetic and non-diabetic

individuals [37]. Nonetheless, the rate of absorption is largely dependent on the rate at which glucose becomes bioaccessible (available for absorption, after cleavage from the carbohydrate polysaccharide). The overall food matrix and its physico-chemical properties influence such parameters, and are also influenced by varying processing techniques [34, 35]. Reducing the rate and extent of small intestinal starch digestion is now accepted as a mechanism to lower glycemic response and to increase starch resistance to digestion, respectively [18]. It is therefore of great importance to understand the structural architecture of starch and physico-chemical factors that may manipulate its digestion kinetics.

2.1.2 Starch Structure

Starch makes up the major source of dietary carbohydrates in the human diet [38]. The chemical structure of starch is widely accepted [39-41] to be composed of D-glucose monomers covalently linked into long polymers. The covalent linkages may result in the formation of amylose, a linear α[1→4] linked glucan, or amylopectin, a branched glucan with an α[1→4] linked glucan backbone and α[1→6] linked glucan branches (Figure 2.1). Amylopectin are 100 times larger molecules than amylose, with molecular mass of $\sim 10^9$ Da and make up $\sim 70 - 80\%$ of the total weight of the native starch granule [39-41]. Molecular structure has a tremendous influence on the physiological functionality of starch. A thorough understanding of this relationship is critical in optimizing industrial applications and consequent prediction of biophysical properties.
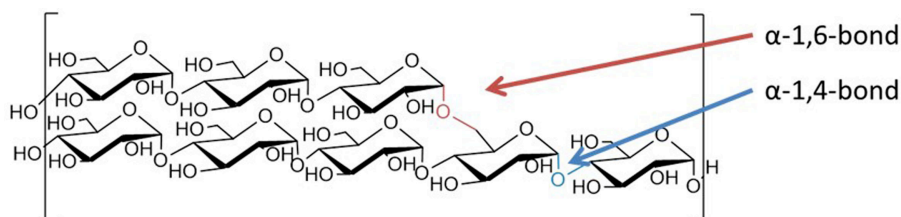
Figure 2.1: α-1,4- and α-1,6- glucans connect glucose monomers to form starch [42].

Starch granules are characterized by their semi-crystallinity [43]. The regions in starch where the α[1→4] linked glucans intertwine results in the formation of double helices (Figure 2.2), that together result in the formation of parallel crystalline regions [44-47]. On the other hand, α[1→6] linked glucans at which amylopectin branching points are initiated contributes to formation of amorphous regions that lack high level of order [44-47]. These distinct regions are called lamellae and are arranged to form growth rings (distinct layers) radiating from the hilum (center) of the grain [43]. The semi-crystalline nature of the starch granule renders it anisotropic, which is the refraction of light at different angles dependent on the orientation of the crystalline lattice with respect to the angle of the incident light. Direction of polarized light onto an anisotropic material (in this case the starch) contributes to its birefringence property, which is the splitting of the light beam into two beams and their refraction perpendicular to each other. The second polarizer within the polarized light microscope then allows passage of only one of these split beams (which is parallel to it) and exhibition of a white image representing the sample against a black background (Figure 2.3) [48]. Further, the radial arrangement of the starch molecules that forms the starch granule is depicted in the form of a dark cross centered on the hilum, also termed Maltese cross (Figure 2.3) [48-51], the relevance of birefringence will be explained in the "Processing of Starchy Foods- Gelatinization" section below.
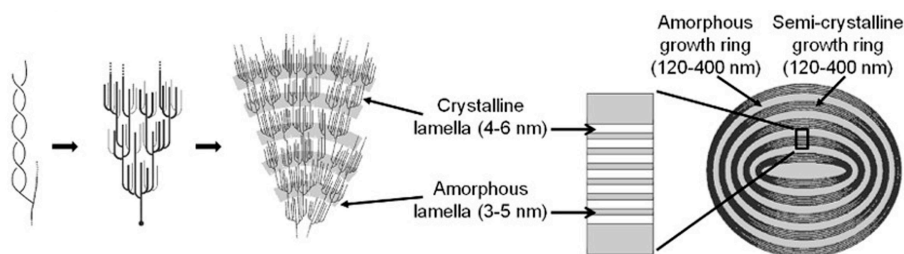
Figure 2.2: Left to right: starch strands are arranged parallel to each other to form a left-handed double helical structure. Multiple helices result in regions of branching and regions of linear polymer in the form of a hierarchical structure, thus forming amorphous and crystalline lamella, respectively. Accordingly, the final starch granule consists of alternating growth rings of explicitly crystalline and explicitly amorphous lamella (regions) [42].
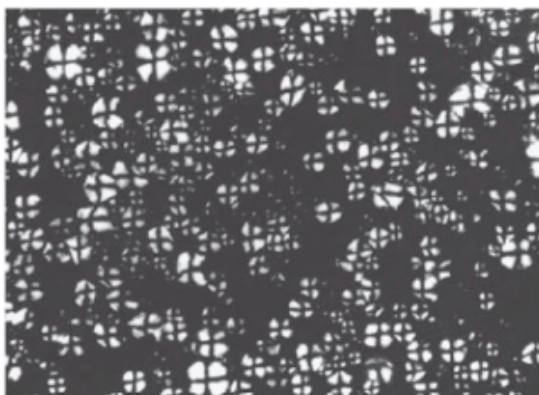
Figure 2.3: Maltese cross of starch granules under polarized-light microscope [49].

2.1.3 Starch Digestion

Starch digestion, also known as amylosis, involves the breakage of α-1,4-glucan linkages in the starch polymer chains via α-amylase enzyme [18]. α-Amylase is endogenous in the human gastrointestinal (GI) tract and is secreted from two glands: the salivary glands, into the oral cavity and the pancreas [52] into the duodenum of the small intestine [53]. Salivary α-amylase is responsible for starch hydrolysis in the oral cavity [54]. The significance of salivary α-amylase in starch hydrolysis is debatable and may be a function of the duration of oral mastication time and starch source [55]. Pancreatic α-

amylase is responsible for starch hydrolysis in the small intestine [54], and is responsible for the majority of the total amylosis [56, 57].

α-Amylase enzyme diffuses to the starch granule-water interface where it is adsorbed, thus starting the starch-degradation process [58]. The starch polymer (25 μm) is approximately 3000 times larger than α-amylase (2-3 nm) [59]. Thus, the starch substrate provides a large surface area for α-amylase [38]. Catalysis is dependent on the occupation of the active site on α-amylase. Human salivary, human pancreatic and porcine pancreatic α-amylase enzyme are structurally similar [60-62]. Experimental simulation of human carbohydrate digestion typically uses porcine α-amylase. Both human [63] and porcine [64] pancreatic α-amylase binding sites (i.e., the point of attachment to the glucose polymer), consists of 5 subsites [64]. Accordingly, starch binds with its first glucose unit to the first or second subsites and results in the cleavage of the glycosidic bond between the first and second, or second and third glucose units [63, 64]. In other words, α-amylase specifically cleaves α-1,4-linkages [65] and excludes the terminal glucose and branching α-1,6-linkages. This process yields maltose, maltotriose, and dextrins [66, 67]. Along the brush border of the small intestine are enterocytes that contain various enzymes responsible for digestion of the dextrins, maltose and maltoriose [66, 68].

There are two phenomena that hinder or attenuate the rate of starch hydrolyzing α-amylase enzyme: first, limiting the binding between the enzyme and starch substrate, which is the rate-limiting stage; and second, structural features as well as meal manipulation (e.g. cooking or processing) may result in disruption of the starch granule

integrity [15]. A thorough understanding of these phenomena will be useful in manipulating starch-based foods to inhibit/slow-down their carbohydrate digestibility.

2.1.4 α -Amylase-Starch Access/Binding Limitations

Food architecture is one parameter that may influence access of the enzymes to starch. Water-soluble fibers (SF) reduce the rate and extent of starch digestion via their ability to increase digesta viscosity. Fibers that contribute to viscosity increase transit time in the GI tract and delay gastric emptying [69]. The viscosity increase associated with SFs results in increasing viscosity of the digesta in the GI tract, impeding motion and access of enzymes to the starch, consequently reducing α-amylase activity on starch [70-72]. Further, increasing viscosity hinders diffusion of the α-amylase hydrolysis byproducts to the luminal brush border and renders absorption less effective [70-72]. A number of randomized studies suggest positive contributions of fibers on controlling postprandial glycemia [73-78]. SF is a type of DF, also known as non-starch polysaccharides (NSP), that are resistant to digestion in the human small intestine and undergo some level of fermentation in the colon [74, 79]. β-glucans have gained interest in the industry due to the authorization granted by US Food and Drug Administration to use health claims relating to diets high in oat bran and oats ($\geq$ 3 g/day), which are high in β-glucans [80-82].

2.1.4.1 β-Glucans

(1$\rightarrow$3, 1$\rightarrow$4)-β-D-glucans are glucan polymer chains linked via β-linkages [83, 84] that are found in the cell walls of cereal grains [37]. β-linkages render the molecules resistant to digestion [85] and result in the formation of linear structures connected at the 1,3 and 1,4 positions [37] (Figure 2.4). The random coiled polysaccharide is not

influenced by pH changes due to their uncharged nature [13]. Ability of SFs, inclusive of β-glucan, to increase digesta viscosity within the GI tract is believed to be the major factor responsible for its health benefits, which include reducing postprandial glycemia [86-92] and prolonging the sensation of satiety. Oats are rich (3-7% [4, 93, 94]) in β-glucans, which are concentrated in the endosperm and aleurone layer and have a molecular weight ranging between $0.065\text{-}3\text{X}10^6$ g/mol [95].
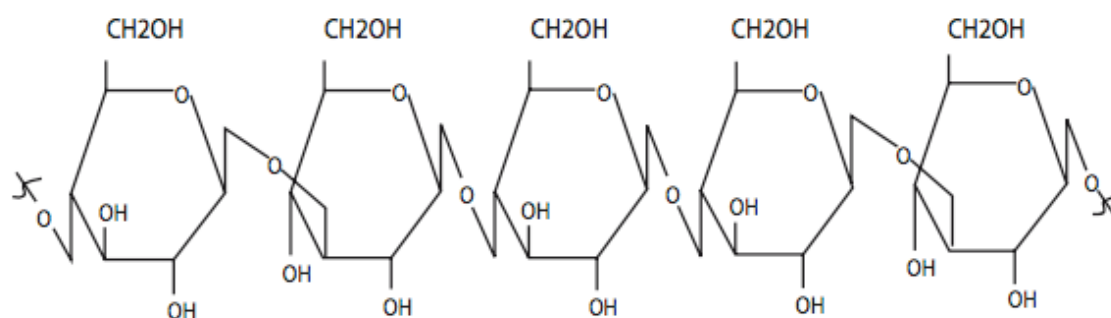
Figure 2.4: β-Glucan linear structure [96].

The mechanism by which β-Glucans modulate postprandial glucose levels is not fully understood. The most widely accepted postulation refers to the viscosity-increasing or thickening property of SFs, inclusive of β-Glucans. Wood *et al.* demonstrate an inverse relationship between viscosity of a 50 g glucose solution (altered via modification of β-glucan (oat gum) molecular weight and dose) and postprandial plasma levels. Plasma glucose and insulin levels were 79-90% inversely correlated to log viscosity of the meal [13]. The linear and unbranched nature of β-glucans [13, 97], in combination with its high molecular weight, provides a high intrinsic viscosity [98, 99]. This allows the polymer coil to overlap and entangle [13, 97], increasing viscosity of the solution at low concentrations (0.2-0.3% w/v) [98, 99]. The ability of β-glucans to resist digestion by

the human GI enzymes, where 88.5% of ingested β-Glucans were recovered in the human ileal efflux [100, 101], allows for retention of viscosity throughout the small intestine.

One factor that influences viscosity is the concentration of SF [97, 102, 103]. Increasing fiber concentrations yield an increase in viscosity to approximately the power of four [99]. Oat bran porridge and cream of wheat, with 10g of added β-glucan significantly reduced postprandial plasma glucose levels compared to the control cream of wheat in both non-diabetic and type II diabetic subjects [104]. The critical role of β-glucan dose on glycemic response attenuation has been observed [105-107]. Meals containing 50 g available carbohydrates with varying β-glucan composition: β-glucan cereal (7.3 g), β-glucan bar (6.2 g), commercially available oat bran cereal (3.7 g), and white bran (0 g) contributed to an inverse correlation between postprandial blood glucose levels and β-glucan concentration [108]. A 4 unit reduction in the glycemic index was observed per gram of β-glucan consumed in a 50 g carbohydrate meal [108]. Beverages containing 5 g oat β-glucan consumed for a 5-week period reduced postprandial glucose concentrations in comparison to a control beverage. However, the reduction was not significantly different from a 10 g oat β-glucan beverage [109]. In another work, diabetic patients that were fed a 12.5 g glycemic carbohydrate load in three forms: oat bran flour, oat bran crisp, and glucose load [110]. The meals varied in β-glucan content: 9.4 g, 3.0 g and 0 g, respectively. The area under the plasma glucose curve showed a statistically significant two-fold decrease for oat bran flour, as compared to commercially available NATUREAL® oat bran crisp. The authors attribute this trend to the higher β-glucan in the bran flour. In addition, the oat bran resulted in a reduction, and flatter curve, in the subjects' postprandial glycemia when compared to the glucose load [110]. Three

breakfast cereals that were controlled to contain 4, 6 and 8.6 g β-glucan via addition of different amounts of oat bran concentrate, were fed to type II diabetes subjects [105]. While the meals resulted in an attenuation in plasma glucose compared to a control, a distinct inverse relationship existed between plasma glucose peak or area under glucose curve and the β-glucan concentration and log viscosity of β-glucan [105]. Breads containing barley β-glucan doses, ranging between 0.1 and 6.3 %, resulted in a linear dose-dependent relationship attenuation in postprandial glycemic levels [111]. Muesli meals containing 4 g oat β-glucan yielded an significant reduction in postprandial glycemic response in healthy subjects as compared to a control meal without muesli and β-glucan [112]; this value appeared to serve as a critical cut-off, below which decreases in postprandial glucose response were insignificant [112, 113].

2.1.4.2 *Effect of Starch-Structure on Amylosis*

Direct contact between the starch substrate and α-amylase is critical to the amylosis process. Since the starch polymer predominately contains α-1,4-glucans chains, with a comparatively limited number of α-1,6-glucans, almost all glycosidic linkages are susceptible to catalysis by α-amylase enzyme [15]. However, the rate of catalysis is governed by various structural and compositional factors, such as ratio of amylose:amylopectin and degree of crystallinity. A tightly packed crystalline structure deters hydrolysis in comparison to a more loosely packed structure. In addition, granule structural features are also susceptible to changes due to processing techniques typically applied to starchy-products, such as cooking and milling, which in turn influences the extent of exposure of the starch glucan polymer to the α-amylase enzyme [15]. It is

therefore important to acknowledge physical characteristics when manipulating the product architecture to yield the desired physiological impact.

2.1.5 *Processing of Starchy Foods - Gelatinization*

Most starches are consumed after exposure to a hydrothermal process. Heating to > 60 °C results in the absorption of water into the starch granule causing an order-disorder transition, where the semi-crystalline nature of the granule is lost. This process is known as gelatinization (Figure 2.5) [114]. During gelatinization, hydrogen bonds are broken within the starch polymer and this disrupts the crystalline structure. The exposed hydroxyl groups of the starch polymer are bound to the surrounding water via hydrogen bonding, which results in swelling of the starch granules [115] to several times its original volume [40, 116-118]. The swelling process is accompanied by the pasting phenomenon, where a rapid increase in viscosity occurs because of the leaching of amylose into the solution [117, 118].
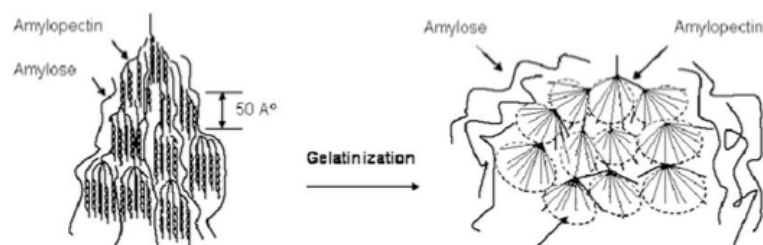
Figure 2.5: Schematic of changes in starch microstructure during the process of gelatinization [119].

Concurrent to loss of crystallinity during gelatinization is a loss in the aforementioned birefringence [116]. Upon hydrothermal processing, the loss in the crystalline structure results in disruption of the molecular organization and a consequent loss in the Maltese cross contour [49]. The point at which all birefringence (~ 95 or 98%) is lost is known as the birefringence end point temperature (BEPT) [116], and is

associated with complete gelatinization of the starch granules and complete loss in crystallinity [51].

Both the loss of structural order in the granule and leakage of amylose increases their susceptibility to α-amylase hydrolysis by facilitating interaction with α-amylase [120, 121]. The water absorption and swelling of starch granules involves disruption of the intra- and inter-molecular hydrogen bonds within the starch polymer, which facilitates access of the enzymes to the starch polymer [122]. The rate of digestion of waxy rice starch was found to be proportional to the degree of its gelatinization [122]. The authors attribute this to the complete disruption of the swollen starch granules in 'fully gelatinized starch samples' due to excess heating [122], this consequently increases accessibility of the hydrolyzing enzyme to the substrate. In comparison, the lack of complete disruption of the swollen starch granules in 'partially gelatinized starch' results in retention of the physical barrier against enzymatic accessibility to the substrate. Numerous authors have found relationships between gelatinization and the rate of starch digestion [123-125].

The correlation between the extent of gelatinization and rate of digestion renders it imperative to acknowledge the influence of different commercial processing techniques on gelatinization. Such variances are exemplified in the processing techniques used in cereal production. Steaming and rolling results in partial gelatinization of starch in thin flakes of instant oat [10] and cooking in boiling water (3 minutes) almost completely gelatinized the starch (deduced from loss of birefringence) [126]. Once the thickness of the rolled oats was increased (old fashioned oats), the extent of gelatinization during cooking (for the same duration) was decreased [10]. The authors attribute this difference

to a thicker particle size and a slower rate of water penetration [126]. Flaked amaranth starch was more readily hydrolyzed than cooked amaranth starch (boiled for 10 min), *in vitro,* due to an increase in gelatinization in the former [127].

2.1.6   *Amylose: Amylopectin Ratio*

Amylose (Figure 2.6) and amylopectin (Figure 2.7) are the two molecules that comprise starch. They are present at variable ratios depending on their source. Amylose makes up around 15-30% of normal starch, 35-70% of high amylose starch, and 0-5% of waxy starch [128]. Although both starches are polymers of glucose, they vary in their molecular weight and extent and length of their branches. Amylose (Figure 2.6) is a linear polymer with a minimal number of long branches, and a molecular weight of around 10^5 - 10^6 Da. Amylopectin (Figure 2.6), on the other hand has a larger molecular weight of around 10^7 - 10^8 Da and is characterized for its large number of short branches [129].
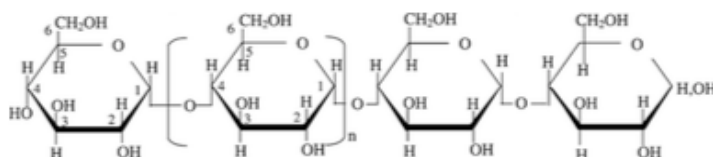
Figure 2.6: Molecular structure of amylose [130].
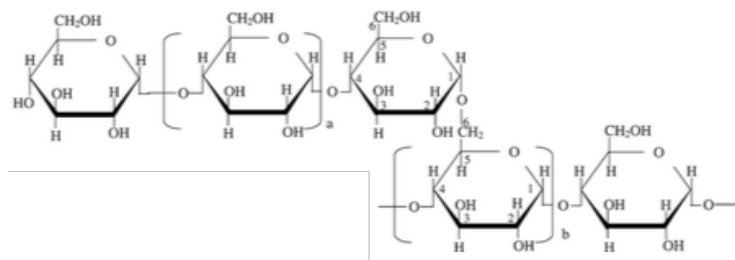
Figure 2.7: Molecular structure of Amylopectin [130].

An inverse relationship was found between amylose content and starch digestibility [129, 131-137]. Four cultivars of rice, each with differing amylose

concentrations, showed a decrease in starch hydrolysis with increasing amylose composition [138]. Barley flour-based bread showed reduced starch hydrolysis with increasing amylose content [139]. High-amylose maize Latin American flat bread (Arepas) showed a reduced extent of *in vitro* and *in vivo (in rats)* starch digestion as compared to the regular maize counterpart [140, 141]. Starch amylose-to-amylopectin ratio was found to be influential on post-gelatinization meal viscosity. A positive correlation exists between amylopectin content and peak starch viscosity, which is attributed to a higher molecular weight of the polymer chains [142] and a more rapid hydration and swelling due to a more ordered/crystalline microstructure [143, 144]. Concurrently, as the amylose content increased both onset of swelling and subsequent gelatinization are delayed [145, 146], also decreasing peak viscosity [147, 148].

2.1.7   Soluble Fiber

We have discussed earlier the influence of SFs in attenuating starch digestion via its effect of digesta rheological behavior. Also, SFs may play a role in reducing adsorption of α-amylase onto the starch surface by creating a barrier surrounding the starch that is resistant to enzyme penetration [149, 150]. Guar gum in bread and pasta has been shown to encapsulate starch granules, thus acting as a barrier between α-amylase and starch, where the extent of the reduction in glucose release was proportional to quantity of fiber [151, 152]. This physical barrier may also trap the nutrients and hinder their ability to reach the intestinal brush border for absorption. Further, SFs compete with starch for hydration, thus reducing the water activity of the solution, and consequent reduction in starch granule swelling, gelatinization, rupture, and amylose leaching [153-156] and consequently reducing susceptibility of the starch granule to hydrolysis.

2.1.8 Conclusions

Starchy foods provide the major source of glucose in the human diet. Therefore it is critical to investigate possible mechanisms to control their physiological response. Such modifications in food processing may prove useful for both the diabetic and non-diabetic consumer. Starch structure and conformation, as well α-amylase-starch access and binding are crucial parameters that influence carbohydrate amylosis. Controlling SF content, determining extent of starch gelatinization, and their collective influence on viscosity is one strategy to attenuate starch digestion kinetics. Such investigations are critical in light of the rapid increase in global occurrence of type II diabetes.

2.2 Human Gastrointestinal Digestion and *In Vitro* Digestion Simulation Models

2.2.1 Introduction

The complexity of the human gastrointestinal (GI) tract and the overall digestion process renders *in vivo* experiments cumbersome, costly, and restricted by ethical considerations [157]. *In vitro* digestion models provide a suitable alternative when they closely mimic human digestion and its physiological conditions [157]. *In vitro* digestion models must accurately simulate the mechanical reduction of food particle size and rate and extent of hydrolysis by enzymes [157]. In order for an *in vitro* model to represent changes in the GI tract, it must be able to mimic pH changes, transit times within each of the GI comprtments, and enzymatic conditions [157]. There are numerous systems used to model the GI tract. Some models are static and designed to serve specific applications; however, most of these systems seldom reproduce the dynamic nature of *in vivo* digestion. Typically, gastric emptying, continuous changes in pH, and secretion flow rates are not accounted for nor included [157]. In addition, these models usually involve use of a magnetic stirrer or shaking bath to simulate chyme mixing, i.e. Twin-Simulator of the Human Intestinal Microbial Ecosystem (TWIN-SHIME), and this does not portray the characteristic mechanical forces of digestion [158]. More complex, dynamic systems include the various compartments to simulate the GI tract. Many of these systems focus on mimicking one or a few of the different compartments of the GI tract, i.e. the Dynamic Gastric Model [159, 160] or the Human Gastric Simulator [161], both of which represent the gastric compartment only. Therefore, such systems do not give insight of the entire

digestion process. One of the few available options in *in vitro* digestion simulation systems that is both dynamic and multi-compartmentalized in nature is the TNO Intestinal Model-1 (TIM-1) [162]. The major pathway of human GI digestion will be summarized, followed by a thorough description of TIM-1 system, which is the digestive simulation system used in all experiments implemented in this dissertation, as well as its compartments and caveats.

2.2.2   *In Vivo Human Gastrointestinal Digestive System*

Digestion of a meal is initiated in the oral cavity via mastication. Salivary glands secrete saliva into the mouth [53] for the purpose of lubrication and initiation of carbohydrate digestion via salivary α-amylase [163]. The mechanically and enzymatically degraded bolus is transported to the gastric compartment via peristalsis. The bolus undergoes mixing with gastric juice in the gastric compartment that is facilitated by the churning activity of gastric muscles [164]. Gastric juice contains HCl that contributes to a progressive decrease in the gastric environment and bolus pH from ~ 6.5 to ~ 1.5. Gastric juice also contains lipase and pepsin enzymes to initiate digestion of protein and lipids. The produced semi-liquid form is now called the chyme [164]. Peristalsis is then responsible for forcefully exerting small gushes of the chyme through the pyloric sphincter into the small intestine [53]. The rate of gastric emptying into the small intestine is a critical factor of chyme digestion and is governed by food structure and composition [165, 166].

The small intestine is approximately 20 feet (6 meters) in length and approximately 1 inch (2.5 cm) in diameter, in the average adult and is made up of three segments: duodenum, jejunum and ileum [167, 168], with the duodenum being the

shortest of the three compartments. Sodium bicarbonate (NaHCO$_3$) is secreted into the duodenum to neutralize the highly acidic chyme, thus providing an optimal pH range for enzymatic activity in the small intestine. Pancreatic juice is secreted from the pancreas into the duodenum and consists of the pancreatic enzymes (proteases, α-amylases and lipases), which are responsible for the majority of the digestion of proteins, carbohydrates and lipids [53, 167]. The liver generates bile, which is secreted through the gall bladder to emulsify fats into smaller droplets [53]. Transit through the small intestine is a result of segmentation motion, which thrusts the digesta down the small intestine and also allows for mixing of the digesta with the digestive enzymes [163, 169]. This segmentation motion, combined with the complex nature of the inner lining of the small intestinal walls, together provide a large surface area for absorption of both nutrients and water [157, 170]. Chyme that has travelled through the small intestine and was not absorbed enters the large intestine or colon. The colon is responsible for: absorption of water and electrolytes, re-absorption of bile, fermentation of polysaccharides and proteins via the inhabitant microbiota, as well as generation and excretion of feces [171].

2.2.3   TNO-Intestinal Model (TIM-1)

TIM-1 is a multi-compartmental and dynamic, computer-controlled system [162] that was developed at TNO Nutrition and Food Research (Zeist, The Netherlands) [172]. TIM-1 mimics the upper part of the human GI tract (stomach and small intestine) and very closely simulates its numerous dynamic physiological processes. TIM-1 regulates pH curves, maintains a 37 °C temperature, secretes gastric and pancreatic secretions in physiological rates and amounts, applies suitable mixing and physiologically representative transit times [173, 174]. In addition, the system facilitates collection of

samples at any time during digestion directly from the compartments or after filtration [173]. Similar to other *in vitro* techniques, the TIM-1 permits accuracy and reproducibility, as compared to *in vivo* analysis [175].

2.2.3.1 TIM-1 Compartments and Principles
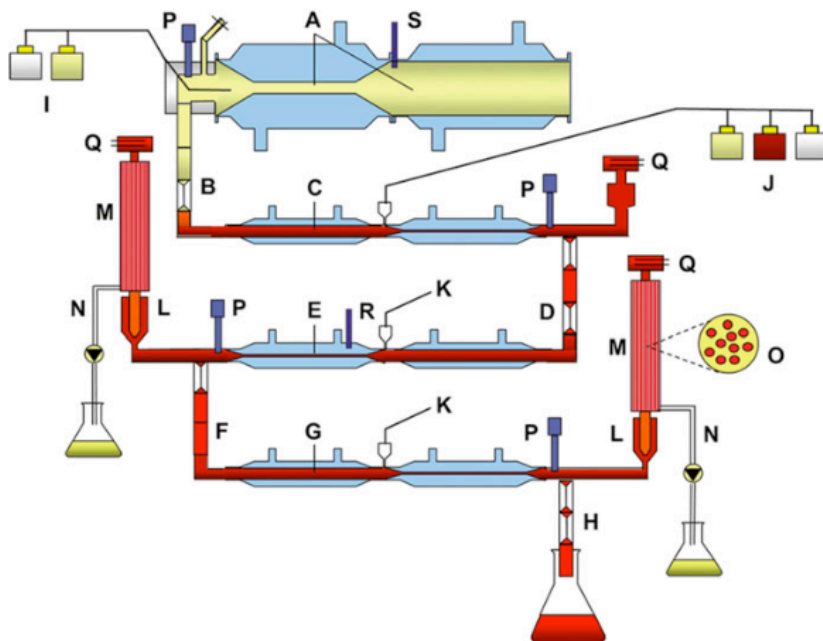
Figure 2.8: TIM-1. A. Gastric compartment; B. pyloric sphincter; C. duodenal compartment; D. peristaltic valve; E. jejunal compartment; F. peristaltic valve; G. ileal compartment; H. ileal-cecal valve; I. gastric secretion; J. duodenal secretion; K. bicarbonate secretion; L. pre-filter; M. filtration system; N. filtrate with bio-accessible fraction; O. hollow fiber system (cross section); P. pH electrodes; Q. level sensors; R. temperature sensors; S. pressure sensor [176].

TIM-1 is composed of four consecutive compartments that function as the GI: gastric cavity (Figure 2.8a), duodenum (Figure 2.8c), jejunum (Figure 2.8e), and ileum (Figure 2.8g) [162, 176]. As shown in Figure 2.8, each of these compartments is composed of an outer glass wall (blue color) filled with water (creating a water-jacket) and an inner flexible silicone wall (yellow in gastric compartment and red in intestinal compartments). Rotary pumps and a computer program are responsible for altering the water pressure in the water jackets and creating alternating compression / relaxation

motion of the flexible walls, mimicking physiological peristalsis on the compartment contents [162, 176]. The temperature is controlled to remain at 37 °C by means of heating water into the glass jackets. Figure 2.8b, d, f and h represent the peristaltic valves that separate the compartments, and are controlled by pressure from a connected nitrogen tank. Applying pressure to these valves almost completely closes the valves and prevents passage of any chyme; the contrary allows full passage of the chyme. Each of these valves has 3 sub-valves within; accordingly, within one valve for a single compartment, when one sub-valve opens, the other two close, this prevents backflow. In order to attain peristaltic motion, the valves are computer-controlled to open and close in a pre-set sequence and timing, accordingly controlling the volume being delivered with every peristaltic cycle [162, 176]. Figure 2.8q is the level sensor at each compartment that controls the volume within to retain a pre-determined level by allowing secretion of corresponding buffer into the compartment. A pH electrode is placed in each compartment (Figure 2.8p), which monitors pH and maintains a pre-determined computer-controlled and physiologically relevant pH curve via secreting 1M HCl (into the gastric compartment) or $NaHCO_3$ (into the intestinal compartments). All secretions including enzymes, bile, and pancreatic secretions are computer controlled [162, 176]. The overall conditions pre-set in the computer program dynamically change with digestion time in a physiologically relevant manner. Peristalsis, pH curves, enzymatic secretions, gastric emptying and transit times, removal of digestates are all based on human *in vivo* data and may all be modified to mimic different types of human subjects (i.e. infant, adult, elderly) in either the fed or the fasted states [177]. The jejunal and ileal compartments are connected to a hollow fiber (Figure 2.8m) filtration device that allows

passage of digestate molecules below ~ 50 nm [178] and collects them in an external beaker (Figure 2.8n) for analysis. The material that leaves the ileal efflux (Figure 2.8h) represents the portion that enters the colon [162, 176].

2.2.3.2 *TIM-1 Caveats*

The first compartment of the TIM-1 is the gastric compartment. TIM-1 lacks simulation of human mastication; application of this step is therefore the responsibility of the researcher to ensure that reduction in particle size of the meal prior to placing the sample in the TIM-1 is similar to that performed *in vivo* (in human oral cavity). Also, similar to all *in vitro* digestion models, the TIM-1 lacks a feedback system that allows individual changes in the dynamic nature of the digestion as per the individual and unique digested meal. This is of major importance with regards to the pre-determined rate of gastric emptying in TIM-1, which would allow passage of particulates into the small intestine in a uniform manner. On the contrary, *in vivo* gastric emptying is dependent on numerous factors: increased liquid viscosity decreases gastric emptying [179, 180]; addition of soluble fibers delays gastric emptying (pectin [181], such as guar gum [182, 183] and locust bean [184, 185]); food consumed at body temperature exits the gastric compartment at a faster rate than colder or warmer foods [186]. Smaller particles have a shorter gastric transit than larger particles [187-189], and liquids and solids have different gastric emptying mechanisms [190]. The researcher must keep the predetermined, uniform, and automated gastric emptying rate into consideration when analyzing bioaccessibility patterns and other related physico-chemical properties.

A critical part of experimental research is the accurate labeling or categorization of the attained sample or results. Accordingly, the question arises: is the collected sample

representative of the bioavailable nutrients? In other words, are the attained nutrients in the collected samples representative of those nutrients that have been absorbed and are now available to perform physiological functions [191]? Or is the collected sample representative of the bioaccessible nutrients? In other words are the collected products of digestion available to be absorbed in the future [176]? For this purpose, it must be noted that water and nutrient absorption involves simple and facilitated forms of diffusion, as well as active transport [157]. However, the hollow fiber filters attached to the jejunum and ileum compartments allow particles below a specific size to pass for collection in the sample intended for analysis. Accordingly, since the TIM-1 does not measure any advanced transport properties across the 'intestinal membrane' it is appropriate to label digestates as bioaccessible and not bioavailable. Attained digested nutrient samples may be representative of the bioavailable nutrients only when the analyzed nutrient is characterized with transport through the intestinal brush border that is not a rate-limiting step [176].

2.2.3.3 Correlation between In Vivo Gastrointestinal Digestion and In Vitro TIM-1

TIM-1 has been used in a large number of experimental works in numerous fields, such as: microbiology [192], pharmacology [172, 193], nutrition and food science [194, 195]. However, validity of any data collected from TIM-1 is dependent on the extent of correlation with *in vivo* data. Accordingly, the FDA has put in place an *in vitro and in vivo correlation* (IVIVC) system that allocates a 'level' of correlation based on ability of the *in vitro* test to provide accurate data when compared to the corresponding *in vivo* data [196], levels include A, B, and C. Level A correlation suggests a point-to-point correlation between *in vivo* and *in vitro* data, yielding a straight line with a slope that

equals to 1. Dissolution of acetaminophen tablets using TIM-1 showed a level A *in vitro/in vivo* correlation, with correlation coefficients of 0.9128 in the fasted state and 0.9984 in the fed state [193]. Partially hydrolyzed guar gum showed a dose-dependent negative correlation with fat and cholesterol bioaccessibility in TIM-1 [197], in-line with *in vivo* findings by Kondo *et al.* [198]. An attempt in increasing bioaccessibility of tangeretin, a major polymethoxyflavone known for its ability to reduce risk of development of degenerative diseases, was performed by altering its oral delivery characteristics [199]. Being a hydrophobic compound, tangeretin was formulated in a lipid-based viscoelastic lecithin emulsion in medium chain triglycerides. The work compared bioaccessibility of the viscoelastic emulsion to tangeretin in a suspension of medium chain triglycerides. The influence of this processing technique on the bioaccessibility of tangeretin was tested both *in vitro* using TIM-1 and *in vivo* from blood samples of orally gavaged mice. TIM-1 results showed a 2.6 fold increase in the bioaccessibility of tangeretin in the viscoelastic emulsion form compared to the medium chain triglyceride suspension form. The *in vivo* experimentation with mice showed that the emulsion oral delivery system resulted in a 2.3 fold increase in the bioavailable plasma tangeretin concentration compared to the medium chain triglyceride suspension system. These results suggest that the TIM-1 provides a good prediction of *in vivo* physiological responses [199]. Verwei *et al.* [195] made use of the TIM-1, in combination with human colon carcinoma (Caco-2) cells to develop a kinetic model describing folate kinetics to predict blood folate concentrations in humans. In the same work, human subjects were fed folate-fortified pasteurized milk, folate-fortified UHT milk, or unfortified milk for duration of 4 weeks. The in-silico model developed from

TIM-1/Caco-2 *in vitro* results was able to accurately predict the increase in blood folate concentrations after the fortified meals, and also accurately predict the decrease in folate concentrations after unfortified meal consumption [195]. In a similar work by the same first author [200], UHT and pasteurized milk were found to be appropriate food matrices for the delivery of supplemental folate, illustrated by a high (60-70%) bioaccessibility [200]. These values coincide with *in vivo* human [201] and rat [202] studies that suggested dietary folate bioaccessibility to range between 40 and 70% of the ingested amounts.

2.2.4 Conclusions

In vitro GI simulation models are desirable alternatives to labor-intensive, costly and ethically constrained *in vivo* digestion experiments. The TIM-1, unlike other *in vitro* simulation models, is able to mimic (via a pre-determined computer controlled system) various physiological properties such as peristalsis, pH and pH changes over time, as well as removal of digestion products. Accordingly, the TIM-1 is considered the closest system currently available to the *in vivo* "gold standard". Numerous studies have shown good correlation between TIM-1 results and *in vivo* data, suggesting the system is reliable in predicting *in vivo* parameters.

2.3 Potential Applications of Luminescent Molecular Rotors in Food Science and Engineering

2.3.1 Abstract

Fluorescent molecular rotors are compounds whose emission is modulated by segmental mobility; photoexcitation generates a locally excited (LE), planar state that can relax either by radiative decay (emission of a photon) or by formation of a twisted intramolecular charge transfer (TICT) state that can relax non-radiatively due to internal rotation. If the local environment around the probe allows for rapid internal rotation in the excited state, fast non-radiative decay can either effectively quench the fluorescence or generate a second, red-shifted emission band. Conversely, any environmental restriction to twisting in the excited state due to free volume, crowding or viscosity, slows rotational relaxation and promotes fluorescence emission from the LE state. The environmental sensitivity of molecular rotors has been exploited extensively in biological applications to sense microviscosity in biofluids, the stability and physical state of biomembranes, and conformational changes in macromolecules. The application of molecular rotors in food research, however, has been only marginally explored. In this review we summarize the main characteristics of molecular rotors, their current

applications in biological research and their current and potential applications as sensors of physical properties in food science and engineering.

2.3.2 Glossary

Bathochromic shift, red shift: A change in the wavelength of an absorption or emission band towards a longer wavelength with a lower frequency.

Fluorescence: Emission from a photoexcited singlet state where the transition from the excited state to the ground state involves emission of light with lifetimes ranging from 10^{-12} to 10^{-7} s.

Fluorescence lifetime: The characteristic time a molecule remains in the excited state before relaxing to its ground state. Fluorescence lifetime is independent of probe concentration while fluorescence intensity is proportional to probe concentration.

Fluorescence lifetime imaging microscopy (FLIM): A technique for measuring the distribution of fluorescence lifetimes in a microscopic image. It provides information on both the spatial distribution of fluorescent molecules as well their local microenvironment.

Fluorophore: A chemical (usually aromatic) compound that can emit fluorescence upon photoexcitation; a fluorescent molecule.

Free Rotor Effect: The ability of a molecular rotor to undergo internal (segmental) rotation that is associated with non-radiative relaxation of the excited singlet state.

Hypsochromic shift, blue shift: A change in the wavelength of an absorption or emission band towards a shorter wavelength with higher frequency.

Intramolecular Charge Transfer (ICT) state: The state adopted by a molecular rotor upon relaxation of the initially photoexcited state; it involves intramolecular transfer of an electron from a donor group to an acceptor group.

Local Excited (LE) state: The planar state of a molecular rotor formed upon direct photoexcitation; it can relax directly back to the ground state with photon emission (radiative decay) or undergo charge transfer to form an ICT state.

Luminescent Molecular Rotor (MR): A molecule that consists of two (or more) segments that can rotate relative to one another (can undergo intramolecular twisting). The rate of twisting, which depends on the free volume, molecular crowding, or viscosity of the local environment, modulates the distribution of the **LE** and **TICT states**. Relaxation is primarily radiative from the LE and non-radiative from the TICT state.

Non-radiative decay rate: The rate of release of excited state energy into thermal energy (i.e., the rate of vibrational relaxation) to return to the ground state. This process does not involve photon emission and is the main mode of de-excitation of the **TICT state**.

Quantum yield: A measure of the radiative yield from the photoexcited state; equal to the ratio of the number of emitted photons to the number of absorbed photons.

Phosphorescence: Emission from a triplet state, formed by intersystem crossing from a photoexcited singlet state, where the transition from the excited state to the ground state involves emission of light with lifetimes ranging from about 10^{-4} to 10 s.

Radiative decay rate: The rate of release of excited state energy via radiative emission to return to the ground state. This process involves photon emission and occurs during de-excitation from the **LE state.**

Ratiometric sensor: A molecule (probe) engineered to consist of a segment, e.g., a luminescent molecular rotor, with specific environmental sensitivity coupled to a reference fluorophore without environmental sensitivity that is able to report on the probe concentration; the use of a ratiometric sensor can correct for the effect of probe concentration.

Resonance energy transfer (RET): Non-radiative energy transfer between two fluorophores. A excited donor (D) fluorophore may transfer energy to an acceptor (A) fluorophore through non-radiative dipole–dipole coupling. RET efficiency is inversely proportional to the sixth power of the distance between D and A and directly proportional to the spectral overlap of D emission and A absorbance.

Stokes shift: The difference in wavelength between the band maxima of the absorption and emission spectra.

Twisted Intramolecular Charge Transfer (TICT) state: The non-planar (twisted) configuration of a molecular rotor, usually with lower excited-state energy; relaxation to the ground state from the TICT state is predominantly non-radiative.

Radiative decay rate: rate of release of excited state energy via photon emission to return to the ground state. This process occurs during de-excitation from the **LE state.**

2.3.3   Abbreviations

BODIPY: Boron-dipyrromethene

CCJV: 9-(2-Cyano-2-hydroxy carbonyl)-vinyl julolidine

CPVDA: p-[(2-Cyano-2-propanedio ester) vinyl] dimethylaniline

DMABN: 4,4-Dimethylaminobenzonitrile

DCVJ: 9-(Dicyanovinyl)-julolidine

DASPI: (Dimethylamino)-styryl-1-methylpyridinium iodide

GRAS: Generally Recognized as Safe

MR: Molecular rotor

SY: Sunset yellow

TEG: Triethyleneglycol ester

2.3.4   Introduction

Luminescence spectroscopy due to its convenience and versatility is commonly used to study the molecular properties and functionality of proteins, lipid membranes, and nucleic acids in the biological sciences[203-207]. The environmental sensitivity of organic chromophores to the physical and chemical properties of their local surroundings, such as pH, ionic strength, polarity, hydrogen bonding, or matrix mobility [208, 209], make these fluorophores excellent *in situ* or even *in vivo* molecular sensors causing minimal or no perturbation to the system. In recent years, the use of spectroscopic techniques in food applications has significantly increased, due, in part, to several factors: a) the identification of suitable Generally Recognized as Safe (GRAS) fluorophores [204, 205], b) instrumental improvements, and c) advances in chemometric methods that facilitate data acquisition, interpretation and implementation of spectrophotometric
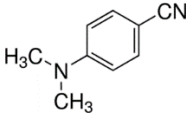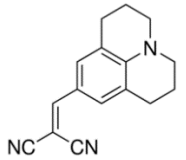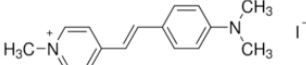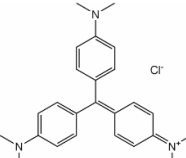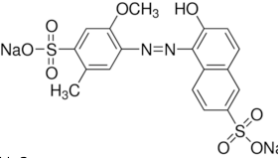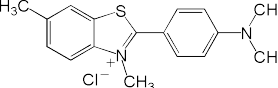
techniques in food matrices [210, 211]. However, in our opinion, luminescence spectroscopy as a tool to study food structure and food properties is still significantly underutilized. This work reviews current and potential applications of a specific class of optical probes, known as luminescent molecular rotors, in the food sciences. Luminescent molecular rotors exhibit a remarkable sensitivity to molecular crowding, free volume, and viscosity and consequently have been proposed as effective intrinsic sensors of quality attributes, particularly of physical properties, in foods [204, 205, 212, 213].

Manufactured foods are complex and often multi-phased [214] systems whilst others such as fruits and vegetables are consumed raw or minimally processed. Regardless, many foods are presented to the consumer after extensive modification, resulting in the development of unique microstructural characteristics. Accordingly, a thorough understanding of the influence of microstructure and composition on organoleptic and physicochemical properties of the foods is crucial to sustain product quality and shelf life [215]. Luminescence techniques based on the use of environmentally sensitive fluorescent probes that function as molecular rotors (MRs) can serve as versatile tools for such a purpose due to their ability to report on various physical properties of their surrounding environment in a noninvasive and non-disruptive way. Luminescent MRs exhibit internal segmental mobility in the excited state that can quench fluorescence. The basis for their environmental sensitivity is hindrance of intramolecular rotation [216]; therefore, interactions of a MR with an interface, a membrane, or a protein, or exposure to variable degrees of molecular crowding will increase the fluorescence emission intensity, quantum yield and lifetime. A molecular rotor may be embedded into a static system, i.e., a food or a cell, and report on properties such as micro (and bulk)

viscosity. Alternatively, MRs can be operationalized into a dynamic industrial setting to monitor changes throughout the processing line and/or to obtain measurements of quality attributes over time at a specific point. Fluorescence lifetime imaging microscopy (FLIM) of MRs can also be used to map the spatial distribution of viscosity in cellular environments [217, 218] and model systems [219, 220]. An overview of the basic operational principles of fluorescent MRs and their current applications in the biological sciences will be presented first, followed by a discussion of the current and potential uses of this class of luminescent probes in food science and engineering.

2.3.5   Fluorescent Molecular Rotors

Table 2.1: Classification, examples, structure and photophysical properties of the major groups of MRs identified to this date.

Type	Examples	Typical Structure	Excitation Wavelength (nm)	Emission Wavelength (nm)	Ref.
Benzonitrile-based fluorophores	DMABN		290	342 / 460 *	[221]
Benzylidene malononitriles	DCVJ		489	505	[221, 222]
Stilbenes	p-DASPI		430	625	[223]
Triarylmethane dyes	Crystal Violet, Fast Green		590 470 /600	630 515 /660	[221]
Azo dyes	Allura Red, Citrus Red		520 520	590 610	[224, 225]
Benzothiazole	Thioflavin T		420	485	[226]

*Dual fluorescence bands

An ideal MR has the following attributes: a) a large Stokes shift (the difference in wavelength between the excitation and emission spectra) that results in good differentiation of excitation and emission spectra, b) high sensitivity to structural rigidity of the surrounding media, c) high brightness [16], and d) no coupling of the response to structural rigidity with sensitivity to other physical and chemical properties such as polarity. Table 2.1 illustrates some of the major groups of molecular rotors that have been identified and studied.

2.3.5.1 Mode of Action

Figure 2.9: Schematic diagram of molecular rotor structure that adopts an "electron donor-π-electron acceptor" (A); 'D' represents electron donor segment, 'A' represents electron acceptor segment; the two segments are connected via a π-conjugation unit. Adapted from Haidekker and Theodorakis [231].
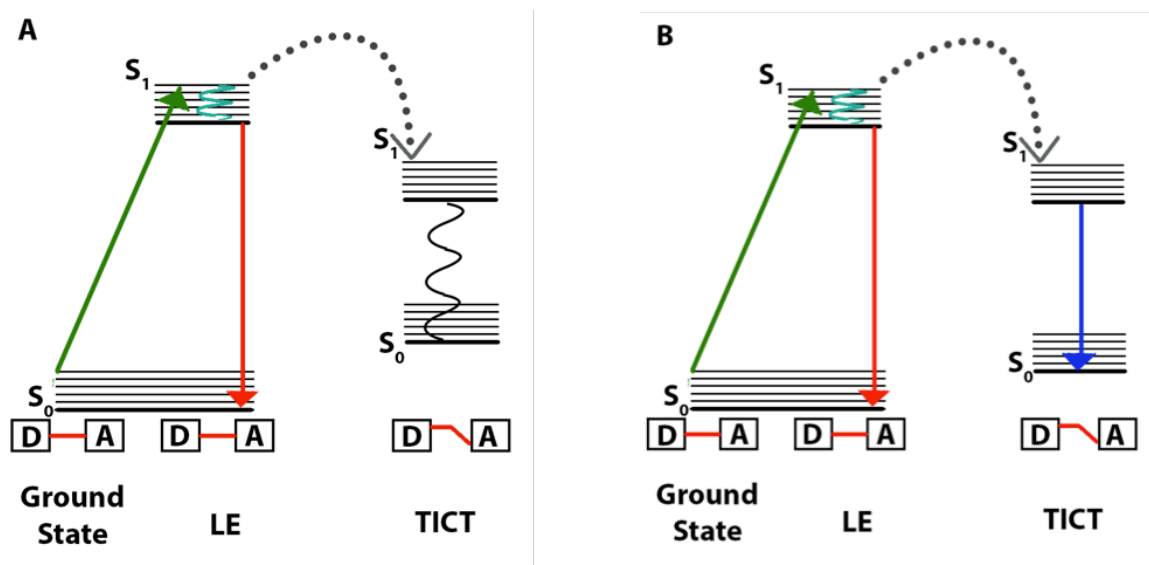
Figure 2.10: Jablonski diagram for single (A), and dual band (B) MRs. Photoexcitation promotes a MR from ground state (S0) to the excited state (S1). The series of parallel lines represent vibrational states. (A) In a single band MR, S1 may

relax by photon emission from the LE state (red arrow) or by non-radiative decay from the TICT state (curved line). (B) In a dual band MR, S1 may relax by photon emission from either the LE or the TICT states (red and blue arrows, respectively).

Molecular rotors (MRs), molecules that can undergo an intramolecular segmental rotational (twisting) motion following photoexcitation [227], typically consist of an electron donor and an electron acceptor group connected by a conjugated network of alternating pi (π) and sigma (σ) bonds (Figure 2.9). Photoexcitation forms a locally excited (LE) intramolecular charge transfer state (ICT) in which an electron is internally transferred from the electron donor to the acceptor [228]. Because of their conjugated system of π orbitals, molecular rotors have a planar ground state configuration. While the initial ICT state formed on photoexcitation is also planar, electrostatic forces resulting from the charge separation induce twisting of the sub-groups on the molecule relative to one another; the resulting non-planar configuration, the twisted intramolecular charge transfer (TICT) state, has a lower excited state energy. Relaxation from the TICT state involves either radiative decay of a photon, giving rise to a bathochromic shift in the emission band, or non-radiative decay via energy dissipating vibrational motions [229, 230] (Figure 2.10). The rate of formation of the TICT state from the LE charge transfer state is dependent on the microenvironment of the matrix, that is, on the free volume around the MR. Molecular crowding, or high medium microviscosity, sterically restricts the formation of the TICT state, thus favoring persistence of the locally excited ICT state; relaxation from the LE state involves direct photon emission, known as fluorescence. The energy gap between the newly formed TICT state and the ground state plays an important role in the subsequent relaxation behavior of the TICT state [212]. If the TICT-ground state energy gap is small, the TICT state relaxes directly to the ground state by fast non-

radiative decay; in this case, there is only a single emission band reflecting radiative decay from the LE state [212] (Figure 2.10A). If the energy gap is sufficiently large, the TICT state can relax by radiative emission, resulting in a second emission band that is red-shifted from the LE fluorescence band [212] (Figure 2.10B). Such dual band emission [216] is exemplified by 4,4-dimethylaminobenzonitrile (DMABN), which belongs to the class of benzonitrile molecular rotors [221]. In either class of MRs, emission from the locally excited ICT state is sensitive to the physical state of the local environment: any increase in molecular crowding/microviscosity increases the probability of emission from the LE state and thus increases the intensity of the LE emission band.

2.3.5.2 Sensitivity to Free Volume (and Molecular Crowding)

The free volume around the MR thus modulates the rate of formation of the TICT state and thus the fluorescence intensity of the LE state [232]: LE emission intensity is low in fluid and high in rigid conditions. Since solution viscosity, which reflects molecular crowding and free volume [233], is easy to modify and measure, the environmental sensitivity of MRs has been mainly evaluated and expressed as sensitivity to solution viscosity.

Loutfy and Arnold's [238] earliest work, which studied the relationship between viscosity and fluorescence quantum yield in a wide range of solvents, suggests that, in low viscosity solvents, hydrodynamics can clearly drive the free rotor effect of MRs. However, in higher viscosity solvents, hydrodynamic predictions are insufficient; instead, free-volume is the primary influence on the segmental relaxation of the probe. They also observed an increase in MR lifetime with solvent viscosity, from liquid ethyl-acetate, a

relatively lower viscosity solvent (11 picoseconds), to viscous glycerol, a relatively medium viscosity solvent (500 ps), to rigid glasses, a relatively higher viscosity matrix (3600 ps). Accordingly, they proposed that the relaxation from the excited state is dependent on the solvent viscosity. A proportional relationship has been established between solvent viscosity and fluorescent quantum yield the Förster-Hoffmann equation [238] describes the following power law relationship between the fluorescent quantum yield, Φ_F, and the viscosity (η) of the solution:
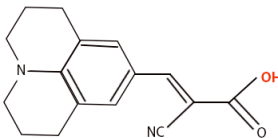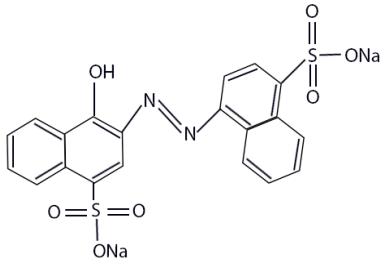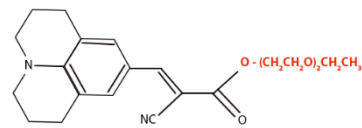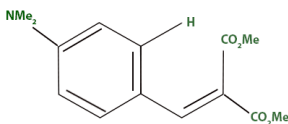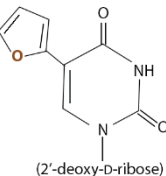
$$\log \Phi_F = C + x \log \eta \qquad (2.1)$$

where C is a dye-dependent constant and x is a constant related to dye-solvent interactions. Since fluorescence emission intensity and quantum yield are proportional, the relationship between the measured fluorescence intensity (I_F) and viscosity can be reworked from Equation 2.1 and is often expressed by the following power law model [216]:

$$I_F = \alpha \eta^x \qquad (2.2)$$

where α is usually considered a measure of the probe's brightness and x a measure of its sensitivity to local viscosity. The sensitivity of novel MRs to viscosity is quantified by the parameter x and is compared to reported values of commonly used MRs. It should be noted that the highest theoretical value for x is considered to be 0.66 [234]. Sensitivity values of novel and commonly used MRs in glycerol-based solutions have been reported in the range of 0.25 to 0.6. Table 2.2 provides selected examples of the values of parameters x and α for several known and recently reported MRs. (See supplementary materials for a complete list of sensitivity parameters for MRs.)

Table 2.2: Reported values for parameters 'x' and 'α' (Equation 2.2) for selected MRs.

Molecular Rotor	Structure	x: Viscosity Sensitivity	α: Brightness	Reference
CCVJ		0.54	147	[234]
Azo Dye (Azorubine)		0.38	-	[235]
CCVJ derivative (addition of ethylene glycol)		0.61	-	[236]
Dimethyl 2-(4-(dimethylamino) benzylidene) malonate		0.52	17	[234]
Nucleoside (pyrimidine – furan)		0.40	-	[237]

2.3.5.3 Sensitivity to Polarity

Solvent polarity generally does not influence the quantum yield of MRs; instead, polarity shifts the emission peak wavelength [239] or broadens the spectrum [230]. Haidekker *et al.* [221] investigated the effect of polarity and microviscosity on the fluorescence emission of 9-(Dicyanovinyl)-julolidine (DCVJ), 9-(2-Cyano-2-hydroxy carbonyl)-vinyl julolidine-triethyleneglycol ester (CCVJ-TEG), and DMABN. The photophysical properties DCVJ and CCVJ-TEG are independent of polarity but are highly sensitive to changes in viscosity [221] while DMABN is an exception as polarity modulates both the Stokes shift and emission intensity. Since the MR is composed of an electron donor (often containing oxygen or nitrogen) conjugated to an electron acceptor (for example, nitrile) [234], the presence of a weaker electron donor (e.g., methoxy, phenyl, or naphthyl group) causes a hypsochromic shift in both excitation and emission peak locations. Additionally, replacing the electron acceptor group with a methyl ester or phenyl sulfonyl group increases the quantum yield, which has been attributed to the dipole moment of the molecule [234]. A recent study on DCVJ and CCVJ revealed a significant difference between viscosity sensitivity of these fluorophores in polar protic and polar aprotic solvents [240]; the differences were attributed to the ability of the solvent to form hydrogen bonds. It is thus evident that the nature of the medium under study must be taken into consideration when selecting a fluorophore as a viscosity sensor.

2.3.5.4 Structure-Property Relationships

The seminal work by Loutfy and Law [239] on MRs investigated the photophysical properties and conformational changes of intramolecular charge transfer in p-N,N-dialkylaminobenzylidenemalononitriles. They concluded that as the

conformational rigidity of the electron donor, i.e., the NR_2, group increases, the quantum yield also increases due to a reduction in the free rotor effect. These authors also suggested that a MR with a smaller NR_2 group exhibits a lower quantum yield since this group will require less free volume to move than bulkier moieties. The influence of the molecular footprint of the rotor on the quantum yield (fluorescence intensity) and viscosity sensitivity was also studied by incorporating substituents on naphthalene-based [234, 241], phenyl-based [234], and boron -dipyrromethene (BODIPY) MR probes [242]. The addition of substituents usually resulted in increases in quantum yield or fluorescence intensity and reduced viscosity sensitivity. This phenomenon is explained by the location of the donor and acceptor groups; when the groups are placed in close proximity, their rotational ability decreases and the energy level of the TICT state increases, resulting in fluorescence without significant passage through the TICT state; consequently, these substituted MRs exhibit higher fluorescence intensity and less viscosity sensitivity [234, 241, 243]. Increased viscosity sensitivity was only reported when the substituents were attached at remote sites on the BODIPY fluorophore, which did not modify the space available for rotation [242]. Sutharsan *et al*. [234] also reported that a modification of the π-conjugation system can increase the electron density between the electron donor and acceptor groups, which increases the quantum yield; however, steric hindrances could limit this increase.

Sinkeldam *et al*. [237] elucidated the role of aryl-aryl bonds in the fluorescence of MRs based on the response of structurally modified nucleosides to changes in viscosity. In this study, pyrimidine was attached in different ways to aromatic moieties of different sizes. Attachment of the pyrimidine to furan or thiophene rings by a single rotatable bond

resulted in similar viscosity sensitivity. By replacing the single bond between the two aromatic ring structures with a conjugating ethynyl bond, the emission intensity was reduced. Fusing the pyrimidine to a thiophene heterocycle completely inhibited emission in response to viscosity changes [237] due to elimination of the rotatable linkage.

Further changes in the structure of the MR have been introduced in order to increase functionality and performance. Traditional rotors, e.g., DCVJ, normally exhibit short excitation and emission wavelengths and small Stokes shifts. Typically, a larger Stokes shift is desirable in fluorescence measurements, to allow greater differentiation between the excitation and emission peaks; a significant overlap of the two spectra hinders detection of maximum fluorescence. To overcome this drawback, a thiophene unit was added to aryl–dicyanovinyl fluorescent MRs, which resulted in larger Stokes shifts and red-shifted emission, facilitating differentiation of the MR emission from that of the background [244]. Self-calibrating MRs composed of an internal reference, a viscosity-independent dye, attached to a viscosity sensitive unit have been synthesized (Figure 2.11A) [245-247]. These ratiometric probes exhibit two emission bands whose intensity ratio can provide a concentration-independent self-calibrating measurement of the viscosity. In these ratiometric rotors, the emission spectrum of the reference dye (viscosity-independent moiety) overlaps the excitation spectrum of the MR probe (viscosity dependent moiety) so that resonance energy transfer (RET) can occur from reference to MR (Figure 2.11b); a single excitation wavelength thus excites both reference fluorescence directly and MR fluorescence by RET. Haidekker *et al.* [245-247] developed a ratiometric viscosity sensor by covalently attaching coumarin-based reference dyes to thiophene or aniline based MRs. Conjugated porphyrin dimers [248]

and a pentamethine cyanine dye substituted with an aldehyde group at its meso position [249] have also been used to obtain fluorescent ratiometric viscosity measurements.
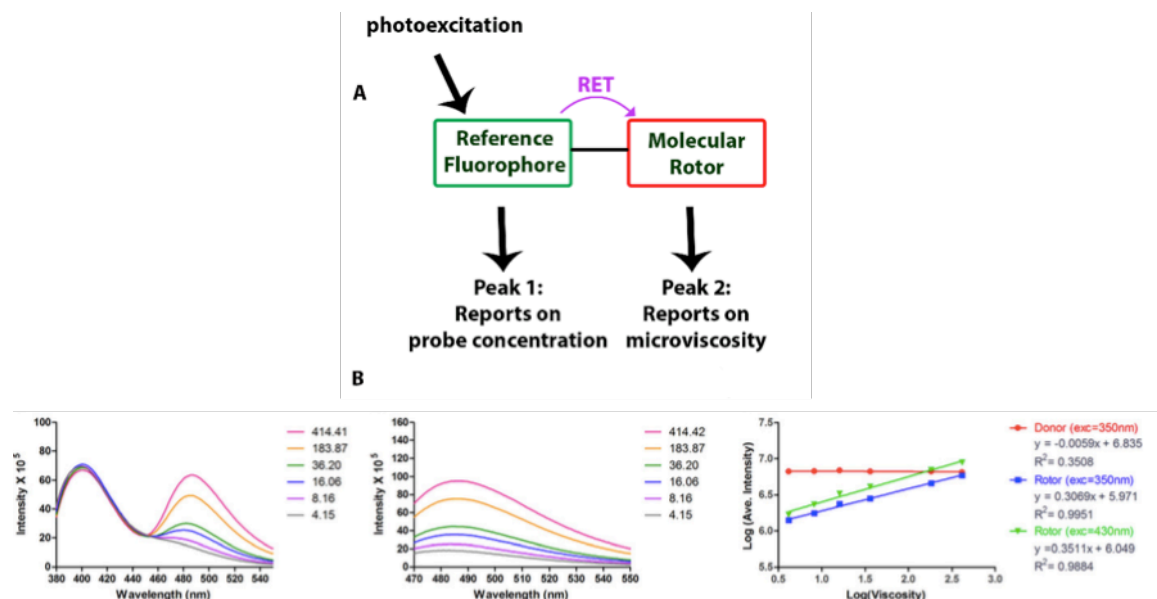
Figure 2.11: (A) Schematic diagram of a ratiometric probe with viscosity sensitivity. (B) Examples of fluorescence emission data (from left): ratiometric MR emission spectra, MR emission spectra alone, and viscosity sensitivity of ratiometric dyes; reproduced with permission from Dakanali, Do [245].

Readers are referred to the review of Uzhinov *et al.* [250] for further details on the influence of chemical structure on the photophysical properties of various MRs and to Haidekker and Theodorakis [212] for an in-depth review of these photophysical properties.

2.3.6 *Applications of Fluorescent Molecular Rotors in Biological Sciences*

MRs have found numerous applications in the biological sciences [218, 249, 251-256] and specifically in molecular biology due to the need of sensors with the ability to report on physical properties such as cytoplasm viscosity or membrane fluidity without perturbing normal system functions. Since spectroscopy of MRs is minimally invasive, it allows for the direct investigation of dynamic properties of proteins, cellular organelles,

membranes, and the cytoplasm within living cells and tissues. This section summarizes some of the most salient reported applications of MRs in biological systems.

2.3.6.1 Biofluids and Intracellular Viscosity

Blood plasma viscosity can be used for early diagnosis of disease [257]. Haidekker *et al.* [258] and Akers *et al.* [259] correlated plasma viscosity and fluorescence emission intensity of julolidine-based MRs. The latter work compared fluorescence-based viscosity assessment to a conventional mechanical method (cone-plate rheometry) in terms of methodology and precision. The results show slightly greater scatter when blood viscosity was determined by cone-and-plate rheometry (< 7.6%) compared to fluorescence spectroscopy using MRs (< 6%), suggesting that non-mechanical sensing can be, at least, equally effective and reliable as mechanical-based methods.

The microviscosity in the cellular cytoplasm is of critical importance to optimal cell functioning due to its effect on processes such as protein folding and other biochemical reactions [260, 261]. The *meso*-substituted BODIPY [255] and *meso*-substituted 4,4'-difluoro-4-bora-3a,4a-diaza-s-indacene [251] MRs have been used to report on microviscosity in live SK-OV-3 human carcinoma cells. A ratiometric viscosity sensitive probe synthesized by Dakanali *et al.* [245] selectively localizes in the cytoplasm and remains in the aqueous phase. Fluorescence lifetime imaging microscopy (FLIM) is used to map the spatial distribution of MR lifetimes (which are independent of dye concentration) that can be correlated with medium viscosity; it is thus possible to map viscosity distribution across heterogeneous cellular environments. A scheme of a FLIM set up using MRs is presented in Figure 2.12. The use of fluorescence microscopy enables spatial and time-based tracking of properties of interest [218, 262]. Intracellular

viscosity in living HeLa cells was estimated with FLIM using a *meso*-substituted BODIPY-C_{12} MR as a probe[263]; Figure 2.13 illustrates the correlation between longer fluorescence lifetime and higher medium viscosity for this probe.

The same technique was used to measure viscosities within the compartments of a primitive cell model consisting of a coacervate core (mimicking a reaction center) coated by oleic acid (mimicking a cell membrane) using Kiton Red and BODIPY-C_{10}, respectively [264, 265]. Fluorescence lifetimes were also found to be organelle-specific within cells and have been used to estimate viscosity values [266]. Another MR, a conjugated porphyrin dimer, was exploited for its unique ability to function as both a photosensitizer that induces cell death upon its irradiation, and a reporter of the resultant dynamic changes in intracellular viscosity [253]. Photoinduced cell death resulted in an increase in fluorescence intensity, illustrating the expected intracellular viscosity increase (~300 cP). This rotor is thus able to report on real-time changes in membrane rigidity as a function of irradiation as well as the longevity of the treated cell.
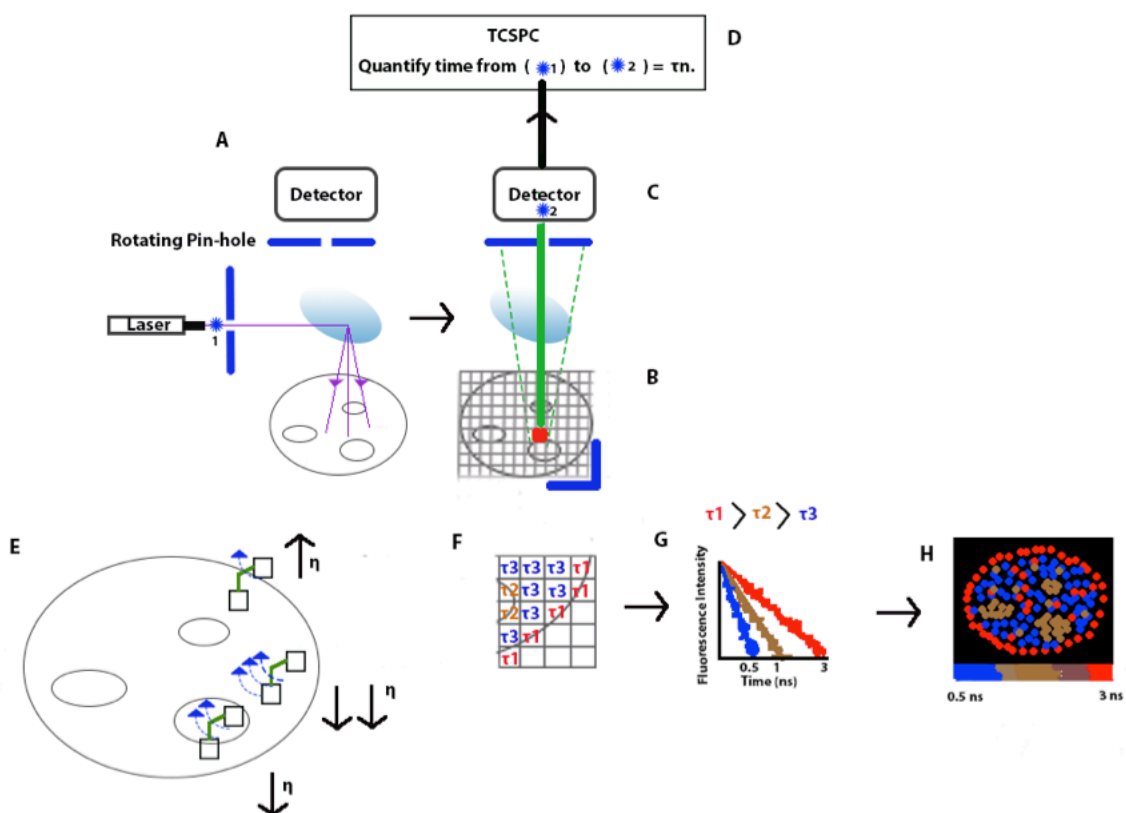
Figure 2.12: Schematic diagram of FLIM to obtain a high-resolution viscosity map of a biological sample. (A) High-resolution fluorescence images are obtained using a confocal scanning microscope. A pulsed laser beam (purple line) is directed towards a dichromic mirror that reflects the light onto a biological sample that has been stained with MR. (B) Sample perceived as multiple pixelated regions; (C) Emission from a single pixel at a time is selectively allowed to pass to the detector through a rotating pin-hole structure while light emitted from other pixels is blocked. (D) A time correlated single photon counting (TCSPC) unit quantifies the duration of the emission; (F) Specific lifetimes (τ) are allocated to each individual pixel. (E) MR decay pathways are microviscosity dependent; increased viscosity (η) hinders rotation (single rotation arrow); longer fluorescence lifetime (τ1); lower viscosity facilitates rotation; shorter fluorescence lifetime (τ3). (F-H) Software is used to compile all τ values into a viscosity map using a false color scale.
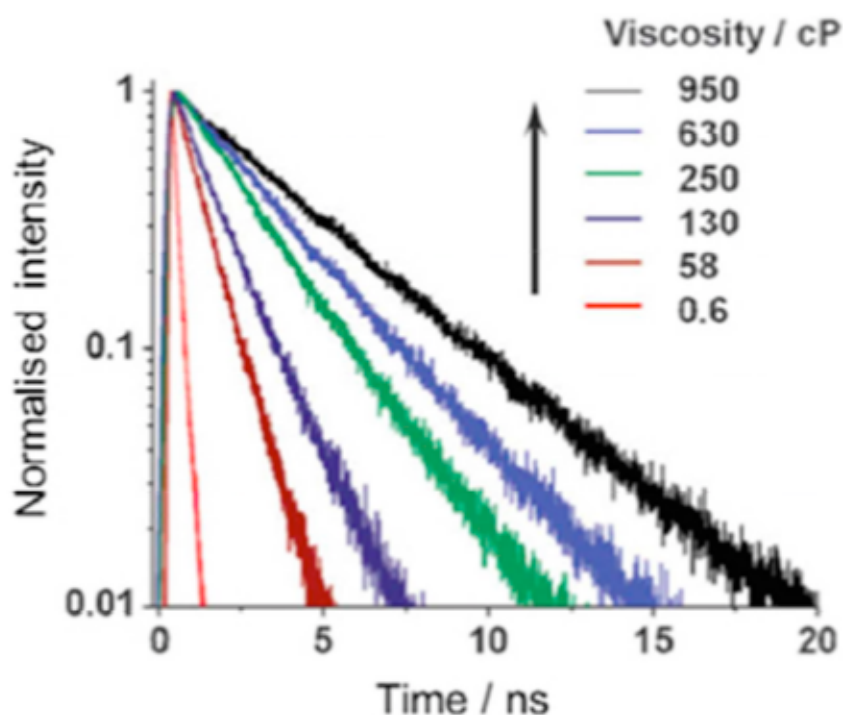
Figure 2.13: Time resolved fluorescence of BODIPY-C10 in methanol-glycerol mixtures of varying viscosity. Reprinted with permission from Thompson, Herling [263].

2.3.6.2 Macroscopic Membrane Properties

Diffusion, packing and permeability are dependent on cell membrane properties such as viscosity and fluidity [267]. The functionality of membrane-bound receptors and enzymes, for example, depends on the membrane viscosity [268, 269] and alterations in membrane properties were found to adversely affect enzyme functionality, active-transport and facilitated diffusion across the membrane, as well as binding of receptors [270]. Numerous health disorders have also been associated with cell membrane viscosity changes, including cardiovascular diseases [271], cell malignancy [272], hypertension [273], hypercholesterolemia [274], diabetes [275], and Alzheimer's disease [276]. Nipper *et al.* [277] investigated changes in the viscosity of a liposome model membrane using a

membrane-entrapped farnesol ester of MR (2-carboxy-2-cyanovinyl)-julolidine, FCVJ. This rotor was found to be sensitive to changes in the membrane viscosity upon addition of viscosity-increasing (e.g., cholesterol) and viscosity–decreasing (e.g., longer chain alcohols) agents.

Lipid membranes and liposomes undergo a temperature-dependent phase change, assuming a gel state below the phase transition temperature and a liquid crystalline state above that temperature [278]. The use of MRs has been explored to distinguish between liquid-ordered (L_o) and liquid disordered (L_d) phase domains in cell membranes; L_o domains have a relatively higher viscosity than L_d domains and play a role in regulating membrane trafficking and signal transduction [279, 280]. An auramine-based MR, conjugated to a cholesteryl group that acts as an anchor into a bilayer lipid membrane was used with epifluorescence microscopy to report on the spatial distribution of lipid membrane viscosity. The images of individual gel-state and liquid-crystalline state liposomes showed regions of bright and weaker green emission, respectively. Similarly, a synthesized membrane with phase-separated L_o and L_d domains showed both high and low-emitting regions, which have been allocated to L_o and L_d domains based on the viscosity-dependent fluorescence intensity of the auramine MR probe (Figure 2.14) [281]. L_o and L_d membrane domains were also investigated using *meso*-substituted BODIPY–C_{10} and –C_{12} aliphatic chains [220] by correlating time-resolved fluorescence decays with temperature-dependent phase state changes in the lipid bilayers. The rotor proved an effective identifier of the two different order regions based on fluorescence lifetimes.
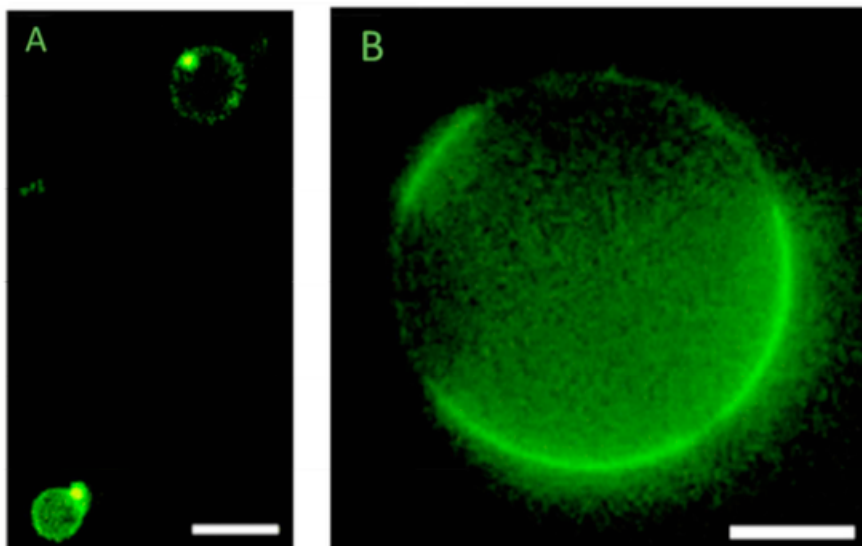
Figure 2.14: FLIM image of an auramine-based MR conjugated to a cholesteryl group embedded into a bilayer lipid membrane. (A) The MR probe is able to distinguish between the gel (bright emission = higher viscosity) and liquid-crystalline (weak emission = lower viscosity) phases of the liposome bilayer membrane. (B) The MR probe can also distinguish between domains in a synthesized giant liposome containing both Lo (more viscous and brighter) and Ld (less viscous and darker region). Reproduced with permission from Yasuhara, Sasaki [281].

2.3.6.3 Protein Aggregation, Degradation and Conformational Changes

The abnormal aggregation of proteins or polypeptides into amyloid fibrils [282] has been associated with numerous diseases such as neurological disorders, type II diabetes and systemic amyloidosis [283]. MRs have been used to identify the presence and formation of amyloids [226, 263] and the effect that therapeutic strategies might have on their stability [227]. For example, Cy3 MR was used to quantify the steric hindrance to the MR at the various stages of amyloid fibril formation, which allowed for comparison of the different amyloid fibrils that resulted from different protein aggregates [264]. A variety of amyloid binding molecules with inherent fluorescent properties have been developed. Among them, thioflavin T derived MRs [226] and novel probes produced by π-conjugation of a diakyl amino group with a 2-cyanoacrylate unit [284] have potential as new diagnostic tools for investigation of amyloid-based diseases.

Additionally, conjugates of MRs and protein ligands have been proposed to track in real-time the degradation of proteins in living cells; upon ligand binding to the target protein, molecular crowding limits the segmental motion of the MR increasing emission intensity; this intensity decreases upon protein degradation [285].

2.3.6.4 Other Applications

Small fluorescent MRs have also been used to report on the viscoelastic properties of microbubbles. The fluorophores bind to the surface of the microbubbles and their fluorescence emission and lifetime are modulated by the local free volume [286]; spatial variations of the fluorescent signal can be correlated to stability and functionality. Expanding the applications of microbubbles into ultrasound imaging and drug delivery [287] requires understanding how composition and fabrication methods affect their surface properties.

These extensive applications of MRs in biological systems provide a roadmap to extend their use to food systems. In the following section we discuss current research using MRs to investigate food properties as well as potential novel applications of these versatile probes.

2.3.7 Potential Applications of Molecular Rotors in Food Science and Engineering

The versatility of MRs offers the potential of direct optical measurement of physical properties related to food quality and stability. Based on the applications discussed above, MR probes can specifically contribute to understanding interactions between food components and the effect of microstructure on food properties, reporting on, for example, polymerization processes, protein degradation, colloidal stability, and phase states and transitions [212, 224, 250]. It should be noted, however, that the limited

solubility, price, and especially toxicity of many conventional MRs limit their application in foods. To overcome this drawback, Corradini and Ludescher [204] have proposed searching for molecular rotors among the many fluorescent molecules found in foods, in order to identify and characterize a library of GRAS probes as intrinsic luminescent sensors of food quality, safety and stability.

2.3.7.1 Micro and Bulk Viscosity of Liquid and Semi-Solid Foods and Food Models

Edible azo and aryl methane dyes, including the synthetic food colors Allura Red, Azorubine, Sunset Yellow, Tartrazine, Citrus Red, Fast Green, and Brilliant Blue, are essentially non-fluorescent in fluid solution but become fluorescent in viscous solutions [204, 205, 224]. Studies of mono-azo dyes in glycerol/water solutions at constant temperature and in glycerol as a function of temperature indicate that its fluorescence intensity follows a power law behavior (Equation 2.2) over variations in viscosity ranging from $1-10^4$ mPa s. Value of 0.35-0.45 for the viscosity sensitivity parameter (x in Equation 2.2) in these systems provides strong evidence that mono azo dyes and by implication other similar food dyes, behaves as a molecular rotor (Table 2.2).

Kashi *et al.* [224] measured the effect of increasing viscosity on the fluorescence intensity of several food dyes in aqueous model systems of identical viscosity (90 mPa s) containing either glycerol, glucose, sucrose or hydrocolloids (Figure 2.15-left). They observed that the sensitivity to bulk viscosity was somewhat lower in the methyl cellulose (MC) and much lower in the carboxymethylcellulose (CMC) solutions. The authors speculated that the lower sensitivity to viscosity was due to extensive hydration and less molecular crowding around the MR in the polymeric hydrocolloid solutions. They used pyranine as a fluorescent sensor of molecular crowding based on its ability to

report on the amount of water in its surroundings (Figure 2.15-right) [288]; this probe exhibits dual emission bands that reflect either protonated (peak ~435 nm) or unprotonated (peak ~510 nm) pyranine; the extent of deprotonation is increased by available water (by available sites for the proton). The intensity of the unprotonated pyranine band varied in a complementary manner to the effect of viscosity on the azo dye emission intensity: those solutions in which the azo dye exhibited high intensity (those containing high concentrations of glycerol, glucose or sucrose) exhibited low intensity of the unprotonated pyranine band, and thus limited hydration, while those hydrocolloid solutions with lower mono azo dye intensity exhibited high band intensity, and thus extensive hydration of the probe. Although these results explain the lack of sensitivity of azo dyes to viscosity modulate by CMC, they do not fully account for the greater effect of methyl cellulose on azo dye intensity. The authors hypothesized that differences in the sensitivity of the dye to bulk viscosity in hydrocolloid solutions may reflect the hydrodynamic size, the structure, or the intrinsic rigidity of the hydrocolloid polymer or with interactions between the probe and the polymer. The use of MRs as sensors of bulk viscosity was also reported by Akers *et al.* [289] who make use of CCVJ in aqueous colloidal solutions of dextran and hydroxyethyl starch and by Dragan *et al.* [290] who designed two novel MRs, PicoGreen and SYBR Green, and tested them in collagen solutions. These MRs effectively responded to the bulk viscosity of these solutions of macromolecules. It is important to note that molecular rotors report on the properties of solutions at the molecular level and their potential use as sensors of bulk viscosity should be verified for hydrocolloids and for specific foods on a case by case basis.
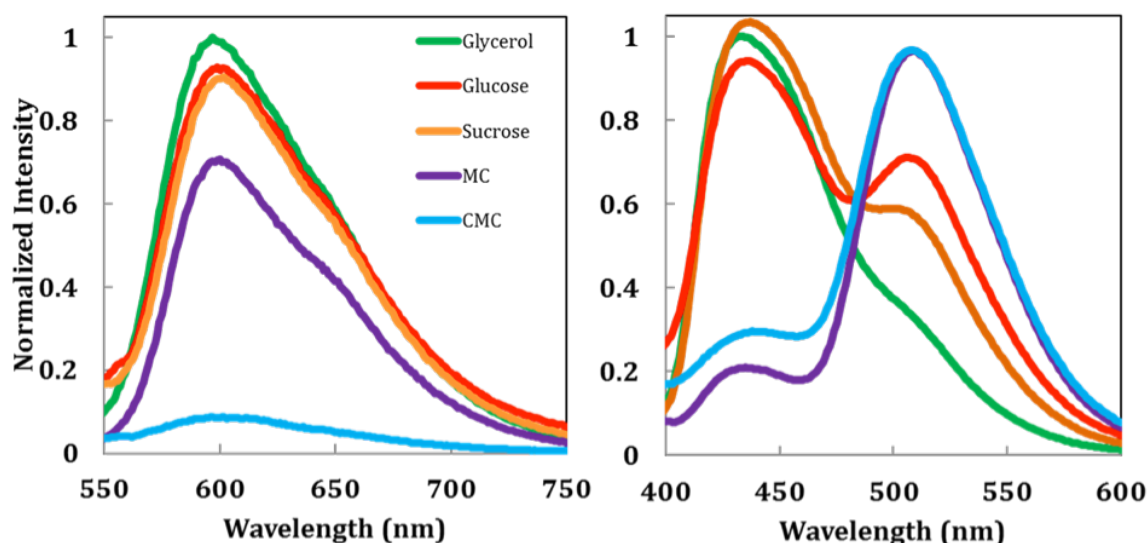
Figure 2.15: Normalized fluorescence intensity of the GRAS MR Azorubine (left) and pyranine (right) in solutions of different composition and equal viscosity (90 mPa s); MC: methyl cellulose, CMC: carboxymethyl cellulose. The two emission bands of pyranine are due to protonated (~435 nm peak) and unprotonated (~510 nm peak) probe. Reprinted with permission from Kashi, Waxman [224].

A lipophilic azo dye, Citrus Red 2, which is also approved in food applications, was used to monitor the micro-viscosity of oil confined in colloidal fat crystal networks [225]. The fluorescence intensity of the dye remained constant when the degree of oil confinement, expressed in terms of the box-counting fractal dimension of the network, was below 1.89 (Figure 2.16). Box-counting fractal dimension, which provides a measure of the microstructural characteristics of the crystalline network, is determined from analysis of microscopic images of the fat crystal network [291]. The fluorescence intensity of the MR increased dramatically above a fractal dimension of 1.98 as the degree of confinement increased, that is, as the molecular crowding increased. In these systems, the bulk viscosity, which is dominated by the formation of a solid crystalline network, does not reflect the actual viscosity of the continuous oil phase; instead the

micro-viscosity monitored by the fluorescence intensity of the embedded MR better describes the physical state of the fluid phase.
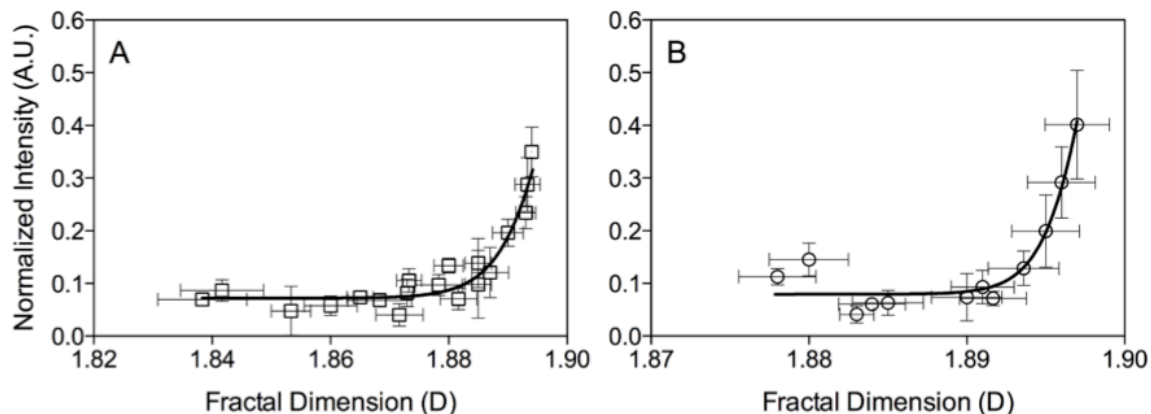
Figure 2.16: Normalized fluorescence intensity of Citrus Red as a function of the fractal dimension of the (A) medium chain and (B) unsaturated triglyceride crystalline networks. Reprinted with permission from Du, Kim [225].

These studies provide insights and experimental opportunities applicable to the food industry. They highlight the often limited correspondence between micro and bulk viscosity found in polymer (hydrocolloid) systems while supporting the potential of MRs as non-mechanical sensors of both micro and bulk viscosity. The identification of non-toxic, non-invasive, and potentially automated non-mechanical sensors of bulk viscosity can have a significant impact on in-line measurements of physical properties of foods. In addition, they also enable completely novel applications such as measurements of viscosity *in vitro* during the process of digestion in model systems or even *in vivo* in living organisms.
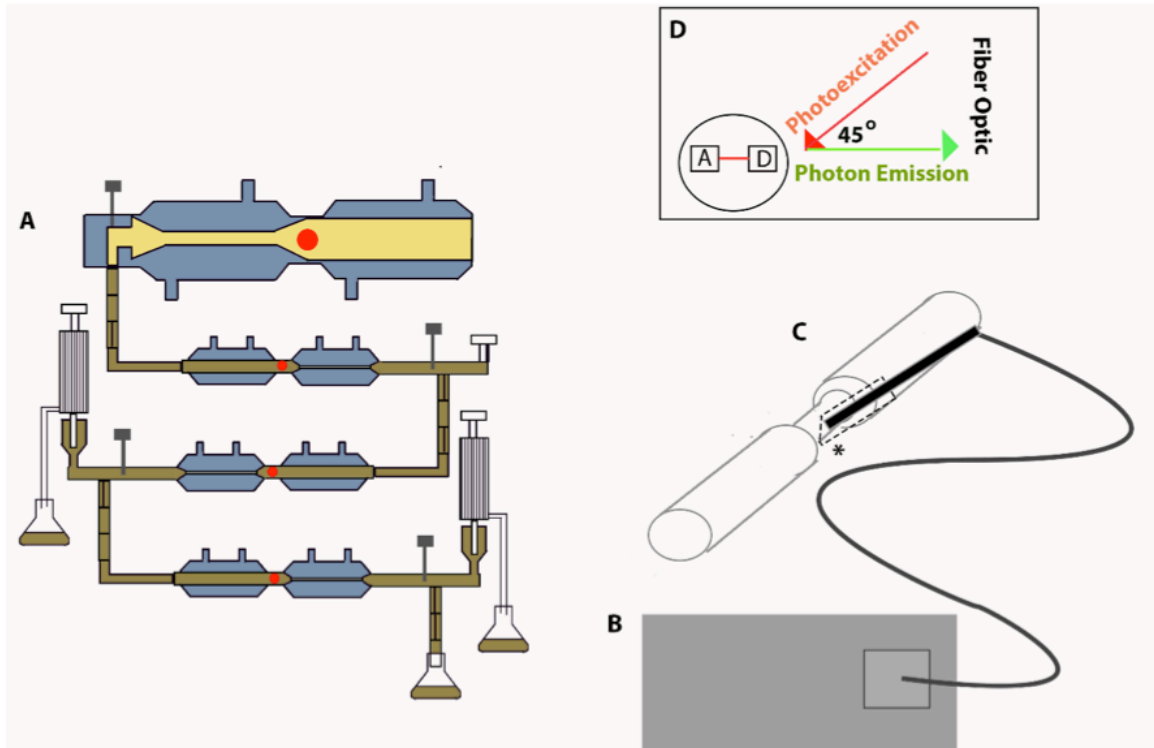
Figure 2.17: (A) Schematic diagram illustrating the coupling of a luminescence spectrometer with the TIM-1 gastrointestinal model system; red dots indicate locations at which (B) a fiber optic can be placed to obtain spectrofluorometric measurements. (C) Schematic diagram of the fiber optic accessory. Note the use of an adapter (dotted line) to allow repeatable positioning of the fiber optic accessory at (D) 45° angle to reduce light scattering.

A potential coupling of fluorescence spectroscopy with a dynamic gastrointestinal model such as the TNO intestinal model (TIM-1), an *in vitro* system that mimics the stomach and small intestinal compartments (duodenum, jejunum, and ileum) of the human gastrointestinal tract, is illustrated in Figure 2.17. This proposed method incorporates a MR probe into the gastrointestinal solutions and uses spectrophotometry with fiber optics to measure probe fluorescence intensity during *in situ* digestion. Such an application could elucidate how postprandial macronutrient digestion, chyme viscosity, and potentially satiety are affected by initial meal viscosity, among other research questions.

2.3.7.2 Colloidal Properties and Dynamics

The fluorescence intensity and lifetime increases 10-100-fold compared to fluid solution when MRs are embedded in micro-organized environments such as micelles, liposomes, or inclusion complexes (e.g., cyclodextrins) [216, 250]. Although there are no published reports on the use of MRs in food colloids, the advances made in a variety of non-food systems exemplify their potential to monitor physical properties and kinetics of formation of colloidal food systems.

Several MRs have been used to monitor the formation of colloidal structures. Thioflavin T shows a progressive increase in fluorescence intensity with increase in surfactant concentration up to the critical micelle concentration [292]; local environmental constraints associated with MR binding to surfactant micelles were deemed responsible for the increase in intensity. The lifetime of a synthetic MR, dubbed AzeNaph1, has been used to monitor the self-assembly of amphiphilic co-polymers into nanostructures; increased solvation of the nanostructures resulted in confinement of the micelle core as indicated by a significant increase in the lifetime of the embedded MR [293]. The fluorescence intensity of a GRAS probe Sunset Yellow FCF (SY; FD&C yellow #6) was used to evaluate formation of surfactant micelles [294]. Self-aggregation of SY in solution resulted in hindered rotation and an enhancement of fluorescence emission intensity; this fluorescence intensity decreased as the dye partitioned within the hydrophobic core of the micelles.

Conventional MRs, including DCVJ, CCVJ, and Thioflavin T, have proved effective in following the self-assembly of dipeptide molecular gelators. The fluorescence intensity increased with fibril formation during gelation and was also sensitive to changes

in structure after fibril assembly [295]. Miguel et al. [296] developed a MR based on the foldamer concept that was used to determine the microviscosity of an organogel formed by a urea-based organogelator and toluene. The end point of miniemulsion polymerization for an in-line process was detected using fluorescence of 1,1-dicyano-4-(4′-dimethylaminophenyl)-1,3-butadiene) [297]; although the initial polymerization steps did not affect the photophysical properties of this MR, at monomer conversions above 50%, the fluorescence intensity showed progressive increases. MRs such as merocyanine dye also have shown potential in mapping hydrophobic regions in micellar systems [298].

Protein Aggregation, Folding, and Interactions

MR binding to proteins has been shown to restrict intramolecular rotation of the probe, increasing its quantum yield, fluorescence intensity and lifetime. Further restriction of movement can be attained by conformational changes and interactions between the proteins or with other components [250]. The stability of proteins in parenteral nutrition products is enhanced by the addition of surfactants such as polysorbate 80, which prevents protein aggregation during the shelf life of the product. Identifying the susceptibility of these preparations to aggregation under different environmental conditions (especially variations in temperature) is crucial to ensure their adequacy and safety. The ability of CCVJ and DCVJ rotors to detect changes in aggregation in protein formulations that contain polysorbate was confirmed using steady-state and time-resolved fluorescence spectroscopy; thermally-induced protein aggregation resulted in increased fluorescence intensity and longer lifetimes [299]. Differential scanning fluorimetry of CCVJ was used to detect the temperature of protein aggregation in the presence of surfactants in a high throughput screening assay [300]. And Iio *et al.*

[301] used a DCVJ derivative to monitor the polymerization of G-actin into F-actin and to study F-actin filament polymorphism.

Due to the high affinity of proteins for MRs it is possible to envision numerous applications of MR-based fluorescence spectroscopy to monitor the structure, dynamics and functionality of food proteins including denaturation and gelation processes, stability to environmental perturbations, and interactions with proteins and other food components.

2.3.7.3 Phase Transitions

Given the centrality of phase transitions in modulating the physicochemical properties of ingredients, the ability of MRs to report on phase transitions can be of significant importance to the food industry. MRs formed of polydiphenylacetylenes (PDPAs) coupled with long alkyl chains were found to be sensitive to the crystallization of paraffin [302]. High rigidity of the solid state hinders intramolecular rotation and increases fluorescence intensity. Paraffins with embedded MRs were used to impregnate wax paper and develop thermo-responsive fluorescent sensor systems. ROBOD, an unconstrained boron dipyrromethene dye, was used to investigate pressure-induced changes in 1,2-dichloroethane including glass formation in the presence of an inert polymer [303]; the high viscosity of the glassy state was found to restrict twisting of the rotor and increase fluorescence emission. Progressive vapor uptake by a polymer film results in the presumptive plasticization of the polymeric matrix; the resulting decrease in matrix rigidity was detected by a decrease in the fluorescence intensity of a julolidine-derived MR dissolved in the film [304, 305]. This application of MRs can be of particular

importance in monitoring the stability and integrity of synthetic packaging and edible films either in the laboratory or even more importantly in the final packaged product.

2.3.7.4 Sensors for Flow

Another relevant application of MRs, one proposed by Haidekker and Theodorakis [231], is their use as flow sensors. Such applications provide opportunities for in-line detection of fluid flow during continuous liquid food or juice pasteurization and in sterilization and dehydration processes where predictions of flow rates and behavior are imperative for effective processing [306]. CCVJ, a julolidine based MR, was able to report on changes in flow as a function of shear stress with a dependence on viscosity and velocity [231]. Mustafic *et al.* [307] imaged the flow patterns in an ethylene glycol solution under four different flow chamber geometries using CCVJ and p-[(2-cyano-2-propanedio ester) vinyl] dimethylaniline (CPVDA) MRs. The images were obtained with LED illumination using a digital camera and were compared with the results of flow modeling using computational fluid dynamics. As anticipated by Haidekker and Theodorakis [231], Mustafic *et al.* identified flow as the driver of the fluorescence intensity increase; however, a complete understanding of the mechanism controlling the sensitivity of MRs to flow has yet to be unraveled. Nonetheless, flow rates as low as 0.1 mm/s were detected in this work, presenting new opportunities for real-time investigations of fluid flow during food processing.

2.3.8   Conclusions

This review has highlighted the ability of MRs to monitor a range of physical properties of foods including bulk and micro viscosity of hydrophilic and hydrophobic liquids and semi solids, the aggregation and colloidal properties of molecules and

macromolecules, the phase behavior and phase transitions of hydrophobic molecules, and fluid flow. These applications can involve measurements of bulk solutions on the macroscopic scale using a spectrometer or measurements on much smaller scales using a fluorescence microscope. MR-based fluorescence spectroscopy as an analytical technique in food systems presents distinct advantages: it is noninvasive, site specific, rapid, sensitive, versatile, and easy to use. The development of a library of edible MRs for use in food applications can enhance the use of this methodology in foods and facilitate the continuous monitoring of the physical properties of food products.

2.3.9   Acknowledgements

3   Research Objectives

It is of critical importance to understand the possible mechanisms which alter form and formulation of food commodities and how they influence their physico-chemical properties and consequent physiological impact. For this purpose, the **global objective** of this dissertation was:

To investigate the effect of food physico-chemical properties on macronutrient digestibility through characterizing digestion kinetics and luminal viscosity trends.

This global objective was achieved via addressing the following **sub-objectives**:

A) To compile a critical review that summarizes and discusses the main characteristics of molecular rotors (MR), their current applications in biological research, and current and potential applications as sensors of physical properties in food science and engineering.

B) To present a method that integrates TIM-1, spectrophotometry and MR technologies to report on changes in *in vitro* gastrointestinal (GI) luminal viscosity.

    i. To evaluate the suitability of the use of fast green (FG) as a molecular rotor (MR) in TIM-1 system by characterizing the influence of possible interaction between FG and the various TIM-1 solutions (bile, gastric enzymes, pH, and electrolyte solutions).

    ii. To verify the suitability of FG to characterize changes in maize starch

chyme viscosity as a function of different amylose-to-amylopectin ratios (AM:AP) by correlating between rheological viscosity and the corresponding fluorescence intensity.

    iii. To estimate the extent of maize starch gelatinization after application of the cooking method by measuring the loss in birefringence under polarized light microscopy.

    iv. To assess method aptitude to accurately reflect on changes in *in situ* luminal viscosity of maize starch samples during *in vitro* TIM-1 digestion.

C) To investigate the relationships between physico-chemical properties of oat-based meals on *in situ* luminal viscosity and digestion kinetics during *in vitro* digestion as function of form and formulation.

    i. To assess the influence of different methods used in commercial processing of oats on their physico-chemical properties and biophysics of digestion, by comparing three commercially available oat-based products: instant oats, steel cut oats, and oat bran.

    ii. To determine the contributions of milk protein concentrate (MPC) to the luminal viscosity trends and parameters of digestion kinetics of instant oat-based and steel cut oat-based meals.

D) To investigate the effect of the physico-chemical properties of human breast milk and infant formula on bioaccessibility of free fatty acids.

4 The Influence of Amylose-to-Amylopectin Ratios on *In-Vitro* Gastrointestinal Viscosity

This chapter was co-authored with Derrick Fondaco, Joe Zuccaro, Maria G. Corradini, Richard D. Ludescher**,** and Michael A. Rogers.

4.1 Abstract

The TNO Intestinal Model-1 (TIM-1) and a luminescence spectroscopic technique with molecular rotors were coupled to facilitate detection of *in situ* changes in luminal viscosity during *in vitro* gastrointestinal (GI) digestion. TIM-1 was used to simulate GI digestion of three maize starch samples that varied in their amylose-to-amylopectin ratio (AM:AP): native, high amylose (AM) and high amylopectin (AP). The fluorescence intensity (FI) of Fast Green (FG), a molecular rotor was recorded and used to monitor and record trends occurring in each of the TIM-1 gastric and small intestine compartments. FI of FG were not affected by the concentration of secretion fluids nor the pH of TIM-1 compartments, and the FI was directly proportional to the viscosity imparted by the starch. This allowed for direct measurements of digesta viscosity during the simulated digestion in situ. The fluorescence intensity measurements suggest that the initial consistency of AP > native > high AM. TIM-1 gastric FI was highest for high AM > high AP > native maize starches. Birefringence loss was lowest for high AM (~ 44%) and similar for native (~ 98%) and high AP (~99%) maize starches. We conclude the validity of the proposed method to facilitate measurement of luminal viscosity, *in vitro,* when the food matrix microviscosity is representative of bulk viscosity. Discrepancy between

micro- and bulk viscosities as well as the presence of numerous and large particulates in the digesta may contribute to increased FI, that may be inaccurately interpreted as high viscosity. Providing a method for monitoring GI digesta viscosity is critical due to its well-accepted influence on rate and extent of nutrient digestion and absorption as well as sensation of satiety.

4.2 Introduction

Digesta viscosity is an important physical characteristic with a wide range of impacts on physiological response. Increased gastric digesta viscosity (1) increases distention in the stomach cavity and contributes to increased sensation of satiety [308-311]; (2) slows down rates of gastric emptying [312]; (3) impedes motion and access of enzymes to the substrate, consequently reducing nutrient hydrolysis [70-72]; and (4) hinders diffusion of the hydrolysis by-products to the luminal brush border and renders absorption less effective [70-72]. A thorough understanding of alterations to digesta viscosity that occur during transit throughout the gastrointestinal (GI) lumen is critical for better understanding of structure-function relationships [313]. Unfortunately, insight on changes in digesta viscosity during digestion typically involves resorting to bench top rheometer equipment that requires extraction of the sample from the digestive system *(in vivo* through ileostomy and/or *in vitro*) at different digestion intervals. In addition, shear rates in the GI tract have not been analyzed due to complexity of the digestive system and variability in shear rates at different locations of the luminal cavity [314]. For example, a shear rate range of $10 - 100$ s^{-1} was proposed to represent shear along the entire GI tract previously [315]; while another research group suggests a shear rate range of 0.1-10 s^{-1} in the small intestine [316]. Other methods used to report on digesta viscosity include

gamma scintigraphy, ultrasound and echo-planar magnetic resonance imaging (EPI), but are exclusively/typically applied *in vivo* [312]. With human *in vivo* experiments being characteristically cumbersome, costly, and restricted by ethical considerations [157]; *in vitro* digestion models provide a suitable alternative if able to closely mimic human digestion and its physiological conditions [157]. There is therefore a need for a non-invasive method for reporting *in situ* luminal viscosity changes throughout GI transit. This work describes and verifies a methodology we previously proposed [317] to potentially facilitate reporting on real-time changes in luminal digesta viscosity using two integrated technologies: TNO Intestinal Model-1 (TIM-1) and luminescence spectroscopy with viscosity sensitive probes, i.e. molecular rotors (MR) (Figure 4.1). TIM-1 is an advanced artificial digestion simulation system that mimics the human stomach and small intestine. In comparison to other *in vitro* techniques, this dynamic computer-controlled system is unique in its ability to regulate pH, temperature, gastric and intestinal emptying, transit time, and GI secretions [162, 318] allowing it to closely mimic the physiological conditions occurring in the human GI tract as a function of digestion time.

Luminescent MRs are optical chromophores that may be used as intrinsic luminescent probes to assess viscosity [319]. The term "molecular rotor" refers to a molecule that consists of two (or more) segments that have the ability to rotate relative to one another (intramolecular twisting). The rate of intramolecular twisting depends on the free-volume (or molecular crowding) of surrounding environment. Photoexcitation of fluorescent MR can result in twisted intramolecular charge transfer (TICT). Deactivation from the TICT state occurs predominantly through a nonradiative pathway. Alternatively, a return to the ground state from the local excited state can occur through a radiative

decay process that results in emission of photons. Since the rate of TICT state formation is lower in more viscous environments, these two competing decay pathways determine the sensitivity of the probe to the micro-viscosity of the surrounding environment [213, 320, 321]. Consequently, any change in the medium rigidity, such as an increase in local (and bulk) viscosity [322], hinders formation of a TICT state and increases FI.
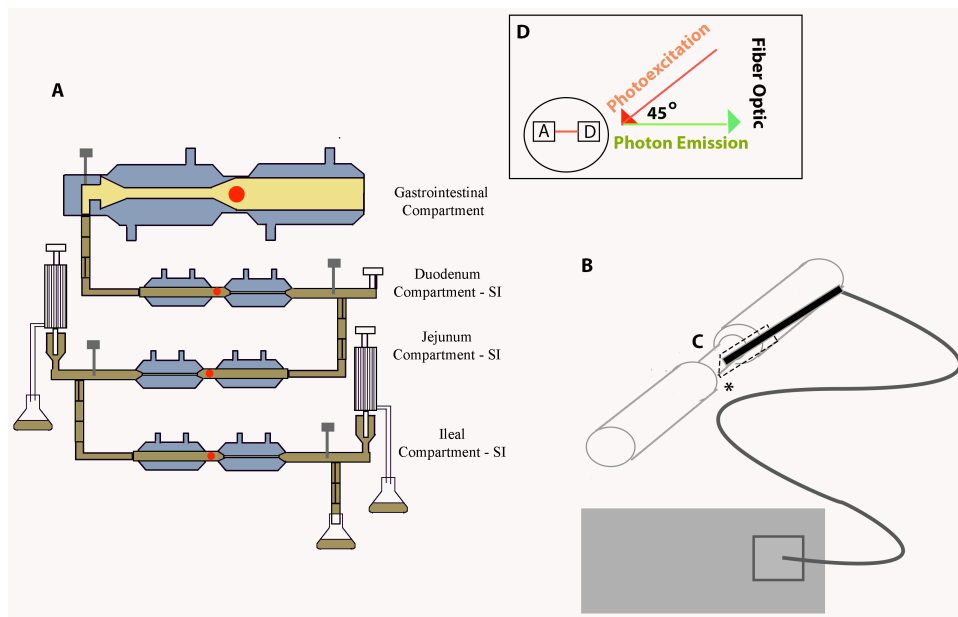
Figure 4.1: Schematic diagram illustrating the coupling of a luminescence spectrophotometer with the TIM-1 GI model system. (A) TIM-1 GI model system; red dots indicate locations at which (B) a fiber optic can be placed to obtain spectrofluorometric measurements. (C) Schematic diagram of the fiber optic accessory. Note the use of an adapter (dotted line) to allow repeatable positioning of the fiber optic accessory at (D) 45° angle to reduce light scattering. [317]

Starch viscosity is greatly influenced by the ratio of its two α-glucans constituents [323]: linear amylose (AM) and branched amylopectin (AP) [130, 324]. Amongst its numerous functional properties [325], starches form a viscous paste if heated above a certain critical temperature, the gelatinization temperature. Gelatinization involves water diffusion and uptake by the starch granule, swelling, leaching of AM [117, 118], and ultimately increased viscosity. Maize starch samples with different amylose-to-

amylopectin ratios (AM:AP), native, high AP and high AM, are digested, *in vitro*, to assess the ability of the proposed method, in which TIM-1 and MR are coupled, on accurately reporting on changes in luminal viscosity due to differences in their amylose-to-amylopectin ratio (AM:AP). Fast Green FCF (FG) is the selected MR; it is a triaryl methane dye, and is Generally Recognized as Safe (GRAS). Selection of FG was based on its: hydrophilic nature, sensitivity to local viscosity, large Stokes shift (excitation and emission wavelengths of 580 nm and 610-750 nm, respectively), and differentiation from the background (excitation at ~580 nm does not excite the other molecules that are present). Method applicability was first verified by investigating possible interactions between FG and TIM-1 solutions. Correlations between rheological viscosity and FI by FG in the gelatinized maize starch samples are then determined to investigate suitability of probe to report in changes in matrix viscosity. Gastric and small intestine FI values are recorded, at predetermined time intervals, throughout digestion in TIM-1 to provide real-time luminal viscosity trends. Method efficiency is then validated against the extent of loss in birefringence within polarized light micrographs.

4.3   Materials and Methods

4.3.1   *Influence of TIM-1 Environmental Conditions on Photophysical Response by FG and Contribution to FG peak*

4.3.1.1 Sample Preparation

4.3.1.1.1   Bile Solutions

Fresh porcine bile was collected from a slaughterhouse (Farm-to-Pharm, NJ, USA), where multiple collections of bile were pooled into a single batch, divided into

single-use quantities, and then stored at -20°C for later use. Bile was thawed on the day of the experiment and filtered using Miracloth (Merck KGaA, Darmstadt, Germany) prior to incorporation into the experimental solutions. Bile was mixed with water to generate solutions ranging from 0 to 2% concentrations at 0.2 % increments.

4.3.1.1.2 Gastric Enzymes - Lipase and Pepsin- Solutions

Gastric enzyme solutions were prepared in duplicate to contain a mixture of lipase (F-AP15, Amano Enzyme Inc., Nagoya, Japan) and pepsin (P7012, Sigma-Aldrich, MO, USA) at 1:1 ratios to make solutions of 0.1 to 0.5 mg gastric enzyme/ml at 0.1 mg/ml increments. This range was selected to incorporate and slightly exceed the physiologically relevant concentration, which are used in TIM-1 (0.2 mg lipase and 0.2 mg pepsin per ml). Samples were prepared with and without (control) 10 μM FG.

4.3.1.1.3 Small Intestinal Electrolyte Solutions (SIES)

Small intestinal electrolyte solution (SIES: 5 g/l NaCl, 0.6 g/l KCl, and 0.25 g/l $CaCl_2$) was prepared in water to make solutions ranging from 10 to 70% at 15% increments, in duplicate.

4.3.1.1.4 pH

The pH of the Fast Green solution was adjusted using NaOH and HCl solution (0.1 M), the pH of the samples was monitored using a benchtop pHmeter (Orion™ Star A211, Thermo Fisher Scientific, Waltham, MA). The dilution due to the addition of the acid or base solution was recorded and the concentration of FG was corrected, if necessary. The concentration of FG of all the samples was corroborated based on the

absorbance of the samples at 580 nm determined using a UVVis spectrophotometer (Cary 60, Agilent, Santa Clara, CA).

4.3.1.2 Measurements

All concentrations for the abovementioned solutions were prepared in glass vials as a control (without FG) and with 10 μM FG. Fluorescence spectra were collected using a Cary Eclipse spectrofluorimeter (Agilent Technologies, Santa Clara, CA) equipped with a fiber optic coupler over the range of 610 to 750 nm, with excitation at 580 nm. Excitation and emission slits were set at 5 nm and 20 nm, respectively. Background spectra were deducted from the corresponding FG-containing sample spectra. Each point was normalized using the maximum FI of the corresponding overall dataset.

4.3.2   Maize Starch Food System- Materials and Sample Preparation

Three maize starch samples (Table 4.1), which varied in AM:AP, were acquired from Ingredion (Bridgewater, NJ, USA). Fast Green FCF (FG) was purchased from Sigma-Aldrich (St. Louis, MO).

Table 4.1: The commercial name, description and AM:AP for each maize starch sample.

Commercial Name	Description	AM:AP
Melojel (Native)	Native/unmodified maize starch	~ 25-27% AM : 73-75% AP
Amioca (High AP)	High AP maize starch	~ 0 AM: 100% AP
Hylon VII (High AM)	High AM maize starch	~70% AM : 30% AP

Sample preparation was controlled to provide 15% starch in the final sample, as is characteristic of most frequently consumed starch products (e.g. mashed potatoes and pasta). 45 g of the maize starch sample was mixed with 105 g of water, 95 g gastric electrolyte solution (6.2 g/L NaCl, 2.2 g/L KCl, and 0.3 g/L calcium chloride di-hydrate),

and 40 µM FG in a glass beaker, and covered with aluminum foil. An FG concentration study (data not shown) was performed to determine the ideal FG concentration and to avoid occurrence of inner filter effect, which would be detrimental to recorded fluorescence intensity (FI). The mixture was placed in a hot water bath at 100 °C for 11 minutes. This water bath temperature was above the gelation temperature (~ 62-72 °C [326]) for both Melojel (Native) and Amioca (High AP) samples. Samples were removed after 2.5 minutes and 5.5 minutes of heating initiation, to be stirred for a 30 seconds duration and then returned to the water bath to complete the 11 minutes total heating duration. After 11 minutes, samples were removed and its contents were mixed. The mixture beaker was covered with aluminum foil and placed in a cold water bath until it reached ~ 36 - 37.5 °C, mimicking human biological temperature, and then analyzed immediately to avoid starch retrogradation.

4.3.3   *Birefringence Loss in Maize Starch Food Systems to Determine Extent of Gelatinization*

Samples were prepared as described above and the heating process was omitted in control samples. Samples for microscopy were prepared for heated and control samples using a drop of samples or a thin layer of the starch samples, which were covered with another glass slide. Birefringence of the starch samples were captured using polarized light and an imaging station (Linkham, Surrey, England) equipped with a Qimaging 2560 x 1920 pixel CCD camera (Qimaging, Surrey, BC, Canada) and a 10x Olympus lens (0.25 N.A.) (Olympus, Tokyo, Japan). Real-time viewing and image capturing was performed using Qimaging MicroPublisher 5.0 software (Qimaging, Surrey, BC, Canada) with resolution of 320 x 240 for Melojel (Native) and Amioca (High AP) and a lower

resolution of 160 x 120 for Hylon (High AM). A total of five micrographs were captured for each imaged sample and the birefringent area was quantified using ImageJ (NIH, Bethesda, Maryland). An average percent value was determined for each of the imaged samples and reported as percent birefringent area. Birefringence data allows depiction of the degree of gelatinization of the samples as a result of the heating process in the form of loss in birefringence.

4.3.4 *Influence of the Viscosity of Maize Starch Food Systems on the Photophysical Response by FG*

Rheological testing of starch samples was performed to verify the sensitivity of FG to changes in viscosity. Starch samples were prepared following the sample preparation procedure indicated in '*Sample Preparation*' section. Samples were then sequentially diluted using water that contains 40 μM FG to prepare solutions of 7, 10, 12, 15, 17, 20 % starch in water. A Discovery Hybrid Rheometer (TA Instruments, DE, USA) equipped with cone and plate 60 mm geometry was used to determine the rheological properties of the sample. The flow curve at 37 °C and 5 points per decade were recorded within a shear rate range of $0.1 - 100\ s^{-1}$. The recorded viscosity at $30\ s^{-1}$ was used for data analysis and correlations between FI and both starch concentration as well as viscosity were conducted.

4.3.5 Luminescence Spectroscopy Coupled with TIM-1 to Monitor Luminal Viscosity of Maize Starch Food Systems

4.3.5.1 TIM-1 Experimental Meal

To mimic the initial gastric conditions, 100 g of prepared starch samples were mixed with 5 g gastric secretion fluid, 95 g gastric electrolyte solution (see *TIM-1 Simulated Digestion* section for formulation) and 50 g water. The meal was fed into the TIM-1 (TNO Triskelion, Zeist, The Netherlands) gastric compartment along with 50 g water for a total experimental meal weight of 300 g.

4.3.5.2 TIM-1 Simulated Digestion

The TIM-1 digestion system (Zeist, The Netherlands) was used to mimic digestion in the adult human stomach, duodenum, jejunum, and ileum. The ileal secretion fluid consisted of small intestinal electrolyte solution (SIES; 5 g/l NaCl, 0.6 g/l KCl, and 0.25 g/l $CaCl_2$). Jejunal fluid consisted of SIES containing 10% fresh porcine bile. A 7% pancreatin solution was prepared with Pancrex V powder (Paines & Byrne, UK). Gastric secretion fluid consisted of 600 U/ml pepsin (P7012, Sigma-Aldrich, MO, USA) and 40 U/ml lipase (F-AP15, Amano Enzyme Inc., Nagoya, Japan) in a gastric electrolyte solution (4.8 g/l NaCl, 2.2 g/l KCl, 0.22 g/l $CaCl_2$, 1.0 g/l $NaHCO_3$). The pancreatin and gastric fluid solutions were placed on ice immediately after preparation. The fresh porcine bile solution (10%) was prepared with bile collected from a slaughterhouse (Farm-to-Pharm, NJ, USA), where multiple collections of bile were pooled into a single batch, divided into single-use quantities, and then stored at -20°C for later use. Bile was thawed on the day of the experiment and filtered using Miracloth (Merck KGaA, Darmstadt, Germany) prior to incorporation into the experimental solutions.

Hydrochloric acid (1 M HCl) and sodium bicarbonate (1 M NaHCO$_3$) were added to the TIM-1 system to control pH levels throughout the digestion experiments. NaHCO$_3$ was used to maintain pH values in the duodenal, jejunal, and ileal compartments at 5.9, 6.5, and 7.4, respectively. HCl was added to the gastric compartment to follow a predetermined pH pattern over time (Table 4.2). To mimic human physiological conditions, solutions were attached to the TIM-1 to facilitate continuous automated flow into the corresponding compartments. Gastric emptying also mimicked human conditions (i.e., gastric emptying half-time of 80 min).

Table 4.2: TIM-1 stomach pH decreased over time during the 1.5-hour digestion period to mimic human adult fed-state GI conditions.

Digestion Time (min)	Predetermined pH value
0	5.5
30	4.5
60	3.0
90	2.0

The TIM-1 compartments were filled with the corresponding start residues to mimic *in vivo* conditions. The duodenal start residue (60 g total) consisted of 15 g SIES, 15 g pancreatin solution (7%), 30 g fresh porcine bile, and 2 mg trypsin (Sigma, T4665-5G). Jejunal start residue (160 g total) consisted of 40 g SIES, 40 g pancreatin solution (7%), and 80 g fresh porcine bile. Ileal start residue (180 g total) consisted of 180 g SIES. After heating the system to the physiological temperature (37°C), the experimental meal (300 g; see *TIM-1 Experimental Meal* section) was immediately fed into the gastric compartment, and the digestion process is initiated. Digestion lasted for 90 minutes (1.5 hours). The jejunum and ileum compartments are each connected to filtration units (M20S-300-01P, MiniKros® filter modules, Spectrum Labs, Breda, The Netherlands) to

remove the digestate fraction. TIM-1 Experiments were performed in quadruplicate for each type of maize starch sample. See *Coupling of a Luminescence Spectrophotometer with the TIM-1 Gastrointestinal Model System to Report on Gastrointestinal Viscosity Changes* section for detailed description of real time FI measurements on TIM-1.

4.3.5.3 Coupling of a Luminescence Spectrophotometer with the TIM-1 Gastrointestinal Model System to Report on Gastrointestinal Viscosity Changes

FI is a concentration-dependent photophysical property [317]. Therefore, a constant FG concentration (throughout an individual experiment and across all experiments) is critical for accurate and reliable correlations between viscosity and FI. TIM-1 GI digestion involves continuous secretion of solutions into each of the GI compartments, which would ultimately dilute the FG concentration in the fed meal. Therefore, FG was added at a final concentration of 40 μM to all TIM-1 secretions and the fed meal to ensure a constant FG concentration throughout. Experiments were performed in quadruplicate for each sample; three of which contained the above-mentioned FG concentration. The fourth run served as a blank/control, and therefore no FG was added.

A Cary Eclipse spectrophotometer (Agilent Technologies, Santa Clara, CA) (Figure 4.1B) equipped with a fiber optic coupler (Figure 4.1C) was used to measure FI changes during TIM-1 (Figure 4.1A) digestion. The yellow and brown regions in TIM-1 (Figure 4.1A) represent the meal digesta, while the blue regions are the water jackets responsible for heating the digesta to a physiological temperature. Within each of the four TIM-1 compartments (stomach, duodenum, jejunum, and ileum) there is a single glass region that is not surrounded by the water jacket (red-dots in Figure 4.1A). The fiber

optic was placed against each of these glass regions (red-dots in Figure 4.1A) to obtain spectrofluorometric measurements. These regions provide a clear view of the sample, and facilitate excitation of FG-MR within the digesta and detection of the emitted photons. Note the use of an adapter (dotted line in Figure 4.1C) to allow repeatable positioning of the fiber optic accessory at an identical 45° angle to reduce light scattering (Figure 4.1D). The TIM-1 and fiber optic were completely covered by a blackout blind to ensure that ambient lighting did not influence the spectroscopic measurements.

The fluorescence spectra were collected over the range of 610 nm to 750 nm, with excitation at 580 nm. Excitation and emission slits were set at 10 nm and 20 nm, respectively. The photomultiplier detector voltage was set at high. Measurements were collected every 5 minutes throughout the digestion period from the four TIM-1 compartments (gastric, duodenum, jejunum, and ileum). An additional measurement at 2.5 minutes of digestion was taken for the stomach/gastric compartment for all samples, to report more precisely on the initial change in viscosity. FI from the fourth TIM-1 run for each starch sample (carried out without FG) was subtracted from the FI of runs with FG, to subtract background FI unrelated to viscosity. To compare samples, all values were normalized relative to the maximum FI for Amioca (High AP).

4.4   Results and Discussion

4.4.1   *Influence of TIM-1 Environmental Conditions on Photophysical Response by FG and Contribution to FG peak*

Preliminary testing was performed using multiple solutions that represent the TIM-1 environment (Figure 4.2). To confirm whether or not the photophysical response of FG is affected by other environmental conditions in TIM-1 besides viscosity, we

recorded FI by FG as a function of changing concentration of SIES solutions (Figure 4.2a) and changing pH value (Figure 4.2b) (within physiologically relevant gastric pH range (1.5 to 6) (Table 4.2)). One-way ANOVA ($p < 0.05$) and Tukey's Multiple Comparison tests suggest changes in both SIES concentration and pH (within the tested range) appear to have no significant influence on FI by FG. MRs have been repeatedly utilized in examinations involving detection of protein aggregation [226, 263, 285, 319] because MR and proteins readily interact. To assess the potential interaction between FG and gastric enzymes (Figure 4.2c), we recorded FI by FG as a function of changing concentration of pepsin and lipase mixture solutions (Figure 4.2d); differences in FI were insignificant. To determine if bile contributes to FI peak by FG and whether or not it can be differentiated from it, we recorded FI by FG as a function of changing bile concentration. Possible contribution of bilin chromophores of bile on FI peak was negated in Figures 4.2c and 4.2d.
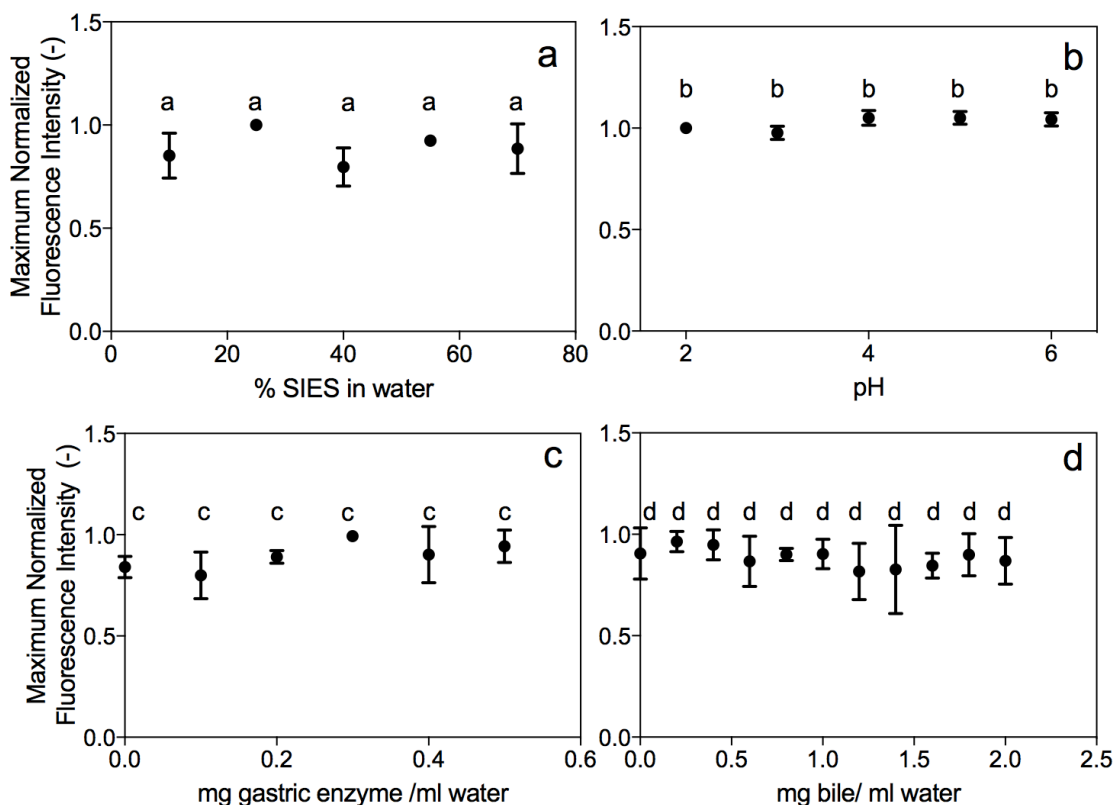
Figure 4.2: Maximum normalized FI of FG-MR as a function of changing the concentrations of SIES concentration (a), pH level (b), gastric enzyme concentration (c), and bile concentration (d). One-way ANOVA (p<0.05) with a Tukey's Multiple Comparison Test was performed for each parameter. Identical letters within each individual graph imply no significant differences (p > 0.05).

4.4.2 Birefringence Loss in Maize Starch Food Systems to Determine Extent of Gelatinization

Starch suspensions, irrespective of their concentration and AM:AP, have low viscosities at ambient temperatures. Starch granules are characterized by their radial arrangement and semi-crystallinity [43], and are therefore anisotropic in nature. This is reflected by their birefringence property [48] in the form of a Maltese cross when viewed under polarized light [48-51]. Processing/cooking of starches typically involves hydrothermal processing. If heated above a certain critical temperature, the gelatinization temperature, an order-disorder phase transition occurs [114], resulting in the formation of

a starch paste. Gelatinization involves water diffusion and uptake by the starch granule, swelling, leaching of AM [117, 118], and ultimately increased viscosity. The increased paste viscosity during gelatinization coincides with disruption of molecular organization, dissociation of the crystalline double helices, disruption of Maltese cross contour, and loss of the aforementioned birefringence [49, 114, 116]. Sample birefringence was therefore captured before (Figures 4.3a-c) and after heating to 100 °C (Figures 4.3d-f), as per the sample preparation method. The attained micrographs provide insight on the extent of gelatinization of the samples that are being fed into TIM-1. Birefringence before and after heating was compared and a birefringence loss (BL) (%) value was quantified. The point at which all birefringence (~ 95 or 98%) is lost is known as the birefringence end point temperature (BEPT) [116], and is associated with complete gelatinization of the starch granules and complete loss in crystallinity [51]. BL for Hylon (High AM) is only ~ 45% (Figure 4.3f), indicating minimal gelatinization and loss in granule crystallinity after the applied heating procedure. Product information provided by supplier indicates elevated gelatinization temperature of 154 °C to 171 °C for Hylon. It may be deduced that the temperature used in sample preparation (100 °C) does not suffice for ideal/complete Hylon (High AM) gelatinization, in agreement with BL data (Figure 4.3f). High amylose maize starches are characterized by a phospholipid composition [327]. Lipids intertwine with linear amylose chains, forming an AM-lipid complex. Although lipids make up a very small fraction (0.15 to 0.55%) of the AM-lipid complexes [130, 328] they can significantly decrease granular swelling and leaching of AM and delay gelatinization temperature [327, 328]. Implications of partial gelatinization of Hylon include diffusion of the water-soluble FG into the intact or partially intact semi-

crystalline granules in which starch-starch associations remain dominant. The increased density in the granule amorphous regions may hinder FG rotation and translate into increased FI emission. BL value for both Melojel (Native) and Amioca (High AP) (Figures 4.3d and 4.3e) exceed the BEPT criteria, suggesting that the majority of the starch granules are gelatinized. Recorded gelatinization temperatures for waxy (High AP) and native maize starches range from (~ 69.5 °C to ~ 82 °C) [142, 327], attribute to their insignificant composition of phosphorus and lipids and thus lack of formation of complexes with lipids, as agreed upon by numerous authors [148, 327, 329]. In consequence, granular damage is expected, accompanied with leaching of amylose, and consequent formation of a three-dimensional polysaccharide network in which the newly exposed hydroxyl groups of the starch polymers form Hydrogen bonds with the surrounding water molecules. In this case, minimal restrictions of FG due to granular confinement are expected. Therefore, the applied heating method exceeds the required critical temperature and ensures sufficient starch gelatinization in these samples.
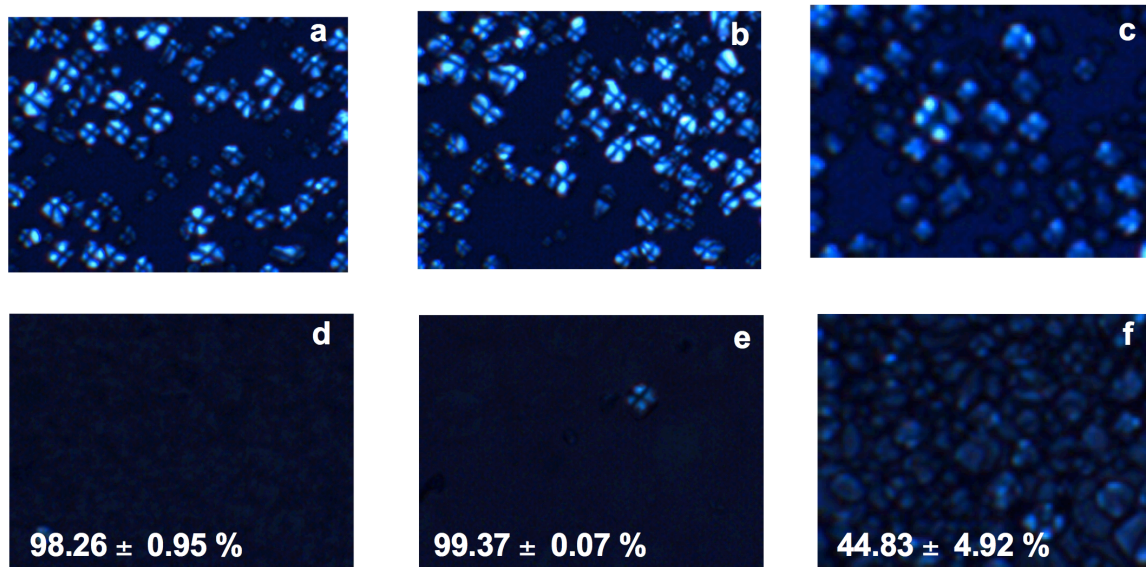
Figure 4.3: Polarized light micrographs of Melojel (Native) (a,d), Amioca (High AP) (b,e), and Hylon (High AM) (c,f), prior to heating (top row) and after heating (bottom row). The numbers presented in d-f represent BL (%) after heating.

4.4.3 Method Verification – Viscosity of Maize Starch Food Systems

To confirm suitability of FG to characterize chyme viscosity of the starch matrix, starch pastes were prepared for each of the samples and sequentially diluted to mimic the viscosity changes (dilution) that would occur during digestion. FI and rheological viscosity (data not shown) measurements of each dilution were measured independently. The recorded maximum FI was correlated with the corresponding maximum rheological viscosity (Figure 4.4), yielding a strong relationship (R^2 = 0.994 - 0.999). Strangely, Hylon (High AM) (Figure 4.4c), with the highest FI, appears to have the lowest rheological viscosity (0 to ~ 90 mPa s). Conversely, Amioca (High AP) and Melojel (Native), with lower FI, yield relatively much higher rheological viscosities (0 to ~ 15,000 and 30,000 mPa s, respectively). This observation will be revisited in the remainder of the discussion for a possible explanation (see *Effect of Starch AM: AP ratio on TIM-1 Luminal Viscosity)*. The plots in Figure 4.4 can assist in quantifying FG

sensitivity to changes in viscosity in the tested starch pastes when fitted using the Förster and Hoffman equation [330] (Eq. 4.1),

$$I(\upsilon) = \alpha \bullet \upsilon^{\chi} \qquad\qquad (4.1)$$

where, $I(\upsilon)$ is the FI, α is proportional to the 'brightness' of the probe , υ is viscosity, and x is a viscosity sensitivity parameter. The viscosity sensitivity parameter 'x' is affected by both the solvent as well as the MR. Parameter 'x' will therefore vary in different matrices as a function of: the interaction between the solvent and MR at the molecular-level, the quantum yield of the system and its bulk viscosity [330]. The values of parameters 'x' as well as 'α' for FG in the tested maize starch matrices are shown in Table 4.3, and are similar to the values reported for effective and commonly used MRs in equivalent media (e.g.: 0.53 for DCVJ, [330] and 0.38 for Azorubine (an Azo Dye) [235]). Table 4.3 suggests similar sensitivity of the FG probe to changes in viscosity in all the tested maize starch matrices. Accordingly, FG is a suitable and sensitive probe to report on viscosity changes in the tested starch food matrix. However, there is a vivid variation in the brightness parameter 'α' (Table 4.3), with the Hylon maize starch sample having a much higher brightness value as compared to both Melojel and Amioca. This suggests a much higher signal from the Hylon sample, and that the intact or partially intact semi-crystalline nature of the granules will influence the measurements (the increased density in the granule amorphous regions would hinder FG rotation and translate into increased FI emission). These assumptions are supported by, and explain, the Hylon sample having the highest FI and lowest rheological viscosity (Figure 4.4c). Additionally, the relationships between FI and apparent viscosity reported in Table 4.3 can assist in obtaining the apparent viscosity from the in line FI measurements (in TIM-1)

(Figure 4.6). It is important to note that MR report on the properties of solutions at the molecular level and their potential use as sensors of bulk viscosity is limited to specific matrices/systems in which the micro- and macro- viscosities are identical [317]. As such, the FI and viscosity are used interchangeably hereafter.
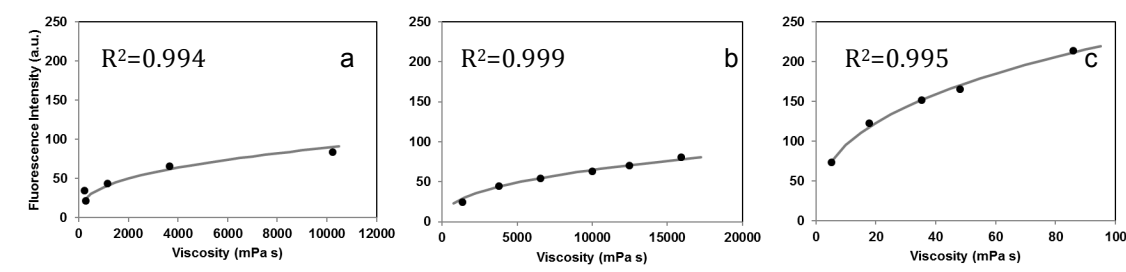
Figure 4.4: Maximum FI as a function of apparent viscosity (mPa s) for various dilutions of heated starch samples, a) Melojel (Native), b) Amioca (High AP), c) Hylon (High AM), after subtracting background FI.

Table 4.3: Parameters of the Förster and Hoffman equation obtained for the FI vs. apparent viscosity relationships of each starch (shown in Figure 4.4)

Starch	Brightness, α	Sensitivity value, x
Melojel (Native)	3.18	0.36
Amioca (High AP)	1.61	0.40
Hylon (High AM)	40.3	0.37

4.4.4   Effect of Starch AM: AP ratio on TIM-1 Luminal Viscosity

FG and TIM-1 are used as per the method illustrated in Figure 4.1 to record real-time FI during *in vitro* digestion, at pre-determined time intervals. The method aims to permit recording real-time changes during *in vitro* GI digestion for different AM:AP in heated maize starch. The three maize starch pastes were each individually digested in TIM-1, and recorded FI were corrected by subtracting the FI of the blank (Figure 4.5). Additionally, the relationships between FI and apparent viscosity reported in Table 4.3 were used to obtain the apparent viscosity from the fluorescence intensity measurements

(Figure 4.6). The changes in maximum FI and apparent viscosity as a function of digestion time point were characterized using an exponential equation (Eq. 4.2):

$$I(t) \, or \, \mu_{app} = IY_{res} + Y_{max} e^{-kt} \qquad (4.2)$$

where Y_{res} is the residual observed FI or apparent viscosity of the sample, Y_{max} is the maximum intensity or apparent viscosity observed and k is the rate of change in FI or apparent viscosity. Fitted parameters from Eq. 4.2 for the apparent viscosity changes are presented in Table 4.4.
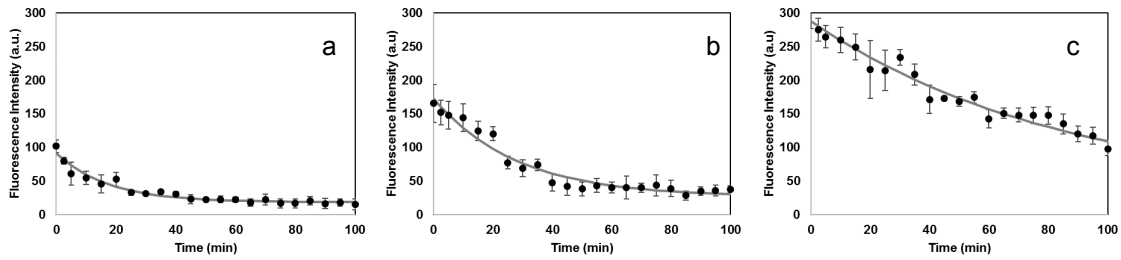
Figure 4.5: Fluorescence intensity recorded at TIM-1 gastric compartment for a) Melojel (Native), b) Amioca (High AP), c) Hylon (High AM) as a function of digestion time.
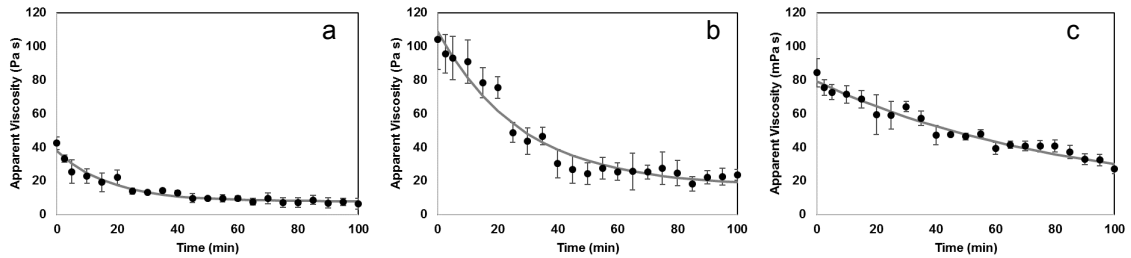
Figure 4.6: Apparent viscosity at TIM-1 gastric compartment for a) Melojel (Native), b) Amioca (High AP), c) Hylon (High AM) as a function of digestion time. Notice that the apparent viscosity for Hylon is reported in mPa s instead of Pa s.

Table 4.4: Parameters of Eq. 4.2 used to fit apparent viscosity values as a function of time for the three starch samples.

Parameters	Melojel (Native)	Amioca (High AP)	Hylon (High AM)
Residual FI 'Yres' (Pa s)	7.7	16.6	0.04
Max FI 'Ymax' (Pa s)	30	92	0.04
Rate of Change 'k' (min⁻¹)	0.06	0.036	0.08

Waxy maize starches (High AP) have higher maximum viscosity in comparison to native and High AM maize starch [142, 327]. AP is the principal starch molecule responsible for increased starch paste viscosity [331, 332]. The larger molecular weight and extensive branching of AP facilitates a greater water retention capacity, as well as rate and extent of granule swelling; which are reflected by comparatively higher peak viscosity [148, 333, 334]. The almost complete BL (Figures 4.3d and 4.3e) implies largely swollen, ruptured granules and leaching of AM content into inter-granular space [335, 336]. AM leaching is considered a pre-requisite for rapid granule swelling, solubility, and formation of a three-dimensional network that increases the starch paste viscosity [329, 335]. The water-soluble nature of FG insinuates its dispersion throughout the newly generated viscous paste. Consequently, FG segmental rotation is restricted to a level that is proportional to the micro- viscosity, and is reflected in a proportionally increased FI. Accordingly, we deduce that the measured FI provide a reasonable approximation of the Melojel (Native) and Amioca (High AP) digesta bulk viscosity during *in vitro* TIM-1 digestion. The apparent viscosity estimations provide additional evidence to this statement. It should be noted that the samples that have undergone rheological testing are similar though not identical to the samples in the gastric compartment. Therefore, differences between fluorescence intensity and apparent viscosity might be attributed to sample composition. The slope of viscosity decay (k) of Amioca (High AP) is smaller than Melojel (Native) (Table 4.4), in other words, higher digesta viscosity is retained for a longer period of time during digestion. Starch hydrolysis/digestion occurs in the small intestine via pancreatic α-amylase enzyme [54,

56, 57] and therefore plays no role in the observed reduction in gastric chyme viscosity [18, 53]. Increased water retention capacity, larger molecular weight, extensive branching, and large number of exposed hydroxyl groups after gelatinization, increased level of ruptured granules may play a role in the observed parameters. The rapid drop in viscosity observed for Melojel (Native) and Amioca (High AP) is accountable to the increased intragastric dilution in response to increased gastric meal viscosity within *in vivo* systems; however, such a phenomenon is not applicable to the pre-determined gastric secretion rates characteristics of TIM-1 *in vitro* system [165]. A limited number of scientific works exist on starch gastric viscosity, and therefore, no relevant previous reportings on maize starch luminal viscosity are available for comparison, as per our knowledge. Other factors affect starch paste behavior [142]: AP and/or AM molecular weight, degree of branching of AP [142], phosphorus and lipid content, and size of granules [334], degree of perfection of the crystalline structure and starch polymorphism [148, 334], starch granule size[337], granule architecture and purity [334].

Increased AM content is associated with a delayed onset of swelling and gelatinization [145, 146], and decreased peak viscosity [147, 148]. The linear AM chains are prone to intertwining with long branches of AP molecules as well as phospholipids, thus physically restricting starch granule swelling and expansion [148, 327]. As a result, the granule is physically of sturdier integrity [338] and has a much elevated gelatinization temperature of 154 °C to 171 °C, as per supplier. It may be deduced that the temperature used in sample preparation (100 °C) does not suffice for ideal/complete Hylon (High AM) gelatinization, in agreement with BL data (Figure 4.3f). In contradiction, the experimental gastric FI for Hylon (High AM) (Figure 4.5c) suggests Hylon (High AM)

yields the highest gastric viscosity. The discrepancy between experimental FI and BL may be a plausible artifact of the photon emission mechanism by MR. This may be explained by the explicit sensitivity of MR to steric hindrance by molecular crowding in its direct microenvironment, rather than the macro-environment of the matrix. Starch pastes typically retain intact granules, partially swollen granules, and granule fragments [339] at an extent that is dependent on the degree of their gelatinization. Limited loss in birefringence (BL ~45%) in the heated Hylon (High AM) meals suggests retention of intact or partially swollen starch granules. Such a finding may lead to several hypotheses that may contribute to high FI values that are not representative of the actual digesta viscosity:

A) The water-soluble nature of FG allows it to diffuse into the intact starch granules. The particulate density within the granule may hinder FG rotation and translate into increased FI emission;

B) The fiber optic is placed at the central glass region of the gastric compartment (Figure 4.1A, red dot) for FI measurement collection. This region tends to be concentrated with particulates, especially during contraction of the water jackets, due to its constrained nature. Accordingly, intact and partially swollen granules tend to be present in this region at a greater concentration than the remainder of the compartment, which results in increased FI detection by the fiber optic.

The values of apparent viscosity obtained using the rheological measurements, provide a more appropriate interpretation of the FI data for Hylon (High AM) . We therefore deduce that FG in combination with TIM-1 is not suitable for measuring the

viscosity of Hylon (High AM) samples or for comparing samples with different degree of gelatinization. The (1) discrepancy between micro- and bulk viscosities and the (2) particulate nature of the paste that causes whole or partial starch granules to accumulate at the point of measurement collection results in FI data that is not representative of the actual matrix viscosity

4.5 Conclusions

A newly developed method is presented herein to facilitate recording real-time luminal viscosity in an *in-vitro* digestion system via the use of three integrated technologies: TNO Intestinal Model-1 (TIM-1) and luminescence spectrophotometry with viscosity sensitive probes (MR). FG is capable of reporting real-time changes in luminal viscosity, *in vitro,* in systems where microviscosity is representative of bulk viscosity. Method limitations: The proposed method is not suitable for systems where microviscosity is not representative of overall matrix viscosity. The resultant emitted FI may be inaccurately interpreted to correspond to elevated total viscosity by an untrained analyzer.

This method provides opportunities for better understanding of digesta viscosity trends and consequent interpretation of structure-function relationships [313]. Meal viscosity has been correlated with a greater sensation of satiety, and reduced hunger and appetite [312, 340]. Correlations between rate and extent of nutrient hydrolysis and luminal viscosity are well accepted [16-18]. The importance of such possible correlations is especially critical in light of the global obesity and diabetes pandemic [14, 19, 20], thus creating an urgent need for dietary intervention and provision of functional foods that improve health. The applicability of the proposed method was tested in three maize

starches: Melojel (Native), Amioca (High AP), and Hylon (High AM). The effect of AM:AP and extent of gelatinization on GI viscosity was observed. AM:AP of starch governs the final functionality and physiological response of individual starches. For example, waxy (high AP) starches are typically utilized as thickener, stabilizers and emulsifiers [41], while high AM starches are used as film coatings for various foods. These physical modifications have physiological impacts that determine postprandial glycaemia and level of resistant starch of the food matrix [139]. Exploitation of such properties may contribute to opportunities for dietary mediation of chronic diseases by foods with pre-determined and targeted health benefits [313].

5 *In vitro* Measurements of Luminal Viscosity and Glucose/Maltose Bioaccessibility for Oat Bran, Instant Oats, and Steel Cut Oats

5.1 Abstract

Three commercially available oat products—instant oats, steel cut oats, and oat bran—were studied using the TNO Intestinal Model-1 (TIM-1) coupled with fluorescence spectroscopy and molecular rotors to evaluate carbohydrate digestion and *in vitro* gastric viscosity as a function of time. A proportional relationship between total bioaccessible sugars and the concentration of available carbohydrates was observed for the different oat-based foods. The rate of starch digestion was greatest for instant oats and lowest for steel cut oats. β-glucan, starch, and total carbohydrate concentrations were proportional to the initial gastric viscosity. Overall, gastric viscosity differed considerably between samples. Instant oat and oat bran viscosities were highest at the onset of digestion and decreased with time, whereas the viscosity of steel cut oats at the onset of digestion was the lowest viscosity observed, increasing with time. These findings suggest

that modification of food form and formulation during processing alters sugar bioaccessibility and luminal viscosity.

5.2 Introduction

Oats attenuate the postprandial glycemic response [37, 108, 341-344] because they contain the soluble fiber $(1\rightarrow3)(1\rightarrow4)$ β-D-glucan [80-82]. This attenuation is attributed to an increase in luminal viscosity [345, 346]. However, variability in the attenuation of the postprandial glycemic response exists because oats are commercially available in several forms, ranging from raw grain to ready-to-eat cereals and cooked oat porridge [2]. Processing of the whole oats changes the physical/structural [347] and chemical characteristics. Many researchers have demonstrated that commercial processing methods modify β-glucan quality (e.g., solubility and molecular weight) [3-5], β-glucan quantity [6], and starch integrity (e.g., gelatinization) [7-10]. A recent systematic review by Tosh and Chu [2] shows a wide range of glycemic indices, ranging between 40 and 88, for differently processed whole oat grains. Nonetheless, the mechanisms underlying the variability in physiological response for commercially available oat products are not yet well understood.

The thickening ability of soluble fiber and the associated decrease in postprandial glucose response is attributed to the ability of oats to bind water and form a water-entrapping non-starch polysaccharide network in the gastrointestinal tract (GIT) [11, 12]. The physicochemical properties of β-glucan also play a crucial role in blood glucose attenuation [348], and research suggests that factors other than increased luminal viscosity play a role in postprandial glucose levels after the consumption of fiber-containing meals [349, 350]. A relationship between the viscosity of the ingested meal

and satiety is now fairly well accepted [308-311], due to resultant increased distention in the stomach cavity with increasing chyme volume. It is of critical importance to understand the mechanisms that correlate physical alterations in oat form to physicochemical properties and physiological impact. For this purpose, oat digestion kinetics and luminal viscosity changes must be determined for different oat-based products.

Few published studies have described luminal fluid viscosity during GIT transit for different oat products. Most of the available studies used static *in vitro* digestion methods, which do not account for the complexity of digestion. Optical chromophores, such as synthetic colors, exhibit molecular rotor behavior and can be used as intrinsic luminescent probes to assess viscosity[319]. The term "molecular rotor" refers to molecules consisting of two or more segments that easily rotate relative to each other [33]. Photoexcitation of fluorescent molecular rotors can result in twisted intramolecular charge transfer (TICT). Deactivation from the TICT state occurs predominantly through a nonradiative pathway. Alternatively, a return to the ground state from the local excited state can occur through a radiative decay process that results in emission of photons. Since the rate of TICT state formation is lower in more viscous environments, these two competing decay pathways determine the sensitivity of the probe to the micro-viscosity of the surrounding environment [213, 320, 321]. Consequently, any change in the medium rigidity, such as an increase in local (and bulk) viscosity [322], hinders formation of a TICT state and increases fluorescence emission intensity. This work involves the first application of molecular rotors paired with a simulated digestion TNO Intestinal Model-1 (TIM-1) to assess 'real-time' luminal viscosity throughout the

simulated gastric environment. The TIM-1 is an advanced artificial digestive system that mimics the human stomach and small intestine. In comparison to other *in vitro* techniques, this dynamic computer-controlled system is unique in its ability to regulate pH, temperature, gastric and intestinal emptying, transit time, and gastrointestinal secretions [318].

In the present work we investigated the physicochemical properties of three different commercially available oat-based products: instant oats, steel cut oats, and oat bran. The TIM-1 system was used to evaluate starch digestion. Coupled with fluorescence spectroscopy and optical chromophores, the TIM-1 system shows changes in luminal viscosity *in vitro*. Total sugar release profiles were described for each of the tested oat-based meals, and a shifted logistic model was used to estimate the rate of sugar release as a function of time. Fluorescence measurements suggest distinctly different trends in viscosity within the gastric compartment for the tested samples.

5.3 Methods

5.3.1 Materials and Sample Preparation

The three tested oat products (instant oats, steel cut oats and oat bran) were supplied by Quaker Oats (PepsiCo, Inc., IL, USA). The composition of the tested oat products are presented in Table 5.1, as per values provided by supplier. Supplier attained the presented values as per the following method: each oat product was pooled from numerous production batches; official reference methods were used to determine percentages of moisture, ash, protein, fat, soluble and insoluble (AOAC 991.43) dietary fiber in the samples; these values were deducted from total weight to estimate the total

carbohydrates (%); AOAC methods 995.16 and 996.11 were used to quantify β-glucan

and starch composition.

Table 5.1: Composition of the tested oat products.

Oat Type	Soluble Fiber (%)	β-glucan (%)	Insoluble Fiber (%)	Starch (%)	Total Carbohydrates (%)
Instant	4.5	3.97	5.2	54.0	62.8
Steel Cut	4.2	3.45	5.1	54.7	64.4
Oat Bran	6.6	6.28	8.1	44.0	55.7

* All results are presented on as-is/wet-basis. The 2 × %RSD (i.e. at 95% confidence interval) for these tests are 12% (soluble fiber and insoluble fiber), 6% (β-glucan), 4% (starch), and 12 % (total carbohydrate).
* Values and standard deviations have been provided by supplier.

Table 5.2: Meal preparation: mixture composition, heating duration, cooling duration, and heating unit.

Oat Type	Oats (g)	Water (g)	Heating Duration	Cooling Duration	Heating Unit
Instant	45	190	65 sec	2 min	Microwave
Oat Bran	45	230	50 sec & 40 sec*	2 min	Microwave
Steel Cut	45	335	25 min **	2 min	Stove top

* Oats were stirred between the two heating periods.
** Oats was stirred occasionally during cooking.

Sample preparation was designed to use a typical serving size (45 g) of each oat

product and the water was adjusted according to the preparation instructions of the

commercial product that was then prepared immediately prior to analysis (Table 5.2).

Instant oats and oat bran were mixed with water in a 1-quart Pyrex cup and heated in a

microwave oven (NN-SD987SA, 1250 watts, Panasonic Corp., Osaka, Japan) on high

power for the time indicated in Table 5.2. The oat bran was heated in two stages and

stirred between the two heating periods for more uniform cooking. To prepare the steel

cut oats, water was brought to a boil in a medium saucepan on an oven-stove top at high

heat, and the oats were stirred into the boiling water. The heat was then reduced to a

simmer, and the oats were cooked on low heat with occasional stirring. All cooked

samples were well-mixed and cooled for 2 min before preparation of the experimental meal (see *Experimental Meals* section).

5.3.2 Experimental Meals

The prepared oat-based meals were masticated immediately after cooling to avoid starch retrogradation. Mastication was performed by a single volunteer using a chew-and-spit method (10 chews) to provide salivary α-amylase and reduce particle size. To mimic initial gastric conditions, the chewed sample (100 g) was immediately mixed with 5 g gastric secretion fluid, 95 g gastric electrolyte solution, and 50 g water. The sample was then promptly fed into the TIM-1 gastric compartment, followed by a 50 g water rinse for a total experimental meal weight of 300 g, which is the upper limit of TIM-1 capacity.

The total available carbohydrates, starch, and β-glucan percentages of each prepared oat product were compared to evaluate their possible impact on the measured parameters (Table 5.3). These values were estimated based on (1) total carbohydrates (%) available in each type of oat (Table 5.1); (2) total amount of oats used during sample preparation (Table 5.2); (3) total amount of water lost during sample preparation (post-cooking weight deducted from pre-cooking meal weight); (4) amount of cooked sample that was chewed and fed into TIM-1 (100 g); and (5) cleavage of glycosidic linkages of starch to yield glucose or maltose (a 10/9 conversion factor was used) [351].

Table 5.3: Estimated total available carbohydrates, β-glucan, and starch of each oat product fed to the TIM-1.

Oat Type	Total Carbohydrates (%)	β-glucan (%)	Starch (%)
Instant	13.21 ± 1.6	0.84 ± 0.05	12.62 ± 0.05
Steel Cut	14.00 ± 1.7	0.75 ± 0.05	13.21 ± 0.05
Oat Bran	11.53 ± 1.4	1.30 ± 0.08	10.12 ± 0.04

* Standard deviations have been calculated as per deviations in composition, shown in Table 5.1.

5.3.3 Molecular Weight of β-glucan

Instant oat- and steel cut oat- based meals were prepared as per cooking methods mentioned above. Samples were then freeze-dried (LABCONCO FreeZone 2.5) and then ground to < 500 μm particle size. 1% (weight/volume) β-glucan samples underwent in vitro digestion by being placed in 25 ml of pH 6.9 buffer containing 75 units of α-amylase (Megazyme E-BLAAM100) and 7.5 units of protease (Megazyme E-BSPRT100) for duration of 2 hours at controlled temperature of 37°C. Following, digesta was filtered through 0.45 μm pore size nylon filter (Whatman^{TM}, GE Healthcare Life Sciences). Size exclusion chromatography post column derivatization fluorescence & refractive index detection (SEC-PCD-FL-RI, 1200 Infinity series, Aligent) was used to analyze peak molecular weight of the samples. Two columns (Column 1: Shodex OH pak, SB-G, 10 μm, 8.0 mm ID X 300 mm L P/N F6429106, Column 2: Waters Ultrahydrogel Linear, 10 μm, 7.8 ID, 300 mm L, P/N WAT011545) coupled in tandem after a guard column (Shodex OH pak, SB-G, 10 μm, 6.0 mm ID W X 50 mm L P/N F6709430) were used for β-glucan chromatographic separation with column temperature at 40 °C. Fluorescence detector was set up at Ex 390 nm, Em 435 nm and RI detector was set-up at 35 °C. Agilent Chemstation (Agilent) was used to collect and process the data.

5.3.4 TIM-1 Simulated Digestion

The TIM-1 digestion system (Zeist, The Netherlands) was used to mimic digestion in the adult human stomach, duodenum, jejunum, and ileum. The ileal secretion fluid consisted of small intestinal electrolyte solution (SIES; 5 g/l NaCl, 0.6 g/l KCl, and 0.25 g/l CaCl$_2$). Jejunal fluid consisted of SIES containing 10% fresh porcine bile. A 7%

pancreatin solution was prepared with Pancrex V powder (α-amylase activity= 25,000 units/g, lipase activity = 25,000 units/g, and protease activity= 1,400 units/g), which was obtained from Paines & Byrne, UK. Gastric secretion fluid consisted of 600 U/ml pepsin (P7012, Sigma-Aldrich, MO, USA) and 40 U/ml lipase (F-AP15, Amano Enzyme Inc., Nagoya, Japan) in a gastric electrolyte solution (4.8 g/l NaCl, 2.2 g/l KCl, 0.22 g/l $CaCl_2$, 1.0 g/l $NaHCO_3$). The pancreatin and gastric fluid solutions were placed on ice immediately after preparation. The fresh porcine bile solution (10%) was prepared with bile collected from a slaughterhouse (Farm-to-Pharm, NJ, USA), where multiple collections of bile were pooled into a single batch, divided into single-use quantities, and then stored at -20°C for later use. Bile was thawed on the day of the experiment and filtered using Miracloth (Merck KGaA, Darmstadt, Germany) prior to incorporation into the experimental solutions. Hydrochloric acid (1 M HCl) and sodium bicarbonate (1 M $NaHCO_3$) were added to the TIM-1 system to control pH levels throughout the digestion experiments. $NaHCO_3$ was used to maintain pH values in the duodenal, jejunal, and ileal compartments at 5.9, 6.5, and 7.4, respectively. HCl was added to the gastric compartment to follow a predetermined pH pattern over time (Table 5.4). To mimic human physiological conditions, solutions were attached to the TIM-1 to facilitate continuous automated flow into the corresponding compartments. Gastric emptying also mimicked human conditions (i.e., gastric emptying half-time of 80 min).

The TIM-1 compartments were filled with the corresponding start residues to mimic *in vivo* conditions. The duodenal start residue (60 g total) consisted of 15 g SIES, 15 g pancreatin solution (7%), 30 g fresh porcine bile, and 2 mg trypsin (Sigma, T4665-5G). Jejunal start residue (160 g total) consisted of 40 g SIES, 40 g pancreatin solution

Table 5.4: TIM-1 stomach pH decreased over time during the 7-hour digestion period to mimic human adult fed-state gastrointestinal conditions.

Digestion Time (min)	Predetermined pH value
0	5.5
30	4.5
60	3.0
120	2.0
210	1.7
360	1.7
420	1.7

(7%), and 80 g fresh porcine bile. Ileal start residue (180 g total) consisted of 180 g SIES. After heating the system to the physiological temperature (37°C), the experimental meal (300 g; see *Experimental Meal* section) was immediately fed into the gastric compartment, and the digestion process is initiated. Digestion lasted for 7 hours to simulate average fed-state physiological conditions of an adult after ingestion of an oat-based meal. The jejunum and ileum compartments are each connected to filtration units (M20S-300-01P, MiniKros® filter modules, Spectrum Labs, Breda, The Netherlands) to remove the digestate fraction. During the experiment, samples were obtained from the duodenum and jejunum filtrates and ileum efflux at 30-min intervals to measure sugar bioaccessibility. These samples were collected in a vial immersed in ice and transferred to the high-performance liquid chromatography (HPLC) system for analysis the same day. Experiments were performed in triplicate for each oat-based meal. The viscosity-sensitive luminescent probe Fast Green FCF (FG; Sigma-Aldrich, ON, USA) (see *Luminescence Spectroscopy coupled with TIM-1* section for details) was added to each of the sample solutions, rinses, and secretion solutions (final concentration 40 μM). A fourth run, in which FG was not added to the solutions, served as a control for luminescence measurements (see *Luminescence Spectroscopy coupled with TIM-1* section for details).

5.3.5 Luminescence Spectroscopy Coupled with TIM-1

The TIM-1 system was coupled with a Cary Eclipse spectrofluorimeter (Agilent Technologies, Santa Clara, CA) equipped with a fiber optic coupler to measure *in situ* fluorescence emission. The TIM-1 and fiber optic probe were placed under a blackout blind to ensure that ambient lighting did not influence the spectroscopic measurements. The fiber optic was placed against the glass surface at a 45° angle, using an adaptor, to reduce backscatter from the glass surface. Based on the results of preliminary studies, FG was selected as a probe because the emission spectra were not affected by naturally occurring fluorophores in the meal or secretion fluids. FG was added at a final concentration of 40 μM to all TIM-1 secretions and the meal being fed into the TIM-1 to ensure a constant concentration of the probe throughout the 7-hour TIM-1 trials, allowing for a more simplified data analysis where no dilution of FG occurs. The fluorescence spectra were collected over the range of 610 to 750 nm, with excitation at 580 nm. Excitation and emission slits were set at 5 nm and 20 nm, respectively. The photomultiplier detector voltage was set at high. Measurements were taken every 10 min during the first 60 min, every 15 min from 60 to 180 min, and then every 30 min from 180 to 420 min. To compare samples, all values were normalized relative to the maximum fluorescence intensity for instant oats. Fluorescence from the fourth TIM-1 run for each oat-based meal (carried out without FG) was subtracted from the fluorescence of runs with FG, to subtract background fluorescence unrelated to viscosity.

5.3.6 Probe Sensitivity Verification using Steady-state Rheology

Rheological testing was performed to verify the sensitivity of FG to changes in viscosity. Oat product samples prepared for the TIM-1 trials were sequentially diluted to

obtain six solutions with oats:water ratios of 1:0, 1:0.5, 1:1, 1:2, and 1:3. FG was added to each of the solutions (final concentration 40 μM) to correlate fluorescence intensity with rheological measurements in a wide range of viscosities. Fluorescence was measured with the method used to determine luminal viscosity. Simultaneously, a Discovery Hybrid Rheometer (TA Instruments, DE, USA) equipped with a 25-mm sandblasted parallel plate was used to determine rheological properties. A flow curve was obtained at 37°C, controlled by the Peltier plate, and recorded within a shear rate range of $0.1–400 \text{ s}^{-1}$.

5.3.7 HPLC Analysis of Sugars

The filtrates and ileum efflux collected from the TIM-1 runs were analyzed using an HPLC system (Alliance Separation Module e2695, Waters Corp., MA, USA) equipped with a 2424 Evaporative Light Scattering Detector (Waters Corp. MA, USA) for each collection time point. A Supelscosil^{TM} LC-NH2 5-μm column (25 cm × 4.6 mm) (Sigma-Aldrich, PA, USA) was used in combination with a 2-cm LC-NH2 Supelguard^{TM} cartridge. The stroke volume for the system was 50 μL, and an isocratic pump mode was used. Ideal separation occurred when the mobile phase was composed of 25% HPLC-grade water (EMD Chemicals, Inc., NJ, USA) and 75% HPLC-grade acetonitrile (EMD Chemicals, Inc., NJ, USA). The column temperature was set at 30 ± 5°C. The area under the curve of the eluted peaks on the HPLC chromatograms was converted to mg of the corresponding sugar (glucose and maltose) using a calibration curve. This conversion yielded the absolute bioaccessible glucose, maltose, and total sugars (glucose plus maltose), which was used to determine cumulative bioaccessible glucose, maltose, and total sugars.

5.4   Results and Discussion

The meals prepared from three commercially available oat products were digested in the TIM-1 *in vitro* digestion system to examine changes in rates of starch digestion and *in situ* luminal viscosity. Although the three products originate from the same grain, they underwent different processing techniques and cooking procedures. Milled oat grains are kiln-dried to inactivate lipase to prevent the development of off-flavors and extend shelf life [6]. The oats are then cut into smaller particles to produce steel cut oats [6]. Steaming and rolling of steel cut oats yields instant oat flakes [6, 352]. Flakes or whole oat groats can be ground into flour, from which the coarse oat bran portion is separated. Oat bran consists of the aleurone and subaleurone layers of the grain [6], which are characterized by a high β-glucan content, as shown in Tables 5.1 and 5.3.

From the three oat-based meals, the cumulative bioaccessible glucose, maltose, and total sugars (glucose and maltose) (Figure 5.1) were determined in the jejunum and ileum compartments of the small intestine and in the ileal efflux (data not shown) collected from the TIM-1 over 420 min. The lowest bioaccessible glucose, maltose, and total sugars at 420 min (Figure 5.1a, b, and c) of digestion was observed for the oat bran. After a lag period of 30–60 min for steel cut and instant oats, and a lag period of 90 min for oat bran, significant amounts of glucose and maltose were cleaved, producing a sigmoidal release profile (Figure 5.1a and b).
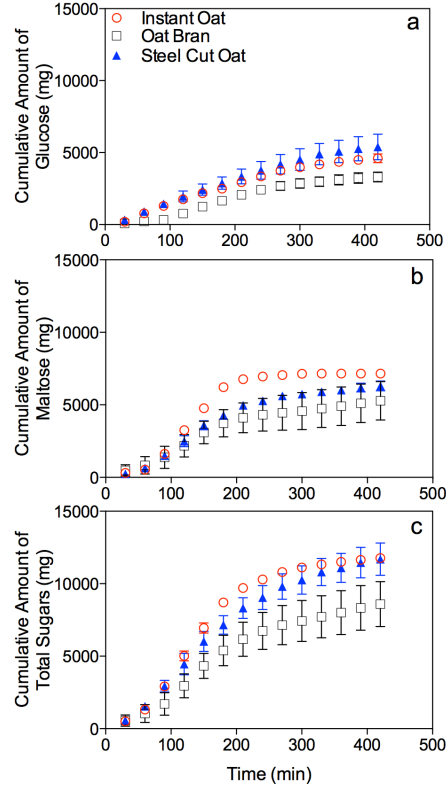
Figure 5.1: Cumulative bioaccessible glucose (a), maltose (b), and total sugars (c) in the jejunum and ileum compartments (combined) for instant oats (red), oat bran (black), and steel cut oats (blue).

A shifted logistic model with three parameters was used to characterize the amount of sugars released in the different TIM-1 compartments as a function of time (t):

$$C(t) = \frac{C_{asymp}}{1 + e^{k(t_c - 1)}} - \frac{C_{asymp}}{1 + e^{kt_c}} \qquad (5.1)$$

where C(t) is the amount of released sugar at a given time, C_{asymp} provides an upper bound to the sugar bioaccessibility curve, k is a rate constant (i.e., mg glucose, maltose, or total sugars per unit time), and induction time (t_c) represents the time at which half of the total bioaccessible sugars have been released.

This model accounts for the lag period and sigmoidal trend (Figure 5.1) and includes a correction term at the right side of the equation, forcing the curve to pass

through the origin and satisfy the condition that at time (t) = 0 min, the amount of bioaccessible sugars is 0 mg. It is important to note that Equation 5.1 was initially applied to lipid systems [353-355] to characterize lipolytic activity. However, the phenomenological characteristics of this model allow its use in diverse applications such as the determination of carbohydrate bioaccessibility. Bioaccessibility refers to the amount of a nutrient that is available for absorption [176], whereas bioavailability refers to the amount of a nutrient that is available to perform its specific physiological function [191]. Since the TIM-1 does not measure advanced transport properties across the intestinal membrane, it is appropriate to label digestates as bioaccessible but not as bioavailable.

Sugar bioaccessibility, rate of release, and induction time (Figure 5.2) for each compartment were determined by fitting the cumulative bioaccessible sugar curves (Figure 5.1) with Equation 5.1 using nonlinear analysis (GraphPad, La Jolla, CA). The theoretical bioaccessibility of glucose, maltose, and total sugars (C_{asymp}) (Figure 5.2a, b, and c) were similar to the experimentally determined bioaccessibility values obtained from the TIM-1 (Figure 5.1). The rate of sugar release (Figure 5.2d, e, and f) varied depending on the measured mono- or disaccharide. For example, the rate of glucose release (Figure 5.2d) was greatest for oat bran, followed by instant oats, and then steel cut oats. The rate at which maltose was cleaved from the polysaccharide was highest for instant oats, followed by steel cut oats, and then oat bran (Figure 5.2e). Finally, the rate of total sugar release from starch was greatest for instant oats, followed by oat bran, and then steel cut oats (Figure 5.2f).

A typical serving of steel cut oats provides a greater concentration of digestible carbohydrates than instant oats, and oat bran yields the lowest amount of sugars. It is now widely accepted that both amount and type of carbohydrate influence postprandial glycemic response [356-359]. Figure 5.2c shows that total bioaccessible sugar is at least in part governed by the concentration of carbohydrates and starch (Table 5.3) for each type of oat-based meal. The rate of starch digestion also influences postprandial glucose response [121, 360, 361] and is again affected by starch type and quantity.
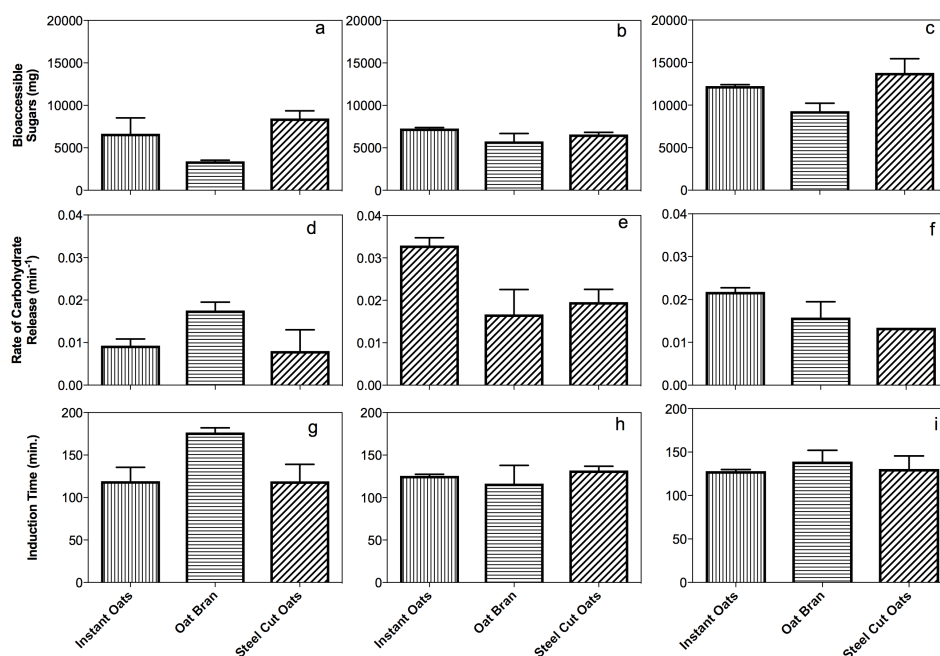
Figure 5.2: Fitted parameters from Equation 5.1 in the jejunum plus ileum compartments, representing total bioaccessible sugar, rate of sugar release, and induction time for glucose (left column: a, d, g), maltose (middle column: b, e, h), and total sugars (glucose plus maltose) (right column: c, f, i).

Oat starch differs from other cereal starches in that it exists as clusters of starch granules [9]. The steaming and flaking processes used to make rolled oats disrupts the cell wall and breaks down these clusters into individual starch granules [8, 9, 362]. This breakdown is greater in thinner flakes [9] characteristic of instant oats. Damaged starch

granules are more readily hydrolyzed by α-amylase than intact granules [10, 363, 364]. It has been hypothesized that the preserved structural integrity of the cell walls in oat bran and steel cut oats may act as a barrier that impedes access of the amylase to starch, thus possibly reducing the rate of starch hydrolysis [365]. Both high-pressure and normal-pressure steaming processes remove the protein network surrounding oat starch granules [362] that functions as a hurdle against starch digestion [366, 367]. Gelatinization also disrupts the native crystalline structure of the starch and allows amylose to "leak" out of the starch granules [117, 118], which facilitates digestion [121]. Steaming and rolling results in partial gelatinization of starch content in thin flakes of instant oat [10]; increasing the groat thickness decreases the extent of gelatinization [10], possibly attenuating water penetration and consequently reducing extent of gelatinization [126]. Elevated β-glucan levels also reduce the extent of gelatinization by competing for water hydration with starch [153, 154] and hindering the motility of digestive enzymes and their access to the starch substrate [153, 368, 369] due to elevated luminal viscosity [13, 345]. These changes may contribute to the more rapid rate of sugar release for instant oats (Figure 5.2f) compared with oat bran and steel cut oats.

The fitted induction times (Figure 5.2g, h, and i) were similar between samples, typically between 120 and 135 min, except for the induction time for glucose in oat bran ($\sim$175 min) (Figure 5.2g). Induction time (t_c) combines the initial lag, rate of sugar release, and duration of hydrolysis. Such a delay in starch hydrolysis in oat bran may be, at least partly, congruent with the above mentioned higher concentration of β-glucan characterized with a much higher water binding capacity as compared to starch [82]. Thus, possibly attenuating starch hydration and gelatinization and consequent

susceptibility to amylosis.

The TIM-1 system was coupled with fluorescence spectroscopy to detect changes in luminal viscosity. The sensitivity of the fluorescent FG probe to changes in viscosity in glycerol/water and concentrated sugar solutions was first evaluated using the Förster and Hoffman sensitivity parameter, x [330], which was found to be between 0.4 and 0.5, supporting the use of this probe as a molecular rotor:

$$I(v) = \alpha \cdot v^{x} \tag{5.2}$$

where $I(v)$ is the fluorescence signal intensity, α is related to the brightness of the probe, and v is viscosity. To corroborate the validity of this probe in our system, the fluorescence intensity and rheological properties of instant oats in various dilutions were independently evaluated and compared (Figures 5.3 and 5.4). We found that fluorescence intensity decreased with decreasing viscosity (i.e., increasing dilution) (Figure 5.3). The rheological measurements indicated a non-Newtonian and shear-thinning behavior for all tested dilutions (data not shown) across the measured shear rate range (0.1-400 s^{-1}). It is important to note that shear rates in the gastrointestinal tract have not been analyzed due to complexity of the digestive system and variability in shear rates at different locations of the luminal cavity [314]. For example, a shear rate range of $10 - 100$ s^{-1} was proposed to represent shear along the entire gastrointestinal tract previously [315]. Another research group suggests a shear rate range of 0.1-10 s^{-1} in the small intestine [316]. We have therefore selected to use the viscosity of the oat samples at an arbitrary shear rate of 30 s^{-1}, which corresponds to the last point of the shear-thinning behavior of the sample, after which a plateau in the sample viscosity is attained. These viscosity values were correlated with the maximum fluorescence emission intensity. A direct correlation ($R^2 =$

0.98) was found between fluorescence intensity and viscosity (Figure 5.4); therefore, the terms "fluorescence intensity" and "viscosity" are used interchangeably hereafter.
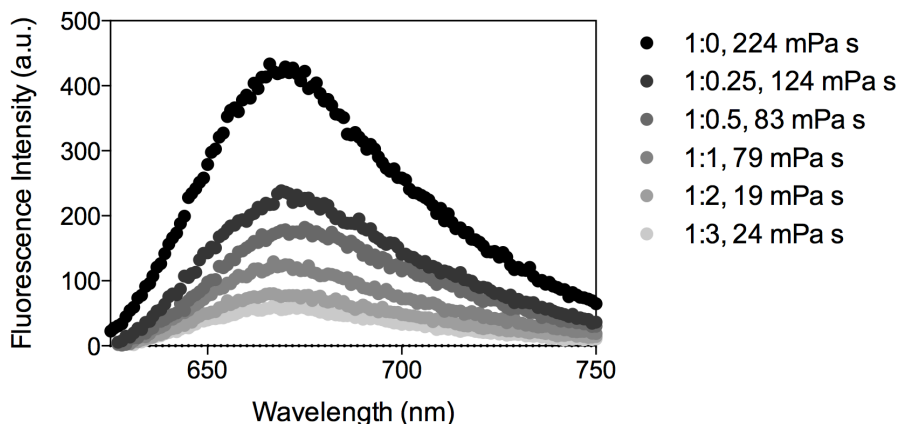
Figure 5.3: Fluorescence intensity spectra for various dilutions of cooked instant oats after subtracting background fluorescence.
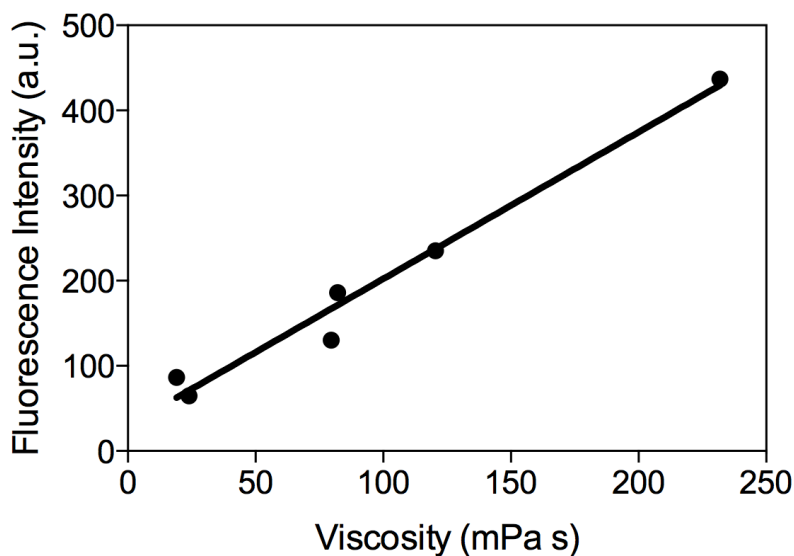
Figure 5.4: Fluorescence emission intensity as a function of viscosity (mPa s) for various dilutions of cooked instant oats after subtracting background fluorescence.

The measured fluorescence intensity for the oat-based meals was normalized to the initial fluorescence intensity of instant oats to facilitate comparison. The maximum intensity in the gastric compartment at each time point (Figure 5.5) was fitted using the logistic equation (Equation 5.3):

$$I(t) = I_{min} + \frac{(I_{max} - I_{min})}{1 + e^{k_1(t_{c1}-t)}} \hspace{3cm} (5.3)$$

where I_{min} is the minimum observed fluorescence intensity, I_{max} is the maximum intensity, k_1 is the rate of change in fluorescence intensity (viscosity), and t_{c1} is the inflection point, at which half of the total change in fluorescence intensity (viscosity) is observed. Fitted parameters from Equation 5.3 are presented in Table 5.5. The normalized fluorescence intensity in the gastric compartment was similar for instant oats and oat bran throughout the digestion period (Figure 5.5a and b), where maximum viscosity was observed at time = 0 min. The thin particles resultant from the rolling step involved in instant oat processing and the widely accepted pre-gelatinized starch content [126] may be hypothesized to translate into attainment of a maximal viscosity at an earlier stage (during cooking); further hydration during digestion results in rapid collapse of the matrix. Initial/maximum intensity for oat bran was greater than that of instant oats (Table 5.5). This may be consequent of a higher proportion of β-glucan in oat bran allowing a greater probability of entanglement between the fibrous polymer chains and increasing the viscosity. The positive correlation between viscosity and β-glucan concentration is widely accepted [3, 314, 370]. There was a longer delay in the degradation of viscosity for oat bran, which does not see a significant decline in fluorescence over the first 70 min, whereas this decline occurs after 10 min for instant oats (Figures 5.5a and b). Oat bran was found to undergo ongoing solubilization in the chyme matrix as the gastric digestion time progressed in pigs [371]; the same research group [372] showed a higher gastric viscosity for oat bran compared to rolled oats in pigs, similar to what was observed in Figures 5.5a and 5.5b. Oat bran β-glucan composition is concentrated within thick aleurone and sub-aleurone layers that are sturdier than the endrosperm cell walls

and retain their structural integrity throughout both the gastric and intestinal digestion, [347, 373, 374]. This resistance to digestion may account for the longer lag period observed for oat bran (Figure 5.5b). Interestingly, the longer lag period observed in the viscosity profile was also seen in glucose bioaccessibility (Figure 5.1a). However, the larger slope of viscosity decay (k_1) combined with a shorter inflection point (time at which half of the total change in viscosity takes place) indicates a more rapid degradation in viscosity in the initially more viscous oat bran chyme compared to instant oats (6). In an *in vivo* system, this rapid drop in viscosity is accountable to the increased intragastric dilution in response to increased gastric meal viscosity; however, such a phenomenon is not applicable to the pre-determined gastric secretion rates characteristics of TIM-1 *in vitro* system [165].

Table 5.5: Parameters of the fit of normalized fluorescence intensity as a function of time using Equation 5.2.

Parameters	Instant Oats	Oat Bran	Steel Cut Oats
Minimum intensity (I_{min})	0.056	0.03	0.57
Maximum intensity (I_{max})	1.01	1.18	0.92
Slope 'k_1' (min^{-1})	-0.027	-0.054	+0.067
Inflection point 't_{c1}' (min)	107	97	124

In contrast, the initial viscosity of steel cut oats was at the minimum (Figure 5.5 c, Table 5.5). Initially, the normalized fluorescence intensity of instant oats (Figure 5.5a, Table 5.5) was approximately twice that of steel cut oats (Figure 5.5c, Table 5.5). The initial/minimum viscosity of steel cut oats was retained for ~ 90 min before a gradual increase was observed. This distinction in the measured fluorescence values may be attributed to the greater thickness of the steel cut oat particles compared to instant oats and oat bran; which may contribute to a possibly slowed penetration of water [10] and
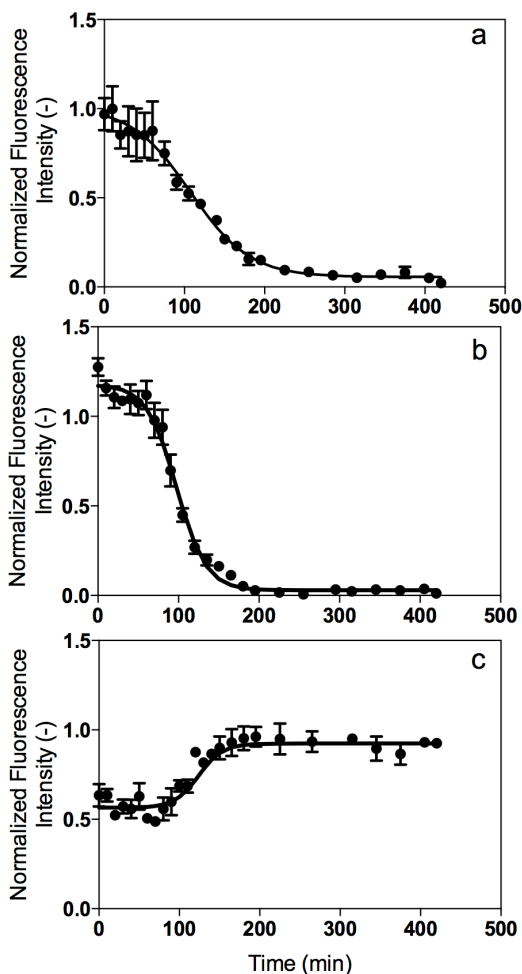
Figure 5.5: Normalized fluorescence intensities in theTIM-1 gastric compartment for instant oats (a), oat bran (b), and steel cut oats (c) as a function of digestion time.

hydration of the β-glucan matrix and thus delaying the onset of increase in gastric

viscosity (Figure 5.5c). However, a very limited number of scientific works exist on steel

cut oats, and therefore, no relevant previous reportings on steel cut oat luminal viscosity

are available for comparison. Further, meal viscosity has been correlated with a greater

sensation of satiety, and reduced hunger and appetite [312, 340]. Accordingly, we

hypothesize a more rapid onset of satiety in instant and oat bran –based meals retained

for a short period of time, and steel cut oats resulting in a delayed yet long-lasting

sensation of satiety; however, scientific experimentation *in vivo* is needed to confirm this

theory.

Recent studies have indicated that the overall viscosity of oat processed products is not only affected by β-glucan content, state, and release kinetics but also it is influenced by starch and protein content and the presence of particulates (Grundy et al, 2017; Zhang et al., 2017). The proposed luminescent technique to measure in situ viscosity allows assessing the viscosity of the combined contribution of the meal components in a noninvasive way.Two more parameters are agreed upon to influence β-glucan viscosity: its molecular weight and solubility [375-377]. Previous studies suggest molecular weight distribution of β-glucan to be positively correlated with viscosity as well as being negatively correlated with rate of *in vitro* starch hydrolysis [376]. Average molecular weights of β-glucan polymers in instant and steel cut oats-based sample meals have been determined (Table 5.6); unfortunately, oat bran sample molecular weight was not analyzed due to sample unavailability (from the same batch) at time of analysis. It is important to note that our current experimental design involves the use of oat grain samples that have been exposed to variable commercial processing techniques. Many researchers have demonstrated that commercial processing methods modify β-glucan quality, such as its molecular weight [3-5]. In addition, the prepared oat-based meals underwent different preparation/cooking methods (Table 5.2) and also contained different quantities of starch and β-glucan in order of attaining a physiological response (*in vitro)* that is most representative of the typical serving of oats. In consequence of these numerous experimental variables, any correlation between viscosity and the corresponding molecular weights would prove insufficient. Solubility, with reference to β-glucans, is used to describe the ability of the polymer to disperse in a liquid [348]; and

was found to be positively associated with viscosity [378]. Solubility of β-glucan extracted from oats that have been kilned, then steamed, then flaked was found to be higher as compared to kilned-only oats *in vitro* [379]. Zhang *et al*. [3] deduce replacement of intramolecular hydrogen bonding of β-glucan with water molecules from steam exposure, thus adopting a more open and linear configuration; which might increase the hydrodynamic volume and possibly increase viscosity.

Table 5.6: Quantified Molecular Weight of β-glucan in tested oat samples.

Oat Type	Molecular Weight (Daltons)
Instant	1.14×10^6
Steel Cut	0.69×10^6

The digestive parameters were closely associated with each other. For example, there was a correlation between oat bran having the highest initial viscosity (Figure 5.5b, Table 5.5), longest induction times for glucose (Figure 5.2g) and total sugar (Figure 5.2i) release, lowest total bioaccessible sugars (Figure 5.2c), and lower rate of sugar release compared with instant oats (Figure 5.2f). Kim and White [380] treated heated oat slurries with α-amylase to hydrolyze starch and lichenase to hydrolyze β-glucan to illustrate the contribution of the two polysaccharides on viscosity. Lichenase treatment resulted in a higher viscosity than α-amylase treatment, suggesting that starch is the major contributor to oat slurry viscosity. The total carbohydrate, β-glucan, and starch concentrations were linearly correlated with initial viscosity in the gastric compartment (Figure 5.6). Although the linear correlations were strong for both β-glucan (Figure 5.6b) and starch concentrations (Figure 5.6c), stronger correlations were observed with respect to total carbohydrates (Figure 5.6a).
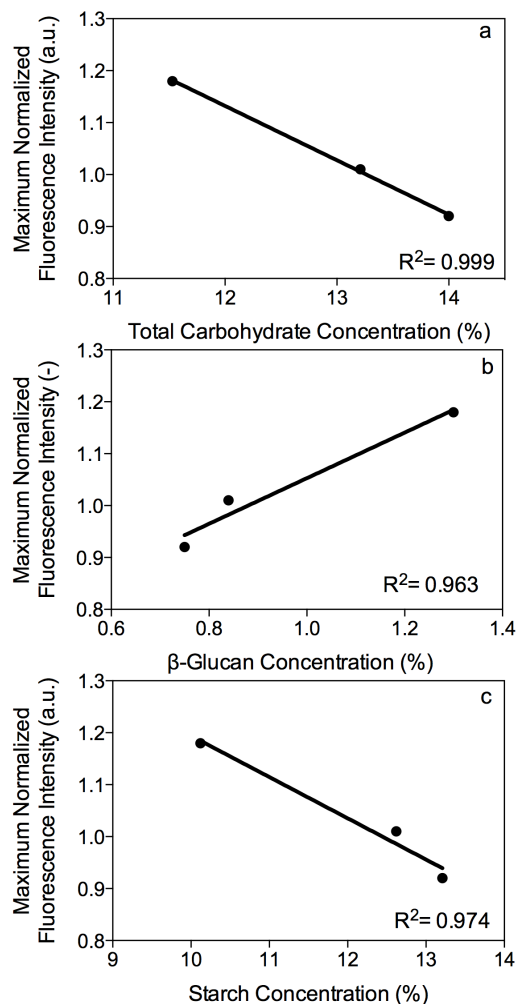
Figure 5.6: Maximum normalized fluorescence intensity at time = 0 min in the gastric compartment as a function of total carbohydrate, b-glucan and starch concentrations.

Figure 5.7 illustrates changes in normalized fluorescence intensities as a function of time for the duodenum, jejunum, and ileum compartments. The results showed an approximately 10-fold reduction in viscosity compared to the gastric compartment viscosity. Although distinct changes in gastric fluid viscosity were observed (Figure 5.5), the viscosity in the intestinal compartments indicates a highly diluted state. Similarly, Villemejane *et al.* reported a 10-fold reduction in the viscosity of the chyme between the stomach and the small intestinal compartments [318]. This result was ascribed to the

automated and pre-determined gastric emptying rate that allows passage of small particulates into the small intestine in a uniform manner, and not to physiologically relevant phenomena. For example, *in vivo* gastric emptying is dependent on numerous factors including meal viscosity, which is not observed in the TIM-1 [308-311] due to an automated and pre-determined gastric emptying protocol. Accordingly, the experimentally observed changes in small intestinal viscosity measurements (Figure 5.7) are unlikely to represent viscosity changes *in vivo*. However, viscosity trends in the gastric compartment (Figure 5.5) may roughly reflect *in vivo* gastric emptying. As an example, echo-planar magnetic resonance imaging in humans fed locust bean gum meals showed longer gastric emptying times with increased meal viscosity [340]. In addition, gastric chyme viscosity was found to be a better predictor of changes in gastric emptying than initial meal viscosity in pigs [381].

5.5 Conclusions

A comparison of three commercially available oat products revealed numerous differences in composition that appear to influence the biophysics of digestion. Our results showed that starch content was directly proportional to total bioaccessible sugars, and the rate of sugar release was slowest for steel cut oats and most rapid for oat bran. Although initial viscosity and rate of degradation of viscosity differed for instant and oat bran, the gastric luminal viscosity trends were similar. However, a different pattern was seen for steel cut oats. These changes in gastric viscosity may influence rates of gastric emptying and the sensation of satiety. The physicochemical properties of the different oat-based meals, which may influence postprandial glycemia in an inadvertent manner, are critical for product development, especially for meals for diabetic patients.
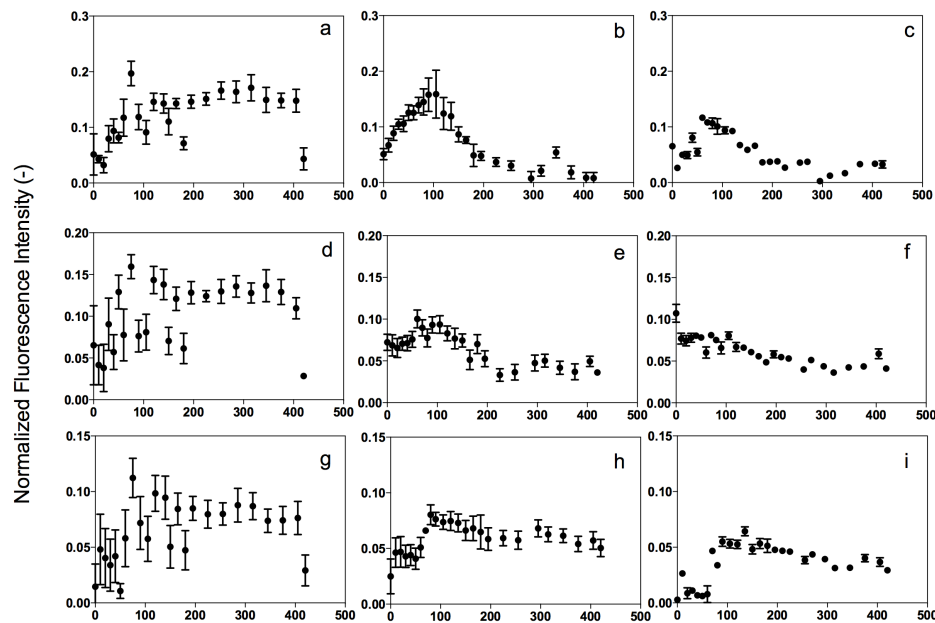
Figure 5.7: Normalized fluorescence intensities recorded at TIM-1 duodenum (top row), jejunum (middle row), and ileum (bottom row) compartments for instant oats (left column: a, d, g), oat bran (middle column: b, e h), and steel cut oats (right column: c, f, i) as a function of digestion time.

5.6 Acknowledgements

5.7 Conflicts of Interest

The views expressed in this manuscript are those of the authors and do not necessarily reflect the position or policy of PepsiCo, Inc.

6 Luminal Viscosity and Sugar Bioaccessibility of Instant and Steel Cut Oat/Milk Protein Blends

This chapter is co-authored with Derrick Fondaco, Karen Ben-Elazar, Maria G. Corradini, Richard D. Ludescher, Douglas Bolster, Gary Carder, YiFang Chu, Yongsoo Chung, Jodee Johnson, Michael A. Rogers

6.1 Abstract

Milk protein concentrate (MPC; 0 g, 5 g, and 10 g) was added to two commercially available oat products, instant oats and steel cut oats, to study its effects on carbohydrate-digestion kinetics and luminal viscosity during *in vitro* digestion. We used the TNO Intestinal Model-1 (TIM-1) to simulate gastrointestinal digestion of the oats-based meals. Meals containing 5 g or 10 g MPC yielded significantly less total bioaccessible sugar compared with those containing 0 g MPC, while the rate of starch digestion was significantly higher in meals containing 5 g or 10 g MPC. The TIM-1 was coupled with fluorescence spectroscopy and a luminescent molecular rotor to report changes in gastric viscosity *in situ*, showing that the gastric viscosity was higher in the meals containing MPC. Those findings suggest that MPC in oats-based meals significantly modifies the kinetics of carbohydrate digestion and increases gastric viscosity.

6.2 Introduction

Designing foods by modifying their form and formulation is becoming a plausible strategy to control how foods behave and are digested in the gastrointestinal tract (GIT). The resultant changes in the physiological impact of modified foods may serve as a dietary intervention to combat diet-related chronic diseases. Starch-rich foods are of special concern, given the persistence of the type II diabetes pandemic [14, 19]. Therefore, there is a great need for dietary interventions that target postprandial glucose levels. Oats are a staple starchy food with an intermediate-to-high glycemic index (~78) [382]. The hydrothermal processing (cooking) of oats involves gelatinization of the starch and the formation of a biphasic paste with an aqueous, continuous phase and a dispersed phase of swollen starch granules [383]. Modifying the meal formulation allows the physical properties of the starch-paste matrix and the response of the starch to physiological conditions to be controlled. For example, hydrocolloids have a high water retention capacity that was found to contribute to an increase in digesta viscosity throughout the GIT [313]. Increased gastric digesta viscosity impedes motion and access of enzymes to the substrate, consequently reducing nutrient hydrolysis [70-72], as well as hinders diffusion of the hydrolysis by-products to the luminal brush border and renders absorption less effective [70-72]. The subsequent reduction in rate and extent of starch digestion, attributed to increased digesta viscosity [69] has been associated with controlling postprandial glycemia [73-78]. β-glucan is a soluble fiber found in oats that is capable of entrapping water in its network [345, 346] and increasing chyme viscosity in the GIT. These properties of β-glucan are hypothesized to be central in the plasma glucose-lowering health claims associated with oats [80, 384].

Milk protein, especially milk protein concentrate (MPC), is another hydrocolloid that has received attention as a food additive. MPC has a casein-to-whey protein ratio very similar to that of milk [385]. The high protein content of MPC makes MPC an ideal thickening agent, capable of binding water and increasing the food-matrix viscosity. The rheological and physiological aspects of blends of MPC and β-glucan are largely unknown. The viscosity of starch paste prepared in milk is greater than that of pastes containing the same amount of starch but prepared in water [386, 387]. Milk proteins are presumed to modify the properties of the dispersed phase of the starch paste and thus increase the overall viscosity of the paste [388]. We hypothesize that the addition of MPC to oat-based meals may increase the chyme viscosity during luminal transit and consequently influence the rate and extent of starch digestion. Such correlations between the contents of meals and the properties of the meals during digestion are vital for altering glucose bioaccessibility [176] and, potentially, the glycemic index of oats-based meals. Glucose bioaccessibility is of distinct importance because it is the rate-limiting step to glucose bioavailability [15].

We evaluated the effects of the addition of two doses of MPC to instant oat-based and steel cut oat-based meals on carbohydrate digestion and gastric viscosity. We used simulated digestion in the TNO Intestinal Model-1 (TIM-1) paired with molecular rotors (optical chromophores) to assess real-time luminal viscosity throughout a simulated gastric environment. The TIM-1 is an advanced artificial digestive system that mimics the human stomach and upper small intestine. In comparison with other *in vitro* techniques, this dynamic, computer-controlled system is unique in its ability to regulate pH, temperature, gastric and intestinal emptying, transit time, and GIT secretions [318].

Real-time viscosity in the TIM-1 was previously monitored using molecular rotors as luminescent probes to assess viscosity [389]. Molecular rotors are molecules that consist of two or more segments that are capable of rotating relative to one another [390]. Photoexcitation of MR causes intramolecular twisting of the two segments at a rate that is dependent on the free-volume (or molecular crowding) of the surrounding environment. Less viscous environments facilitate a non-planar (twisted) configuration of the molecular rotor in the excited state, thus favoring twisted intramolecular charge transfer (TICT) state. Relaxation from TICT to the ground state is predominantly in the form of non-radiative decay (without photon emission). Rigid or more viscous environments hinder the rotation of the two MR segments relative to one another, yielding a planar configuration in the excited state, and favoring the local excited (LE) state. Relaxation from LE to the ground state involves photon emission (radiative decay). The rate of formation of the TICT state is slower in highly viscous materials, and the two competing decay pathways determine the sensitivity of the probe to the micro-viscosity of the surrounding medium [213]. We analyzed digestates from the TIM-1 to obtain total sugar-release profiles for each of the tested mixtures of oats and MPC. We used a shifted-logistic model to estimate the rate and extent of sugar release as a function of digestion time. The luminescence emitted by the molecular rotors during *in vitro* digestion suggests that mixtures of oats and MPC have a higher viscosity than oats-only meals.

6.3   Methods

6.3.1   *Materials and Sample Preparation*

Quaker Oats (PepsiCo, Inc., IL, USA) supplied the oat products (instant oats and steel cut oats) and MPC80 (MPC, 80% protein) tested in our experiments. Oats were

pooled from numerous production batches. We used standard methods to measure the moisture, ash, protein, fat, and soluble and insoluble (AOAC 991.43) dietary fiber compositions of the oat products (Table 6.1). We then subtracted those values from the total weight to estimate the total carbohydrate content [Total Carbohydrates (%) – Table 6.1]. We used AOAC methods 995.16 and 996.11 to quantify the β-glucan and starch compositions.

We prepared a 45-g serving of each type of oatmeal sample immediately prior to analysis. We mixed the instant oats with various amounts of water and MPC80 (Table 6.2) in a 1-quart Pyrex® measuring cup and heated them in a microwave (NN-SD987SA, 1250 watts, Panasonic Corp., Osaka, Japan) on high power (Table 6.2). The steel cut oats were mixed with various amounts of MPC80, stirred into boiling water in a medium saucepan on a stovetop at high heat, and allowed to simmer on low heat for 25 to 30 min (Table 6.2).

Table 6.1: Compositions of the tested oat products.

Oat Type	Soluble Fiber (%)	β-glucan (%)	Insoluble Fiber (%)	Starch (%)	Total Carbohydrates (%)
Instant Oats	4.50	3.97	5.20	54.00	62.80
Steel Cut Oats	4.20	3.45	5.10	54.70	64.40

* All results are presented on an as-is/wet basis. The 2 × %RSD (i.e., 95% confidence interval) for the tests are 12% (soluble fiber and insoluble fiber), 6% (β-glucan), 4% (starch), and 12% (total carbohydrates).

Table 6.2: Meal preparation: mixture composition, heating duration, cooling duration, and heating unit.

Oat Type	Oats (g)	Water (g)	MPC80 (g)	Heating Duration	Cooling Duration (min)	Heating Unit
Instant Oats + 0 g MPC80	45	190	0.00	65 s	2	Microwave
Instant Oats + 5 g MPC80	45	215	5.88	90 s [u]	2	Microwave
Instant Oats + 10 g MPC80	45	240	11.76	124 s [u]	2	Microwave
Steel Cut Oats + 0 g MPC80	45	335	0.00	25 min [v]	2	Stovetop
Steel Cut Oats + 5 g MPC80	45	380	5.88	28 min [v]	2	Stovetop
Steel Cut Oats + 10 g MPC80	45	425	11.76	30 min [v]	2	Stovetop

[u] The microwave cooking was stopped at 60 s and 90 s for stirring, after which the heating process was continued.
[v] Occasional stirring during cooking.

6.3.2 Experimental Meals

After the meals were allowed to cool for 2 min, a single volunteer masticated the prepared meals using the "10 chew-and-spit" method. The chewing allowed the oats to be masticated and exposed to salivary α-amylase. To mimic the initial gastric conditions, we mixed 100 g of the chewed samples with 5 g gastric-secretion fluid, 95 g gastric-electrolyte solution, and 50 g water. We then fed the samples into the TIM-1 (TNO Triskelion, Zeist, The Netherlands) gastric compartment along with 50 g water for a total experimental meal weight of 300 g. Available total carbohydrates, starch and β-glucan of the meals (Table 6.3) were calculated based on the total carbohydrate content of each type of oat (Table 6.1) and the total weight of the meal (accounting for water loss during cooking) fed into the TIM-1 (Table 6.2). Calculating the available total carbohydrates

required a 10/9 conversion factor to account for the cleavage of the glycosidic linkages of starch to yield glucose or maltose [351].

Table 6.3: Estimated total available carbohydrates, β-glucan, starch, and water-to-starch ratio of each oats-based meal fed into the TIM-1.

Oat Type	Total Carbohydrates (%)	β-glucan (%)	Starch (%)
Instant Oat + 0 g MPC80	13.21 ±1.59	0.84 ± 0.05	12.62 ± 0.50
Instant Oat + 5 g MPC80	11.68 ± 1.40	0.74 ± 0.04	11.20 ± 0.45
Instant Oat + 10 g MPC80	10.46 ± 1.26	0.67 ± 0.04	9.99 ± 0.40
Steel Cut Oat + 0 g MPC80	14.00 ± 1.68	0.75 ± 0.05	13.21 ± 0.53
Steel Cut Oat + 5 g MPC80	13.04 ± 1.74	0.70 ± 0.05	12.42 ± 0.55
Steel Cut Oat + 10 g MPC80	12.07 ± 1.45	0.65 ± 0.04	11.40 ± 0.46

* Standard deviations were calculated as per deviations in composition, shown in Table 6.1.

6.3.3 TIM-1 Simulated Digestion

The TIM-1 mimics the digestive process of a healthy adult and replicates the stomach, duodenum, jejunum, and ileum. The ileal-secretion fluid consisted of small intestinal electrolyte solution (SIES; 5 g/l NaCl, 0.6 g/l KCl, and 0.25 g/l $CaCl_2$). The jejunal fluid consisted of SIES and 10% fresh porcine bile. A 7% pancreatin solution, prepared with Pancrex V powder (α-amylase activity = 25,000 units/g, lipase activity = 25,000 units/g, protease activity = 1,400 units/g), was obtained from Paines & Byrne, UK. The gastric-secretion fluid consisted of 600 U/ml pepsin (P7012, Sigma-Aldrich, MO, USA) and 40 U/ml lipase (F-AP15, Amano Enzyme Inc., Nagoya, Japan) in a gastric-electrolyte solution (4.8 g/l NaCl, 2.2 g/l KCl, 0.22 g/l $CaCl_2$, 1.0 g/l $NaHCO_3$). The pancreatin and gastric fluid solutions were placed on ice immediately after preparation. The porcine bile was collected from a slaughterhouse (Farm-to-Pharm, NJ, USA); multiple collections of bile were pooled, divided into single-use quantities, and stored at -20°C. Bile was thawed and filtered using Miracloth (Merck KGaA, Darmstadt,

Germany) prior to incorporation into the experimental solutions. We used 1M NaHCO$_3$ to maintain the following pH levels in the duodenal, jejunal, and ileal compartments: 5.9, 6.5, and 7.4, respectively. HCl was added to the gastric compartment to generate a predetermined pH pattern over time (Table 6.4). The gastric emptying was set to mimic human conditions (i.e., gastric emptying half-time = 80 min).

Table 6.4: The TIM-1 stomach pH decreased over time during the 5-hour digestion period.

Digestion Time (min)	Predetermined pH value
0	5.5
30	4.5
60	3.0
120	2.0
210	1.7
300	1.7

To simulate digestion, each TIM-1 compartment was filled with the corresponding start residues to mimic *in vivo* conditions. The duodenal start residue consisted of 15 g SIES, 15 g pancreatin solution (7%), 30 g fresh porcine bile, and 2 mg trypsin [Sigma, T4665-5G; trypsin activity ≥ 7,500 Nα-Benzoyl-L-arginine ethyl ester (BAEE) units/mg solid]. The jejunal start residue (160 g total) consisted of 40 g SIES, 40 g pancreatin solution (7%), and 80 g fresh porcine bile. The ileal start residue (180 g total) consisted of 180 g SIES. After warming the system to physiological temperature (37°C), the experimental meal (300 g) was fed into the gastric compartment and the 5-hour digestion process was initiated. The jejunum and ileum compartments were connected to filtration units (M20S-300-01P, MiniKros® filter modules, Spectrum Labs, Breda, The Netherlands) to remove the digestate. During the experiment, samples were taken from the duodenum and jejunum filtrates as well as from the ileum efflux at 30-min intervals. These samples were immersed in ice until they could be transferred to the high-

performance liquid chromatography (HPLC) system for analysis.

6.3.4   Statistical Analysis

Statistical significance of variability in the total cumulative % bioaccessible sugars at the end-point of digestion and on the fitted parameters was determined with one-way analysis of variance (ANOVA) ($p<0.05$) and Tukey's Multiple Comparison Test using GraphPad Prism 7 (La Jolla, California, USA). Statistical significance was defined as p value < 0.05.

6.3.5   Luminescence Spectroscopy Coupled with TIM-1

The TIM-1 system was coupled to a Cary Eclipse spectrofluorimeter (Agilent Technologies, Santa Clara, CA) and a fiber optic attachment to measure *in situ* fluorescence intensity (FI). The viscosity-sensitive luminescent probe, Fast Green FCF (FG; Sigma-Aldrich, ON, USA), was added to each of the TIM-1 sample solutions, rinses, and secretion solutions (final FG concentration = 40 μM). FG was used as the fluorescent probe because its emission spectrum is easily differentiated from the background noise generated by naturally occurring fluorophores in the oatmeals, MPC, and TIM-1 secretion fluids. Because FI data are dependent on the probe concentration, FG was added at a concentration of 40 μM to each of the TIM-1 secretions and meals fed into the TIM-1. This step ensured a consistent concentration of FG throughout the 5-hour TIM-1 trials, allowing for simplified data analysis that assumed no dilution of FG during digestion. The TIM-1 and fiber optic probe were placed under a blackout blind to prevent ambient light from influencing the spectroscopic measurements. We used an adapter to place the fiber optic probe against the glass surface of the sample container at a 45° angle to reduce backscatter from the glass surface. The fluorescence spectra were recorded

between 610 nm and 750 nm, using an excitation wavelength of 580 nm. The excitation and emission slits were set at 5 nm and 20 nm, respectively. The photomultiplier detector voltage was set at high. Measurements were taken every 10 min during the first 60 min of digestion, every 15 min from 60 min to 180 min of digestion, and then every 30 min from 180 min to 300 min of digestion. For comparisons between samples, we used values normalized relative to the maximum FI for instant oats + 0 g MPC80.

Experiments were performed in quadruplicate for each oat type and MPC80 quantity combination (Table 6.2); three of which contained the above-mentioned FG concentration. The fourth run served as a blank/control, and therefore no FG was added. The FI of the blank (control) runs were subtracted from the FI of the corresponding FG-containing runs to eliminate the background fluorescence unrelated to the changes in viscosity trends as a function of digestion time; i.e. the contribution of light scatter from the TIM-1 glass surface, if any. We also performed control runs in which we added FG to 5 g or 10 g MPC80 meals without oats to determine if the MPC80 changed the sensitivity of the FG to the matrix viscosity during *in vitro* digestion. Experiments were performed once for each MPC80 quantity (5 g and 10 g) with FG and once without FG (blanks). FI from blanks (without FG) were subtracted from the FI of FG-containing runs to eliminate background FI unrelated to changes in viscosity.

6.3.6 *Probe Sensitivity Verification using Steady-State Rheology*

A Discovery Hybrid Rheometer (TA Instruments, DE, USA) equipped with a 25-mm sandblasted parallel plate was used to determine the rheological properties of the instant oats prepared with 0 g or 10 g MPC80. A flow curve was obtained at 37°C and recorded within a shear rate range of 0.1–400 s^{-1}. Samples were sequentially diluted to

obtain six oat:water ratios (1:0, 1:0.25, 1:0.5, 1:1, 1:2, and 1:3). We added 40 μM FG to each solution to correlate the FI with the rheological measurements. FI was measured by the same method used to determine luminal viscosity, described above.

6.3.7 HPLC Analysis of Sugars

At each collection time point, the filtrates from the jejunum and ileum as well as the ileal efflux from the TIM-1 were analyzed using HPLC (Alliance Separation Module e2695, Waters Corp., MA, USA) equipped with a 2424 Evaporative Light Scattering Detector (Waters Corp. MA, USA). A SUPELCOSIL^{TM} LC-NH2 5 μm column (25 cm × 4.6 mm; Sigma-Aldrich, PA, USA) was used in combination with a 2 cm LC-NH2 SUPELGUARD^{TM} cartridge (Sigma-Aldrich, PA, USA). The stroke volume was 50 μL, and an isocratic pump mode was used. Ideal separation was achieved when the mobile phase was composed of 25% water (HPLC grade, EMD Chemicals, Inc., NJ, USA) and 75% acetonitrile (HPLCE grade, EMD Chemicals, Inc., NJ, USA). The column temperature was set at 30°C. The area under the curve of the eluted peaks on the HPLC chromatograms was converted to the mass (mg) of the corresponding sugar (glucose or maltose) using a calibration curve. The conversion yielded the absolute bioaccessible glucose, maltose, and total sugars (glucose + maltose), which were used to determine the cumulative bioaccessible glucose, maltose, and total sugars.

6.4 Results and Discussion

Six meals, composed of either steel cut or instant oats and one of three quantities of MPC80 (0 g, 5 g, or 10 g), underwent *in vitro* digestion in a TIM-1 to examine the influence of MPC80 on parameters of starch digestion and luminal viscosity. The TIM-1 does not measure advanced transport properties across the intestinal membrane [176].

Accordingly, the experimentally quantified digestates represent sugar bioaccessibility (i.e., the amount of a nutrient that is available for absorption) [176] and not bioavailability [191]. Cumulative bioaccessible glucose and maltose were determined individually in the jejunum and ileum compartments individually; however, for the purposes of analysis they were combined to represent the total bioaccessible sugars (Figure 6.1a and b). All of the meals produced similarly shaped sugar-release profiles (Figure 6.1a and b). An initial lag period (the first 90 min) was followed by a gradual sigmoidal increase that was attenuated by the addition of MPC80. The addition of MPC80 required more water to hydrate the added protein, and the carbohydrate levels in the digestates varied accordingly (Table 6.3). To correct for that variability, the cumulative percent bioaccessible total sugars (Figure 6.1 c and d) were determined by dividing the cumulative values (Figure 6.1 a and b) by the estimated total fed carbohydrates (Table 6.3).

The total sugars hydrolyzed from the instant oats significantly decreased after the addition of MPC80, with no significant dose dependence (5 g versus 10 g MPC80; Figures 6.1a and 6.1c). Steel cut oat-based meals with 0 g and 5 g MPC80 yielded similar total bioaccessible sugars; significant attenuation was only evident in steel cut oats-based meals containing 10 g MPC80 (Figures 6.1b and 6.1d). There is a wide consensus on the glucose-lowering properties of whey and casein [391-393]. The digestion of milk proteins releases bioactive peptides and amino acids that induce hormones that regulate insulin secretion and blood glucose [394]. Because the TIM-1 system lacks feedback mechanisms [176], it cannot account for hormonal factors, so other factors must be responsible for the reduction in the sugar bioaccessibility upon the addition of MPC80.
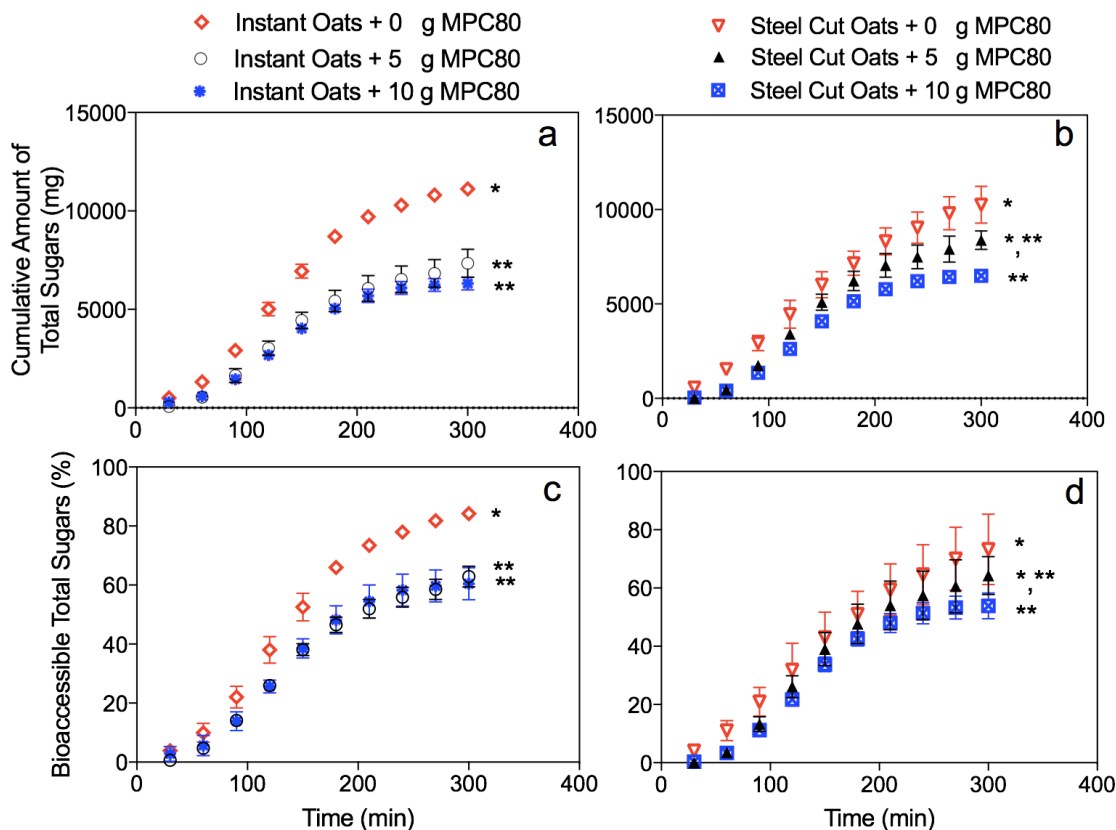
Figure 6.1: Cumulative (a and b) and percent (c and d) bioaccessible total sugars (glucose + maltose) in the jejunum and ileum compartments (combined) for instant oats (left column: graphs a and c) and steel cut oats (right column: graphs b and d) with 0 g MPC80 (red), 5 g MPC80 (black), and 10 g MPC80 (blue). One-way ANOVA (p < 0.05) with a Tukey's Multiple Comparison Test was performed on the total cumulative percent bioaccessible total sugars (glucose + maltose, mg) endpoints (at 300 min of digestion). Different number of asterisks (*) within each graph suggests statistically significant (p < 0.05) differences in total cumulative percent bioaccessible total sugars at 300 min of digestion. The same number of asterisks (*) within each graph suggests no statistically significant differences.

A more descriptive approach was required to characterize and analyze the changes during amylolysis. Therefore, we applied a shifted-logistical model (Eq. 6.1), originally applied to lipid systems [353-355] to characterize lipolytic activity, to analyze the cumulative bioaccessible sugars in our experiments. The phenomenological characteristics of the shifted-logistic model allow it to be used in diverse applications.

The shifted-logistic model characterizes the amount of sugars released in the TIM-1 compartments as a function of time (t):

$$C(t) = \frac{C_{asymp}}{1 + e^{k(t_c - 1)}} - \frac{C_{asymp}}{1 + e^{kt_c}} \qquad (6.1)$$

where $C(t)$ is the amount of released sugar at a given time (t), C_{asymp} is the maximum sugar bioaccessibility attained, k is a rate constant (i.e., glucose, maltose, or total sugars per unit time), and the induction time (t_c) represents the time at which half of the total bioaccessible sugars have been released. This model accounts for the lag period and sigmoidal release profile of the bioaccessible sugars (Figure 6.1) and includes a correction term at the right side of the equation, forcing the curve to pass through the origin and satisfy the condition that at time (t) = 0 min, the amount of bioaccessible sugars is 0 mg.

Sugar bioaccessibility, rate of release, and induction time (Figure 6.2) were determined using the shifted-logistical model (Equation 6.1) fitted to the experimental bioaccessible glucose (data not shown), maltose (data not shown), and total-sugar curves (Figures 6.1a and 6.1b). The addition of 5 g MPC80 to either instant or steel cut oats significantly reduced the glucose, maltose, and total-sugar bioaccessibility (Figure 6.2a–c). The results shown in Table 6.3 suggest that the samples with 0 g MPC80 had the highest levels of available starch compared with the samples with 5 g or 10 g MPC80 and, furthermore, that the extent of starch amylosis is greatly dependent on the amount of available starch substrate. The instant oats with 10 g MPC80 had a greater reduction in total sugar bioaccessibility than the instant oats with 5 g MPC80; however, the steel cut oats had the same amounts of bioaccessible sugars irrespective of the amount of MPC80 added. Therefore, factors beyond the amount of starch were driving the reduction in

bioaccessible sugars (Figure 6.2c). The extent of hydrolysis has been correlated to the integrity of starch granules [10, 347], the degree of gelatinization [117, 118], and the β-glucan quality and quantity [153, 154].
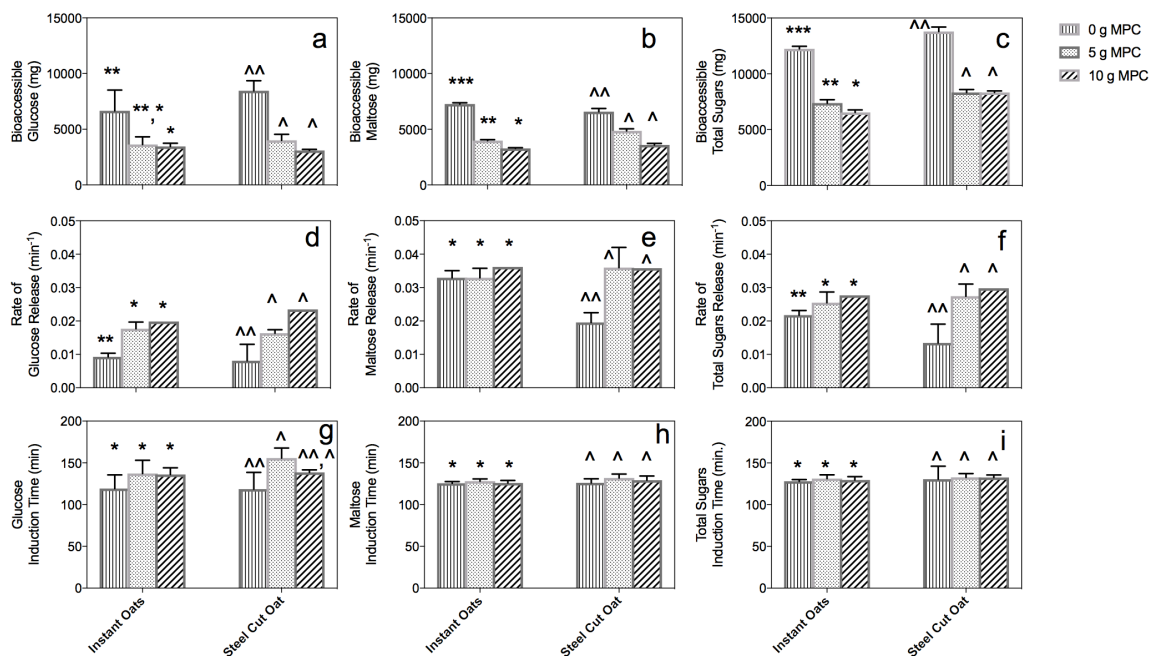
Figure 6.2: Parameters from the shifted-logistical model for glucose (a, d, g), maltose (b, e, h), and total sugars (c, f, i) in the jejunum plus ileum compartments for each oat type and MPC80 quantity. One-way ANOVA (p < 0.05) with Tukey's Multiple Comparison Test was performed for each of the estimated parameters and sugar type for each type of oats-based meals. Different number of asterisks (*) or carets (^) within each graph suggests statistically significant (p < 0.05) differences between the different combinations of MPC0 and instant or steel cut oats, respectively. The same number of asterisks (*) or carets (^) within each graph suggests no differences between the different instant oats and MPC80 combinations for the corresponding parameters. Different number of carets (^) within each graph suggests statistically significant (p < 0.05) differences between the different combinations of MPC0 and instant or steel cut oats, respectively.

The rate of total sugar release significantly increased with the addition of 5 g MPC80, and there was no further increase with the addition of 10 g MPC80 (Figure 6.2 d-f) for either type of oats. Tables 6.2 and 6.3 indicate an inverse relationship between the amount of water added to the meals, which increased with the addition of MPC80, and the percent starch available in the meals. The hydrothermal treatment of starch permits

the starch to gelatinize, rendering its amylose composition more susceptible to interaction with α-amylase and consequent hydrolysis [121]. A study in which biscuits enriched with protein and fiber were digested in a TIM-1 found that both the degree of starch gelatinization and the degree of starch hydrolysis were greater in samples enriched with fiber and protein than in those enriched with fiber only [395]. The β-glucan content of the meals in our study decreased with increasing MPC80 content (Table 6.3). β-glucan is naturally present in oat grain and competes with starch for hydration, thus reducing the water activity of the solution and, consequently, the swelling, rupture, and amylose leaching of the starch granules [153, 154]. Elevated β-glucan levels have therefore been associated with reduced rates of starch digestion [13, 345]. The fitted induction times in our experiments (Figure 6.3g–i) were similar among the samples, typically between 125 min and 135 min, suggesting that the addition of MPC80 had no influence on that parameter.

6.4.1 *In Situ Gastric Viscosity Measurements*

Luminal viscosity was determined by coupling the TIM-1 with fluorescence spectroscopy using the molecular rotor FG. We first evaluated the sensitivity of the FG to changes in viscosity in glycerol/water and concentrated sugar solutions using the Förster and Hoffman equation [330] (Equation 6.2)

$$I(\upsilon) = \alpha \bullet \upsilon^{x}$$

$$(6.2)$$

where I(v) is the FI, α is proportional to the 'brightness' of the probe, v is the viscosity, and x is a viscosity sensitivity parameter. The value of x for FG in the model systems was between 0.4 and 0.5, similar to the values reported for effective and commonly used molecular rotors in equivalent media [e.g., 0.53 for DCVJ [221]]. To verify the suitability

of FG for the characterization of chyme viscosity, we prepared instant oats with 0 g or 10 g MPC80 and sequentially diluted the preparations to obtain six solutions (oats + MPC80:water 1:0, 1:0.25, 1:0.5, 1:1, 1:2, and 1:3). We evaluated the FIs of the diluted solutions independently. The results shown in Figure 6.3a and b suggest a decrease in FI with increasing dilution of both the oats + 0 g MPC80 solution and the oats + 10 g MPC80 solution. The FI was ~400 a.u. for the undiluted oats + 0 g MPC80 solution (Figure 6.3a) and decreased to 200 a.u. at the 1:3 dilution. The range was wider for the oats + 10 g MPC80 solution (Figure 6.3b), ranging from ~900 a.u. with no dilution to ~200 a.u at the 1:3 dilution. The broadening of the fluorescence range had two possible causes. The desired cause would be an increase in viscosity due to the added protein. The undesirable cause would be the formation of protein-FG complexes, which would hinder the FG rotation upon photoexcitation. Complex formation would yield high FI values, which an untrained analyst might falsely interpret as high viscosity of the medium. More importantly, FG-protein interaction would hinder the technique from characterizing the actual chyme viscosity in the samples with MPC80. Therefore, we performed rheological viscosity measurements, which are independent of molecular rotor interaction, on the same diluted samples to better characterize the relationship between the FI and the viscosity. The rheological findings indicated a non-Newtonian, shear-thinning behavior for all of the tested dilutions (data not shown) across the measured shear-rate range (0.1–400 s^{-1}). It is important to note that shear rates in the GIT have not been adequately analyzed because of the complexity of the digestive system and variability in the shear rates at different locations of the luminal cavity [314]. For example, a shear-rate range of 10–100 s^{-1} was previously proposed to represent the shear along the entire GIT [315],

whereas another research group suggested a shear-rate range of 0.1–10 s^{-1} in the small intestine [316]. In our experiments, the maximum FI was correlated with the corresponding rheological viscosity (Figure 6.3c), yielding a direct linear relationship (R^2 = 0.92) and suggesting that FG is a suitable probe to measure viscosity changes in the oats-based food matrix (with or without MPC80). Therefore, we considered the FI to be a direct indicator of the viscosity.
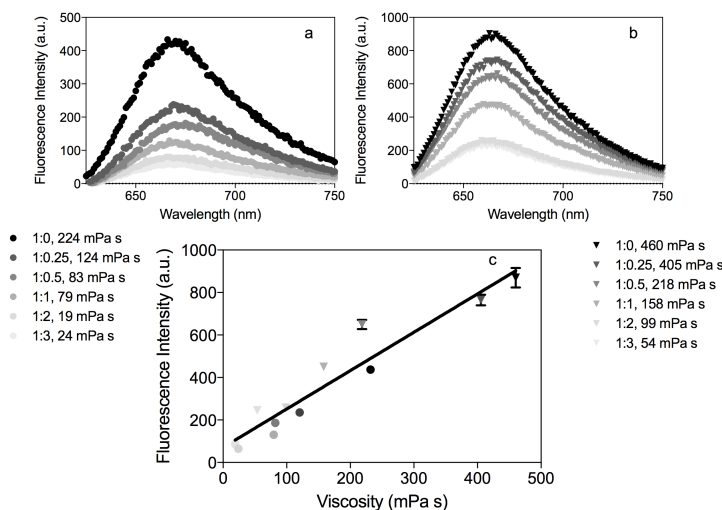
Figure 6.3: FI spectra for dilutions of cooked instant oats with 0 g MPC80 (a) and 10 g MPC80 (b) after the subtraction of the background FI. FI as a function of viscosity (mPa s) (c) for dilutions of cooked instant oats with 0 g MPC80 (•) and 10 g MPC80 (▾).

FG was added to all of the solutions of the TIM-1 apparatus at identical concentrations and the FI was recorded as a function of time in the stomach, duodenum, jejunum, and ileum compartments of the TIM-1. Initially, MPC80-only meals (5 g or 10 g MPC80 mixed with the corresponding amount of water without oats) were fed into the TIM-1 (Figure 6.4); no error bars are presented in Figure 6.4 because those runs were performed only once for each amount of MPC80. The purpose of the initial TIM-1 runs was to obtain gastric digestion-viscosity profiles of MPC80 to be compared to those of the blends of oats and MPC80 (see Figure 6.5). The maximum FI of the MPC80-only

samples recorded for the stomach compartment decreased exponentially and was fitted to

Equation 6.3:

$$I(t) = ae^{-k_2 t} \qquad (6.3)$$

where a corresponds to the initial FI, k_2 is the rate-of-decay curve, and t is time. Table 6.5

shows the parameters of the exponential model (Equation 6.3). The fitted parameters of

the normalized FI vs. time relationships (Table 6.5) suggest a slightly more rapid decay in

oats with 5 g MPC80 (k value of -0.012 min^{-1}) compared with that in oats with 10 g

MPC80 (k value of - 0.01 min^{-1}).
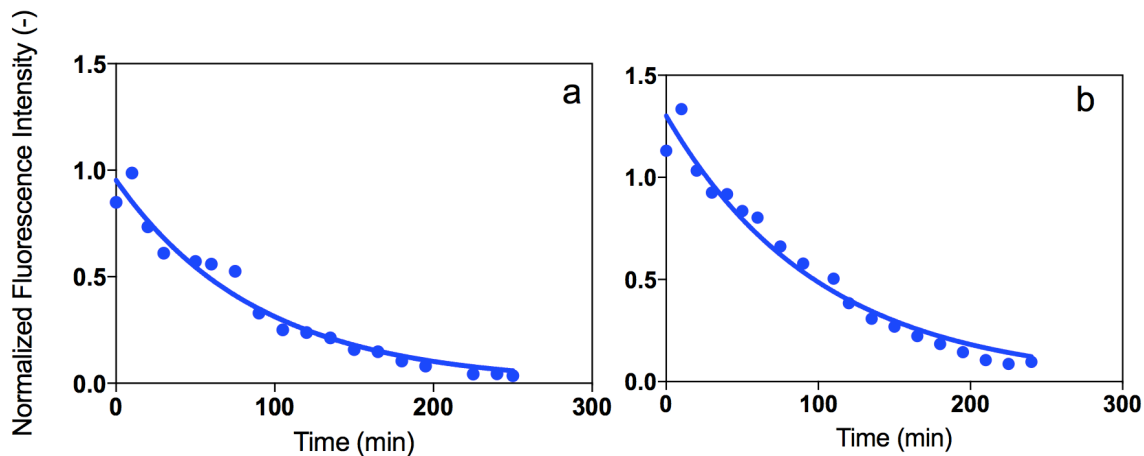
Figure 6.4: Normalized FI in the TIM-1 gastric compartment for a) 5 g MPC80-only meal (5.88 g MPC80) and b) 10 g MPC80-only meal (11.76 g MPC80) as a function of digestion time. Values were normalized to the initial FI of instant oats (Figure 6.5e) to facilitate comparison.

Table 6.5: Parameters of the exponential decay (Equation 6.3) of normalized FI as a function of time for 5 g and 10 g MPC80-only (no oat grain) meals (from Figure 6.4).

Parameters	5 g MPC80	10 g MPC80
Initial intensity in exponential decay (a)	0.88	1.3
Slope of exponential decay (k_2)	0.01	0.01
Mean Squared Error ^	0.0210	0.0046

^ Presented with four decimal digits to better reflect the accuracy of the estimated parameters.

As previously mentioned, the measured FI for all the samples was normalized to

the initial FI of instant oats to facilitate comparisons. We recorded the normalized

maximum FI of the instant oats-based meals with 0 g, 5 g, and 10 g MPC80 (Figure

6.5a-c) in the stomach compartment and fit the measurements to a Fermi model (Equation

6.4):

$$I(t) = I_{min} + \frac{I_{init} - I_{min}}{1 + e^{k_1(t_{c1} - t)}} \tag{6.4}$$

where I_{min} is the minimum observed intensity, I_{init} is the initial observed intensity, k_1 is

the rate of intensity decay, and t_{c1} is the inflection point. Table 6.6 presents the

parameters of the Fermi model. We recorded the normalized maximum FI of the steel cut

oats-based meal with 0 g MPC80 (Figure 6.5d) in the stomach compartment and fit the

measurements to a logistic model (Equation 6.5):

$$I(t) = I_{min} + \frac{I_{max} - I_{min}}{1 + e^{k_3(t_{c2} - t)}} \tag{6.5}$$

where I_{min} is the minimum observed intensity, I_{max} is the maximum observed intensity, k_3

is the rate of intensity increase, and t_{c2} is the inflection point. Table 6.7 (first column)

shows the parameters of the logistic model. The Fermi function is mirror image of the

logistic function [396], which denotes the differences in behavior of the two types of oats.

The gastric viscosity varied depending on the type of oat and the concentration of

MPC80 (Figure 6.5a and d). The gastric viscosity for instant oats (Figure 6.5a) had a

maximum value at the onset and decreased during digestion. Conversely, the gastric

viscosity for steel cut oats increased during digestion (Figure 6.5d). We previously

correlated the gastric viscosity and physico-chemical properties of instant oats-based and

steel cut oats-based meals [389]. Numerous factors contribute to differences in the gastric

viscosity, including: (a) the physical properties of the oat and starch granules, (b) the

consequent influence on the rate of starch gelatinization, and (c) the β-glucan quantity

and quality. The addition of MPC80 to the instant oats resulted in a dose-dependent
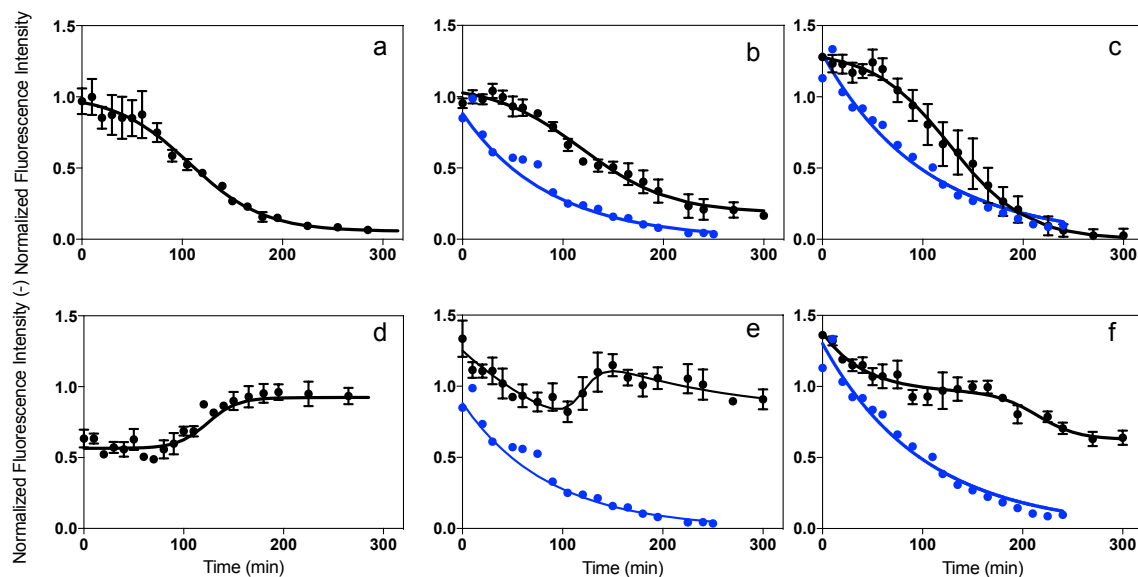
Figure 6.5: Normalized FI in the gastric compartment as a function of digestion time for instant oats (a, b, c) and steel cut oats (d, e, f) with 0 g MPC80 (a and d), 5 g MPC80 (b and e), and 10 g MPC80 (c and f) fitted with the respective models. The MPC80 gastric FIs (Figure 6.4) are re-plotted with the corresponding oat-protein meals (blue data set).

increase in both the initial FI and the inflection point (t_c; Figure 6.5a–c; Table 6.6). The

increase in the initial FI indicates a possible increase in the viscosity of the meal paste

during the hydrothermal meal-preparation process. The apparent viscosity of starch-milk

pastes was previously reported to be higher than that of starch-water pastes [386, 388,

397]. Starch-water pastes are characterized as bi-phasic. The continuous phase is an

aqueous solution containing the amylose leached from the starch granules during

gelatinization, while the dispersed phase is made up of swollen starch granules that

mainly consist of amylopectin [383]. The presence of milk proteins, such as caseins and

whey, has been shown to increase the viscosity of the dispersed phase [398]. Matser and

Steeneken [399] postulated that the gelatinization process in starch-milk pastes creates a

bicontinuous system. The authors suggested that casein micelles are excluded from the starch granules and reside within the voids between the starch granules. That structural alteration is presumed to increase the rigidity and viscosity of the medium [386, 388]. Increases in starch-paste viscosity have been associated with the entanglement of whey proteins [400] and possible cross-linking between starch and casein hydrophilic groups (i.e., –OH, -NH$_2$, -COOH, and –SH) [386, 399, 401].

Table 6.6: Parameters of the Fermi model (Equation 6.4) used to fit the normalized FI values as a function of time for instant oats with various amounts of MPC80.

Parameters	MPC80 (g) Added to Instant Oats		
	0 g MPC80	5 g MPC80	10 g MPC80
Minimum intensity (I_{min})	0.06	0.19	0.1
Initial intensity (I_{init})	1.01	1.08	1.32
Slope (k_1, min^{-1})	0.03	0.02	0.03
Inflection point (t_{c1}, min)	107.00	119.00	127.00
Mean Square Error ^	0.0010	0.0018	0.0017

^ Presented with four decimal digits to better reflect the accuracy of the estimated parameters.

Table 6.7: Parameters of the logistic model (Equation 6.5) and the additive-contributions model (Equation 6.6) that were used to fit the normalized FI values as a function of time for steel cut oats with different amounts of MPC80.

Parameters	MPC80 (g) added to Steel Cut Oats		
	0 g MPC80 *	5 g MPC80 **	10 g MPC80 **
Minimum intensity (I_{min})	0.57	0.31	0.96
Maximum intensity (I_{max})	0.92	0.79	0.63
Slope (k_3, min^{-1})	0.07	0.10	0.05
Inflection point (t_c, min)	124.00	121.00	215.00
Initial FI in exponential decay (a)	-	0.94	0.42
Rate of exponential decay (k_2, min^{-1})	-	0.01	0.02
Mean Square Error ^	0.0018	0.0005	0.0013

Asterisks indicate the model used to fit the experimental data in Figure 6.5: * Equation 6.5 and ** Equation 6.6.
^ Presented with four decimal digits to better reflect the accuracy of the estimated parameters.

The inflection point represents the time required to produce half of the total change in FI, implying an ability of the gastric chyme to resist reductions in viscosity during digestion with the addition of MPC80. Caseins are the most abundant protein in MPC80 and are able to form gels under acidic conditions by denaturing [402]. MPC80-only gastric FI trends (Figure 6.4) were re-plotted (blue data set) with the corresponding oats + MPC80 meals in Figures 6.5b and 6.5c to illustrate that the two sets (blue vs. black) follow different trends. This suggests that the recorded fluorescence indicated changes in the instant oats + MPC80 chyme. The addition of MPC80 to the steel cut oats modified the FI over time (Figure 6.5d vs. Figure 6.5e and f). The addition of MPC80 contributed to the degradation in the FI of the steel cut oats-based meal between the initiation of digestion and 100 min of digestion in a manner that resembled the corresponding MPC80-only gastric FI trends (blue data set). Beyond 100 min of digestion, the mixtures of 5 g MPC80 and steel cut oats (Figure 6.5e) underwent an increase in FI comparable to that of steel cut oats + 0 g MPC80 (Figure 6.5d). In addition, the experimental data of the oats + 5g MPC80 (Figure 6.5e) corresponded very closely to the sum of the independent contributions of steel cut oats + 0 g MPC80 (Figure 6.5d) and 5 g MPC80 only (Figure 6.4a). Those observations imply the possibility of an additive effect between MPC80 and steel cut oats. We therefore generated an equation (Equation 6.6) in which the logistic (Equation 6.5) and exponential (Equation 6.3) models are summed to express the respective contributions of steel cut oats and MPC80 to the overall FI trends in Figures 6.5e and 6.5f:

$$I(t) = \left\{ I_{min} + \frac{(I_{max} - I_{min})}{1 + e^{k_3(t_{c2} - t)}} \right\} + ae^{-k_2 t} \qquad (6.6)$$

The experimental initial FI value was 1.25 (Figure 6.5e) and is depicted in Table 6.7 as the sum of the *a* and I_{min} parameters (0.94 and 0.31, respectively). The initial FI value attained from the experimental data was larger for the steel cut oats + 5 g MPC80 (1.25) than for the steel cut oats without MPC80 (0.75), suggesting that the addition of 5 g MPC80 to the steel cut oats increased the luminal viscosity in the gastric compartment. The k_2 term (Table 6.7) illustrates the slope of the initial decrease in FI (0.01). Subsequently, the FI of steel cut oats + 5 g MPC80 increased from 100 min to 150 min of digestion (Figure 6.5e). In comparison, the 5 g MPC80-only meal (blue data set, Figure 6.5e) showed a minimal contribution to the FI during the corresponding time frame. Given the complexity of the system, we deduced that the increase in viscosity is a function of the interdependence of the system components. Soluble fiber (1→3)(1→4) β-D-glucan is a constituent of oat grains [80-82]. β-D-glucans are widely acknowledged for their thickening ability due to the binding of water to form a water-entrapping, non-starch polysaccharide network in the GIT [11, 12]. Kim and White [380] treated heated oat slurries with α-amylase to hydrolyze starch and with lichenase to hydrolyze β-glucan to illustrate the contribution of the two polysaccharides to viscosity. The lichenase treatment resulted in a higher viscosity than the α-amylase treatment, suggesting that starch is the major contributor to oat-slurry viscosity. The k_3 term (Table 6.7) represents the slope (0.1) of the increase in FI between 100 min and 150 min of digestion, during which the inflection point occurs at 121 min, which is slightly more rapid than the inflection point of 0 g MPC80 (~124 min). In the case of the addition of 10 g MPC80 to steel cut oats (Figure 6.5f), the effect of both contributions is less discernible, and the interpretation of the parameters is less straightforward. We also used Equation 6.6 to fit the data from the

stomach for the steel cut oats + 10 g MPC80 (Figure 6.5f). Although the first part of the dataset shows a decrease that could be characterized by the sum of the protein exponential decay, the second part of the graph shows a different regime from that of 0 g and 5 g MPC80 + steel cut oats, probably because of changes in the matrix. Therefore, the obtained parameters of Equation 6.6 for the steel cut oats + 10 g MPC80 sample are not representative of the same regions of the curve represented by those parameters for the steel cut oats + 0 g and 5 g MPC80 samples. We also analyzed the normalized FI as a function of time in the duodenum, jejunum, and ileum compartments (data not shown). In a previous publication [389], we observed an approximately 10-fold reduction in intestinal viscosity compared with the gastric-compartment viscosity. We ascribed that result to the automated and pre-determined gastric-emptying rate that allows for the uniform passage of small particulates into the small intestine.

6.5 Conclusion

We added MPC80 to instant oats-based and steel cut oats-based meals at two doses, 5 g and 10 g, to determine the changes in luminal viscosity and carbohydrate digestion *in vitro*. The total bioaccessible sugars significantly decreased with the addition of increasing amounts of MPC80 and increased with increasing available starch content. The rate of starch hydrolysis was positively correlated to the amount of MPC80 in the meals. The metabolic response to dietary starch is a function of the rate of starch hydrolysis/digestion [16, 17]. Therefore, an understanding of the kinetics of starch digestion offers opportunities to control the postprandial glycemic response [18]. FI measurements suggest a progressive increase in gastric viscosity with increased addition of MPC80. Luminal viscosity decreases both α-amylase motility and access to the starch

substrate and glucose bioaccessibility [72, 153, 369]. Gastric viscosity has also been associated with increasing distention in the stomach cavity, which was repeatedly correlated with increasing sensations of satiety [310, 311]. A better understanding of such relationships between food form and formulation may be useful in the design of food products intended for patients with specific diet-related chronic diseases, such as diabetes, with pre-determined physiological impact.

7 Biophysical Aspects of Lipid Digestion in Human Breast Milk and Similac$^{\text{TM}}$ Infant Formulas

7.1 Abstract

Physico-chemical properties of human breast milk were compared to four Similac$^{\text{TM}}$ infant formulas, and correlated with *in vitro* free fatty acid bioaccessibility using a simulated gastrointestinal system (TIM-1). Viscoelastic measurements, as a function of pH (pH 6.5 to 3.0) and shear rate, showed lower viscosities in breast milk compared to infant formulas. Droplet size and distribution measurements showed distinct differences between the tested formulas and breast milk. During lipid digestion, a lag period was observed for only breast milk. The rate of lipolysis was found to be higher in breast milk compared to Similac$^{\text{TM}}$ formulas. The total bioaccessible free fatty acids for Advance infant formula and breast milk were not statistically different for the *in vitro* TIM-1 model and the shifted-logistical model using one-way ANOVA ($p < 0.05$) with a Tukey's Multiple Comparison Test. All other infant formulas had significantly lower free fatty acid bioaccessibilities at the end of the simulated digestion. A positive correlation between rate of lipolysis and droplet surface area per gram for the Similac$^{\text{TM}}$ infant

formulas was found. However, breast milk did not follow that trend, suggesting the possible involvement of other factors in rate of lipolysis for breast milk.

7.2 Introduction

Childhood obesity is an alarming universal epidemic where the rate of incidence has precipitously increased over the last 25 years.[403-409] It was reported in the 1980s, that 7.2% of 6 to 23 month old children in the United States were classified as obese and this has increased to 11.6% by 2000.[410-412] Amongst the numerous adverse health effects associated with childhood obesity is Type 2 diabetes; once a disease explicit to adults, now half of recently diagnosed incidences of diabetes are adolescents.[20] It has also been noted that the prevalence of childhood obesity is lower in breast-fed infants compared to formula fed infants.[21-23] Regrettably, the mechanism responsible for this correlation is not understood.[24] Numerous hypothetical links between obesity and breast feeding pertain to the passive nature of bottle-feeding, regardless of the type of milk, versus active suckling when infants are fed directly at the breast, [24, 25] the hormones and adipokines in breast milk,[26-32] the rates of gastric emptying,[413, 414] and the rate of the ileal break in emulsions.[415] Accordingly, supplemental in-depth studies comparing the physico-chemical properties and digestibility of breast milk and infant formula are imperative.

The high caloric density and functionality of the lipid composition in both breast milk and infant formulas may be considered an important marker of their nutritional quality. At birth, there is a switch from a glucose-dominated to a lipid-dominated energy supply since fat constitutes half of the energy content in breast milk and infant formulas.[416] This presents major challenges to the digestive system, because of the

poor solubility of lipids, which must first be converted to structures that are less insoluble and available for uptake. Despite these limitations, the human digestive system is effectively designed at digesting and absorbing most lipids.[417] Key reactions, such as adsorption of digestive lipases and emulsification of fatty acid and monoglyceride during digestion, must take place at the oil-water interface to solubilize lipids and lipid soluble nutrients.[418]

Lipid hydrolysis depends on the ability of lingual, gastric and pancreatic lipases, to access the interface, which depends on both the action of bile salts and co-lipase. It is believed during infant digestion, lingual lipase, which does not require co-factors, may play a more significant role in digestion due to the immaturity of the pancreatic lipase system.[419] von Ebner's glands of the human tongue secrete lingual lipase [420]; which facilitates initiation of digestion of triglyceride components of the milk when it reaches the stomach. [421] It is reported that milk fat globular exposure to lingual lipase prior to exposure to pancreatic lipase results in increased rate of lipolysis.[422] Another lipase that is considered to be of interest with regards to infant digestion of milk fats is bile salt-stimulated lipase (BSSL); [423] which is understood to be of maternal origin, produced in the human mammary glands.[424, 425] BSSL is unique, in its ability to hydrolyze the 3 *sn*-positions of a triglyceride, thus generating free fatty acids and glycerol.[426, 427] BSSL is reported to withstand (dormant) the infant stomach pH, while resuming its activity in gastrointestinal areas where elevated levels of bile salt are available.[428-430] [431-433] Bile salts not only facilitate the adsorption of co-lipase and lipase, but also aid in the solubilization of the lipolysis products as they accumulate at the interface, into mixed micelles, allowing the transport to and through the gut mucosal surface.[417] The

gut cell lining is then able to sense these nutrients and in response, secrete hormones and peptides that slow digestion and send signals to the brain that reduce appetite.[434] Michalski *et al.* [435] found infant formula fat droplets to be smaller than human milk fat droplets and that the milk fat globule surface area, required for lipolytic activity, is relevant to lipid digestion.[436] In addition it has been shown that human milk has a greater lipid bioaccessibility during the gastric digestion than infant formula. [437] We hypothesize that a correlation lies between the physico-chemical properties of these different infant formulas and breast milk and the bioaccessibility/digestion of their lipid composition. Digestion refers to the process of disassembling food macronutrients into absorbable units, [438] while bioaccessibility of a nutrient refers to its potential to be absorbed.

In the present work, we investigate the physico-chemical properties of human breast milk and infant formula by light scattering, to illustrate droplet size and distribution, as well as rheological viscosity measurements. The TNO Intestinal model (TIM-1), an *in vitro* model that simulates the upper gastrointestinal tract, was used to monitor the bioaccessible free fatty acids generated throughout a 5-hour simulated digestion. A study on the effect of partially hydrolysed guar gum on fat bioaccessibility showed good correlations between the TIM-1 and *in vivo* bioaccessibility data.[439] Free fatty acid release profiles are described for each of the tested infant milks and a shifted logistical model, developed by Troncoso *et al.,*[354] was used to elucidate the rate of lipolytic generation of free fatty acids as a function of time.

7.3 Method

7.3.1 Materials and Sample Preparation

Similac ^{TM} (Abbott Nutrition, OH, USA) infant formulas (Total Comfort, Sensitive, Soy, and Advance) were prepared, immediately before analysis, as per the label instructions. ~8.8 g of dry powered formula was added to 2 oz of distilled tap water and mixed with a magnetic stirrer until homogenous. Human breast milk was expressed (as per IRB Protocol 13-824M) on the same day of the corresponding experiment and stored at 4°C while being mixed thoroughly to prevent creaming.

7.3.2 Light Scattering

Droplet size in the infant formulas and breast milk were studied using light scattering (Masterisizer 2000, Ver 5.54, Malvern Instruments Ltd., Malvern UK). The ultrasound was not used to ensure that particle size reduction did not occur. Instead, constant stirring at 2700 rpm was used to prevent creaming. A refractive index (RI) of 1.42 (approximate RI of oils) was used for particle size determination.[440] Five replicates were conducted for each sample and the average droplet size distribution (in μm) was used for data analyses. Standard deviation of the maximum, minimum, and mean diameters, as well as the surface area and Sauter mean diameter (D[3,2]) values were determined for each of the five formulas and averaged.

7.3.3 Viscosity at different pH

The initial pH of the infant formulas and breast milk all fell between 6.5 and 7.0. Using 1 M hydrochloric acid, each sample was acidified from pH 6.5 to 3.0 in 0.5 increments. For each pH, six replicates were run on a Discovery Hybrid Rheometer (TA

Instruments, DE, USA) to measure viscosity as a function of shear rate. A temperature controlled peltier plate and a 6 cm stainless steal cone (cone angle (3 deg: 59 min: 20 sec) and truncation (105 μm)) was set at 37 °C, and a logarithmic shear rate sweep from 0.5 to 500 s^{-1} was used to determine the rheological properties. The points per decade of data collection were limited to ensure that the run did not exceed 5 min, this was in part to prevent phase separation from occurring, no macroscopic separation was observed during the viscosity measurements.

7.3.4 TIM-1 Simulated Digestion

The TIM-1 (TNO, Zeist, The Netherlands) simulated gastrointestinal tract was used to mimic the gastrointestinal tract of infants and the lipid digestion of breast milk and Similac^{TM} formulas. TIM-1 consists of four compartments representing the stomach, duodenum, jejunum and ileum. Duodenal start residue (60 g; 15 g SIES, 30 g fresh porcine bile, 2 mg trypsin solution (bovine pancreas (7500 N-α-benzoyl-L-arginine ethyl ester (BAEE) units/mg, T9201) was obtained from Sigma Aldrich), 15 g pancreatin solution), jejunal start residue (160 g: 40 g SIES, 80 g fresh porcine bile, 40 g pancreatin solution), and ileal start residue (160 g SIES) were injected into their respective compartments prior to heating the system to physiological temperature (37 ˚C) in preparation for feeding. Also, prepared solutions simulating bile, gastric and pancreatic secretions were attached to the TIM-1. Pancreatin was obtained from Sigma Aldrich, USA. Fresh pig bile (Farm-to-Pharm (Warren, NJ, USA)) was collected from a slaughterhouse, standardized by pooling numerous collections, aliquoted into single use amounts for individual TIM experiments, and then stored at -20 ˚C until use. Enzyme solutions were placed in ice, until they were used to fill the TIM-1. Although the same

lot of each enzyme was consistently used for each run, it is important to note that biological differences exist between commercially available enzymes and enzymes present *in vivo*. Therefore, the absolute values obtained from the simulated digestions may not be biologically relevant, however, the changes observed between each sample are relevant.

Also, Modifications to the solutions (a), software program (b), fed sample(c), and total digestion period/run (d) were implemented to mimic the human infant gastrointestinal conditions.

(a) Modified solutions attached to the TIM-1 to simulate infant conditions: only 75 % of the 7 % pancreatin solution (Pancrex V powder, Paines & Byrne, UK) was utilized; the small intestinal electrolyte solution constituted of NaCl 5 g/L, KCl 0.6 g/L, CaCl2 0.25 g/L. the initial gastric enzyme solution included 150 g gastric electrolyte solution, 28.1 mg of lipase (Rhizopus lipase (150,000 units/mg F-AP-15), obtained from Amano Enzyme Inc. (Nagoya, Japan)), and 22.5 mg pepsin (from porcine gastric mucosa, lyophilized powder, >2,500 units/mg protein, Sigma Aldrich) (pepsin and lipase quantities used are 75% of the quantity typically used in an adult-digestion simulated TIM-1 experiment); the solution was mixed for 10 min at room temperature.

(b) In addition, the TIM-1 system protocol used was that of the 'infant fed-state'; thus controlling peristaltic movements, nutrient and water absorption, gastric emptying, pH, enzyme secretion rates and transit times to be similar to the *in vivo* gastrointestinal environment of the human infant.[353] The software provides the following conditions in the respective TIM-1 compartments (Table 7.1).

Table 7.1: Software pH values of TIM-1 stomach throughout 5-hour digestion period to mimic human infant gastrointestinal conditions.

Digestion Time (Min.)	pH value
0	6.5
30	6.5
150	4.5
240	3.5
300	3.5

(c) The total sample fed into TIM-1 was reduced to 200 g (67 g of gastric electrolyte solution and 133 g meal), while an adult run would involve feeding 300 g of total fed sample.

(d) Five hour simulated digestions were performed to mimic the suggested transit time to the cecum in infants.[441] Samples were collected from the jejunal and ileal filtrates and ileal efflux at 30, 60, 90, 120, 180, 240, and 300 min and then frozen ($\sim$ -40 ^{o}C) until extraction.

7.3.5 *Experimental Meals*

The gastric electrolyte solution (8.25 mg of amylase and 5 g of the above mentioned gastric electrolyte solution) was mixed with 133 g of the sample, and fed into TIM-1 after the four GI compartments were heated to 37 °C. 133 g of the mixed sample was then fed to the TIM-1 standardizing the amount of fat ($\sim$5 g fat in each meal) fed to the TIM-1 allowing the bioaccessibility to be approximated. To fill the gastric compartment a 200 g meal was fed for the infant model, therefore 67 g of gastric electrolyte solution was added to the 133 g meal.

7.3.6   Free Fatty Acid Extraction

The fatty acid concentrations from the jejunum, ileum and ileum efflux, at each of the aforementioned time intervals, were thawed and extracted in duplicate. Fatty acids were extracted by first adjusting the pH of 5 mL of filtrate to a pH value between 10-12 using 10 N NaOH. 200 μl of 5 mg/ml nonanoic acid was added to serve as an internal standard and 15 ml dichloromethane was added. After 24 hrs, the organic and aqueous layers were separated and the bottom dichloromethane layer was discarded. 1 N HCl was added reducing the pH to between 1-2 and 5 mL dichloromethane was added. After 24 hrs the layers were separated and the bottom layer was collected and frozen at -20 °C until further analyses.

7.3.7   High-Performance Liquid Chromatography (HPLC) analysis of Free Fatty Acids

The extracted free fatty acids, from the TIM-1 runs (completed in duplicated) were analyzed using High-Performance Liquid Chromatography (HPLC) (Alliance, Waters e2695) with 2424 Evaporative Light Scattering (ELS) Detector (Waters). A reverse phase free fatty acid HP 4μm (3.9x150 mm) column (Waters, Milford, MA, USA) was used. The stroke volume for the system was 50 μL; and a gradient pump mode was used. Ideal separation occurred when the solvents selected were: 35% Water HPLC Grade 0.22 micron filtered (Pharmco-Aaaper, Brookfield, CT, USA), 20% Tetrahydrofuran (THF) stabilized with 250 ppm BHT (OmniSolv, Bellerica, MA), and 45% Acetonitrile HPLC Grade (EMD Chemicals, Inc., Gibbstown, NJ, USA). The column temperature was set at 30 ± 5 °C. Each of the extractions was run in the HPLC and two injections were taken for each replicate. Accordingly, twelve chromatograms

were attained for each sample at every collection interval (30, 60, 90, 120, 180, 240, and 300 min) at each of the small intestine locations (i.e., jejunum, ileum, and ileal efflux).

7.3.8   Determination of Bioaccessibility

Samples fed to the TIM-1 were controlled to contain 5 g of fat allowing the bioaccessibility to be determined. The % dispersed phase volume, determined with light scattering, for the infant formulas and breast milk were not statistically different and assuming that the fats have the same density it was assumed that they had similar fat contents (albeit it should be mentioned that differences in density may be a potential source of error). From a computational standpoint, the triglyceride composition in the samples was assumed to have the molecular weight of triolein and that 2 mols of oleic acid are released per mol of triolein (i.e., of the 5 g of fat fed 3 g of fatty acids may be released) (Equation 7.1):

$$\text{Maximum Bioaccessability} = \frac{\text{feed fat}}{MW_{TO}} \text{ x2 MWOA} \tag{7.1}$$

where MW_{TO} is the molecular weight of triolein, MW_{OA} is the molecular weight of oleic acid.

7.3.9   Statistical analysis

A one-way ANOVA ($p < 0.05$) with a Tukey's Multiple Comparison Test (Graph Prism 5.0 (La Jolla, CA) was used to determine the statistical significance in the means.

7.4   Results and Discussion

Lipid droplet size distributions of Sensitive, Total Comfort, Advance, and Soy formulas were compared to human breast milk (Figure 7.1). Breast milk has three primary distributions of particle sizes (~ 0.1, 1 and 7 µm), which have been previously

reported,[442] while the Total Comfort infant formula has a single distribution of particles at ~ 0.4 μm and Advance, Soy, and Sensitive formulas have two distinct peaks, one at 0.4 μm and the other at 3 μm. Variations in the individual particle size volumes are shown in Figure 7.1. Based on these results, it is evident that the particle size distribution varies distinctly between infant formulas and breast milk.

The effects of pH on viscosity (Pa s^{-1}) were determined, for the formulas and breast milk, using strain rate sweeps from 5 – 500 s^{-1} (data not shown). Initially, the pH for each sample was between 6.5 and 7, following they were incrementally (every 0.5) acidified using HCl to the pH of an infant's stomach pH ~ 3.[443] Upon feeding, the pH of the gastric compartment is buffered to near the initial pH of the formula/milk, after which the pH decreases until it returns to the initial pH of the stomach.[443] It was apparent that the non-acidified formulas behave as Newtonian fluids and the viscosity is independent of pH. However, as the meals are acidified the viscosity not only increases but the solution behavior changes to a non-Newtonian shear-thinning fluid (data not shown). Since non-Newtonian fluid behavior is observed, a single strain rate of 20 s^{-1} was arbitrarily selected and was plotted against each pH value to allow statistical comparison (Figure 7.2). Enzymatic reactions are dependent on the solution properties, including the viscosity, and can possibly play a role in digestion. Viscosity alters the rate of gastric emptying, postprandial glucose concentrations, and satiety.[444] Various researchers agree upon the presence of a positive correlation between the viscosity of the ingested meal and both gastric emptying and satiety sensation.[308-311] However, the role of viscosity, throughout its transit time in the gastrointestinal tract, is not understood. The question remains, if it is the initial viscosity of the meal or its changing viscosity in

the gastrointestinal tract that plays a role in satiety. The viscosity of both Sensitive (Figure 7.2A) and Advance (Figure 7.2C) remain unchanged from their initial pH value to pH 5.5. Upon further acidification there is a dramatic increase in the viscosity after followed by decrease in viscosity. Similar patterns are seen in Total Comfort (Figure 7.2B) and Soy (Figure 7.2D); however, these samples have the same viscosity at the extreme pH values tested. Breast milk does not follow similar trends to the infant formulas; instead, the viscosity of breast milk does not drastically change between pH values of 6.5 and 4.0, and it is not until a pH of 3.5 that an increase, albeit not dramatic, in the viscosity is observed.
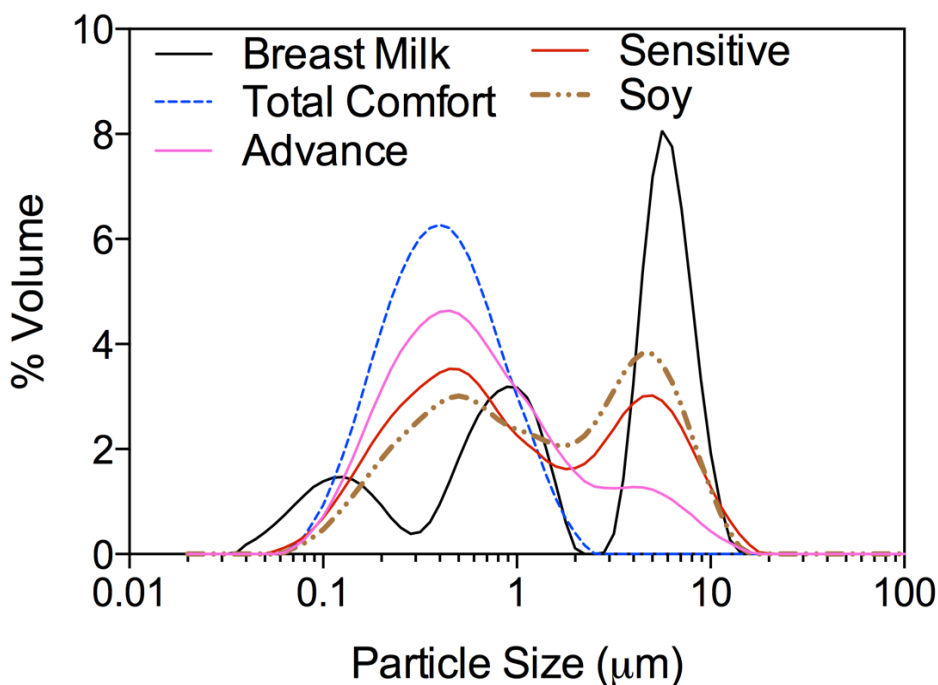
Figure 7.1: Particle size distribution for Similac [TM] **brand types: Sensitive, Total Comfort, Advance, and Soy compared to human breast milk.**

The maximum viscosity for Sensitive is pH 5.0 (Figure 7.2A), for Total Comfort 4.5 (Figure 7.2B), Advance and Soy are 4.0 (Figure 7.2C and 2D), and breast milk is 3.0. Advance, Total Comfort, and Soy had statistically similar viscosities between pH 5.5 and

6.5; while Sensitive was significantly higher at pH 6.5 and 6 and lower at 5.5. Similar pattern are seen at pH 4.5; however, there is no significant difference between Sensitive (0.023 Pa s^{-1}) and Advance at this pH. At all pH values tested, the viscosity of breast milk is statistically lower than the infant formulas with the exception of at pH 3.0 where both Total Comfort and Soy had lower viscosities. In addition, breast milk had the lowest viscosity between 4.0 and 6.5. It is clear that significant differences exist in both the droplet sizes and the viscosity profiles between infant formulas and breast milk; however, it is unclear if these physical differences correlate to differences in lipid bioaccessibility.
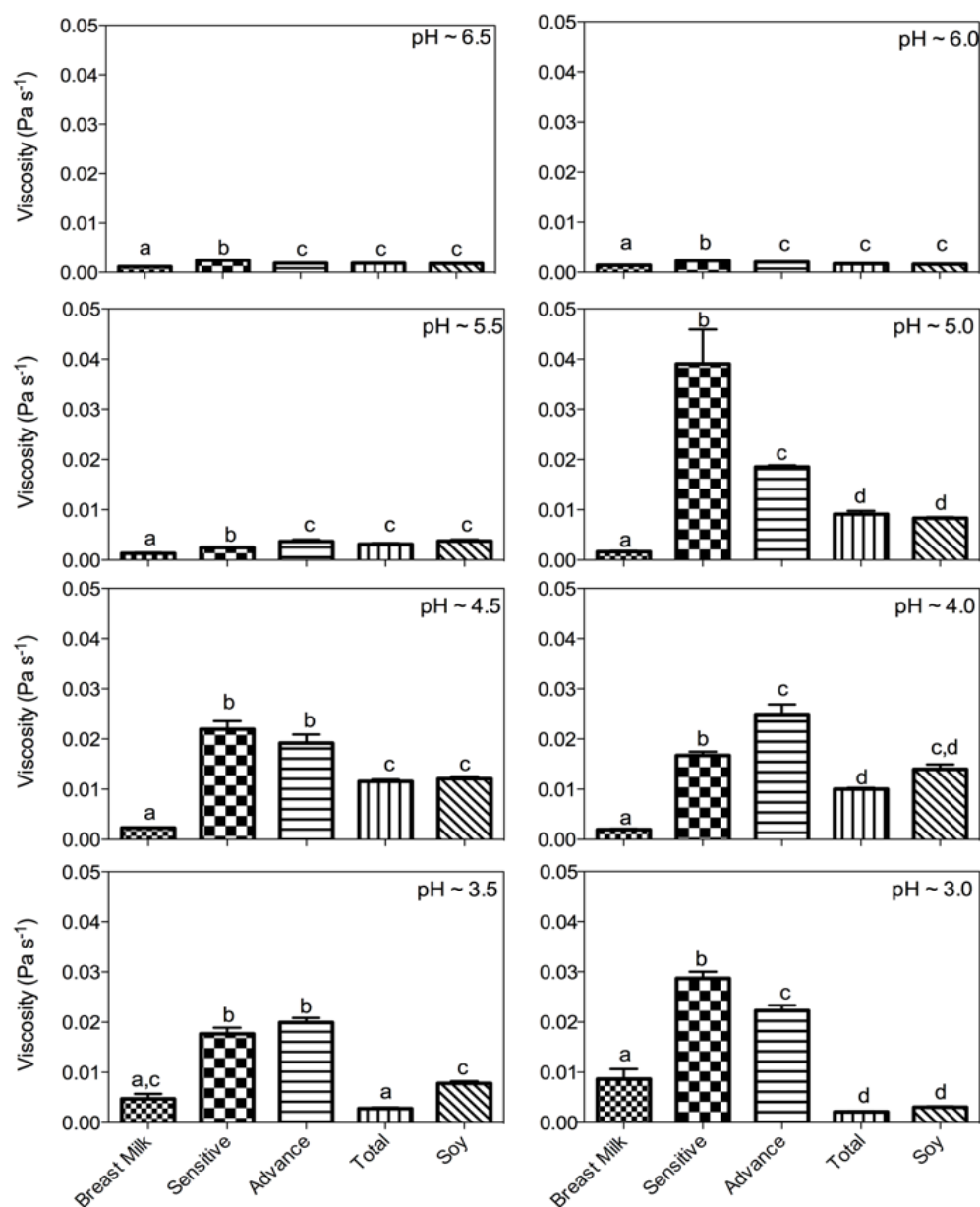
Figure 7.2: Viscosity determined at 20 s^{-1} for Sensitive, Total Comfort, Advance, and Soy based infant formulas compared to human breast milk at pH values between 3.0 and 6.5. Different letters represent significant differences determined using a one-way ANOVA (P<0.05) and a Tukey's Multiple Comparison Test.

The TIM-1 (TNO, Zeist, The Netherlands) simulated gastrointestinal tract was used to quantify the absolute, non-cumulative bioaccessible fatty acids in the jejunum (Figure 7.3), ileum (data not shown) compartments of the small intestine, as well as the

ileal efflux (data not shown). In the Sensitive, Total Comfort and Soy, there is an initial rapid release of fatty acids at the first time point measured and as time progressed the concentration of free fatty acids decreased in the jejunum (Figure 7.3A, B, and D). Fatty acids bioaccessibility increases with time and plateaus at ~200 min for the Advance formula (Figure 7.3C). In all infant formulas, no lag time for lipolysis is observed. Interestingly, in only the breast milk, there is a significant lag (~90 min) before appreciable amounts of fatty acids are released (Figure 7.3E) in the jejunum.

The cumulative free fatty acid, in the jejunum (Figure 7.4A) and ileum (Figure 7.4B), have similar release profiles for Sensitive, Soy and Total Comfort; while the Advance has a greater free fatty acid bioaccessibility. After 300 min of digestion, approximately 1850 mg and 500 mg of fatty acids were bioaccessible in the jejunum and the ileum for Advance. On the other hand, in Sensitive, Soy, and Total Comfort ~250 mg and ~150 mg fatty acids are bioaccessible in the jejunum and ileum. Unlike the infant formulas, breast milk has a significant lag period and even with this delay in lipid digestion, breast milk still provides a total of ~1000 mg and ~400 mg of bioaccessible free fatty acids in jejunum and ileum. Given that breast milk contains maternal BSSL, endogenously, this could lead to the conclusion that the initial interfacial layer is extremely apt at preventing pancreatic lipase from accessing the lipid droplet interface.
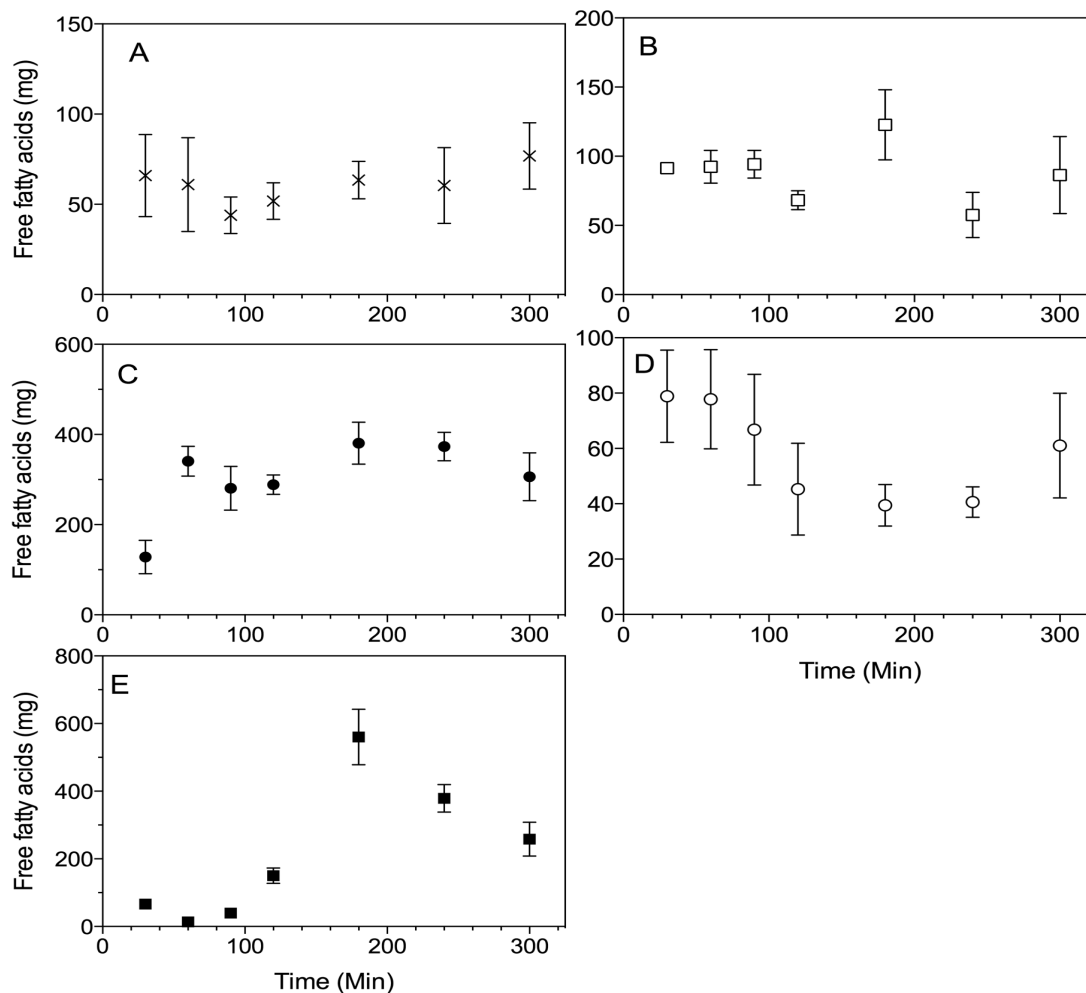
Figure 7.3: Total fatty acids per given time point in the jejunum and ileum (TIM) for (A) Sensitive, (B) Total Comfort, (C) Advance, and (D) Soy based infant formulas compared to (E) human breast milk.

This lag phase was also reported by Bernback *et al.* [427] in human breast milk triglycerides upon *in vitro* hydrolysis with gastric lipase, colipase-dependent lipase, and BSSL. Similarly, Berton *et al.* reported a similar lag phase for hydrolysis of triglycerides in raw, non-homogenised cow's milk by human pancreatic lipase.[445] Structurally, breast milk fat globules differ from those of infant formula. Breast milk fat globules consist of a triglycerides core, enveloped by a membrane of phospholipids, cholesterol and protein;[446] whilst infant formula fat globules consist of a triglycerides

core, surrounded by phospholipids.[437] Lindstrom *et al.,*[447, 448] found barrier properties of phospholipids against BSSL hydrolysis and that pancreatic colipase-dependent lipase hydrolysis activity was found to be constrained by the presence of phospholipids and proteins.[449] Accordingly, the constituents of the human breast milk fat globule membrane could play a role in delaying the initiation of the triglyceride hydrolysis process, thus resulting in the lag period evident in lipid digestion. It is reported that minimal hydrolysis does occur during this lag phase;[450] hence possibly modifying the fat globule membrane composition by increasing its fatty acid and diacylglycerol composition.[445] As a result, the lipases' access to the human breast milk fat globules' triglyceride core is facilitated following the lag phase, allowing for hydrolysis to take place.[445]

The absence of the lag phase in infant formulas could be explained by referring to Figure 7.1, which illustrates that the bulk of the droplet size distribution in the various infant formulas is ~ 0.4 μm. Thus, the lipase will be more capable of accessing the triglyceride core when compared to the breast milk fat globules, whose particle size distribution contains mostly larger size droplets (i.e., 1 μm and 7 μm diameters). These differences in the rate of fatty acid release and the presence of a lag period in breast milk, in both the jejunum and ileum may play a role in satiety. It is extremely important to note however, there is not scientific evidence as of yet to support this.

The overall fatty acids bioaccessibility (Figure 7.4C) is a combination of the fatty acids released from the jejunum and ileum. Fatty acids that were not removed via the jejunal and ileal filtrates were measured at the outlet of the ileal compartment (Figure

7.4D). Similar trends, albeit at much lower concentrations, were observed between the

jejunum and at the ileal efflux.
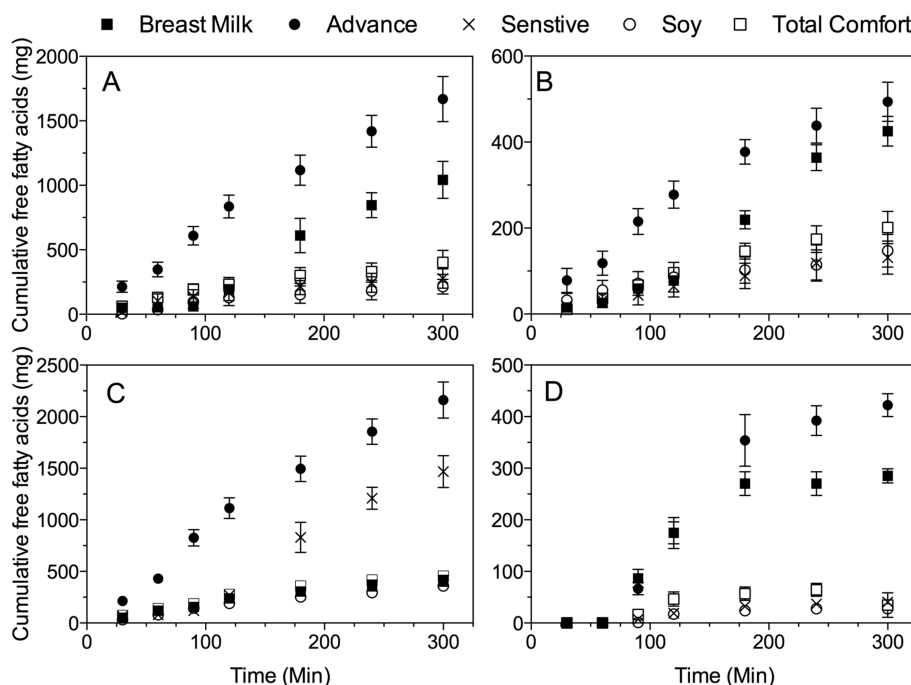
Figure 7.4: Total fatty acids bioaccessibility for Sensitive, Total Comfort, Advance, and Soy based infant formulas as well as human breast milk in various parts of the simulated *in vitro* (TIM) gastrointestinal tract; A) jejunum, B) ileum, C) combined jejunum and ileum, and D) efflux.

The total fatty acid bioaccessibility, in Figure 7.4C at 300 min, was the sum of the

fatty acids measured in the ileum and jejunum filtrates. The bioaccessibility from highest

to lowest are: Advance (~74.5 ± 6.1 %), breast milk (~50.6 ± 5.3 %), Total Comfort

(~24.5 ± 5.56 %), Sensitive (~14.1 ± 3.9 %) and Soy (~12.4 ± 2.7 %). Using a one-way

ANOVA, no significant differences between fatty acid bioaccessibility in breast milk and

Advance was found and Total Comfort, Sensitive, and Soy are not statistically different

from one and other. Breast milk and Advance fatty acid bioaccessibility are significantly

higher than the remaining Similac[TM] infant formulas tested.

A three-parameter shifted logistic model (Equation 7.2) [353-355] was used to characterize the free fatty acids generated as a result of lipolytic activity in each digestive compartment as a function of time, t:

$$C(t) = \frac{C_{asymp}}{1 + e^{[k(t_c - t)]}} - \frac{C_{asymp}}{1 + e^{[kt_c]}}$$

(7.2)

where C_{asymp} is the total amount of fatty acids released, k is the rate of release of fatty acids per unit time, and t_c is the critical time at which half of the total amount of fatty acids is released.[353] Through the use of nonlinear analysis in Graphpad Prism (La Jolla, CA), the three bioaccessibility parameters determined from Equation 7.2 (C_{asymp}, k, and t_c) were analysed.

Upon fitting the shifted logistic model to the free fatty acid bioaccessibility curves (Figure 7.4C), the theoretical bioaccessibility (C_{asymp}) (Table 7.2) showed similar trends compared to what was observed at 300 min of simulated digestion from the *in vitro* digestion. The critical time, t_c, is a parameter which combines the initial lag time, the rate of fatty acid release and the duration of lipolysis. It is evident that breast milk had a much longer T_c compared to the infant formulas, coinciding with our *in vitro* observation of a lag time presented earlier. It has been well established that there is an inhibitory effect of the native milk fat globular membrane on pancreatic lipase activity.[451] No major differences were found between the studied infant formulas. The rate constants, K, for the infant formulas were very similar while breast milk had a much higher rate of release.

Table 7.2: Fitted parameters from equation 7.2 including the total fatty acids released, induction time, and rate of release in jejunum and ileum in the TIM-1.

	Sensitive	Total Comfort	Advance	Soy	Breast Milk
FFAs released (C_{asymp}) (mg)	725	796	3000	739	1534
Induction time (T_c) (min)	48	41	79	38	175
Rate constant (K) (mg/min)	0.0106	0.012	0.0099	0.0083	0.0245

Two different phenomena can account for the differences observed in the rate constants. First, interfacial lipase activity is dependent on the amount of surface area available for the reaction to progress. Therefore, the particle size and particle size distribution may account for differences in the reaction rates, as discussed earlier. As well, breast milk has endogenous maternal BSSL, which could account for the elevated reaction rate in breast milk. Bernback *et al.,*[427] show that the addition of only gastric lipase and colipase-dependent lipase to human milk, *in vitro,* results in an increase in the release of the free fatty acids up to 60 minutes of digestion, beyond which, a stagnant release profile is evident. When they added BSSL to the same mixture, the stagnant free fatty acid release profile was replaced with a continuous increase in the rate of free fatty acids generation. This supports our hypothesis that the presence of BSSL in breast milk influences the rate of free fatty acid release (Table 7.2) and total free fatty acids released (Table 7.2 and Figure 7.4C), despite the initial lag phase. This further explains the stagnant pattern observed in all the infant formulas over the entire digestion period in both the jejunum and ileum compartments (Figure 7.3A-D). To our knowledge, no data exists pertaining to the quantitative rate of free fatty acid release in both infant formula and breast milk in the small intestinal compartments. However, Armand *et al.*[437] compared the rate of gastric free fatty acid release *in vivo*, and found, similar to our

findings, a significantly higher rate of gastric lipolysis in breast milk than in infant formulas. This suggests consistency in the hydrolysis pattern by varying enzymes, since gastric lipase is the predominant hydrolysis performer in the gastric compartment of the gastrointestinal tract; while pancreatic lipase and BSSL (in case of human breast milk) are the predominant hydrolysers in the small intestinal compartments.
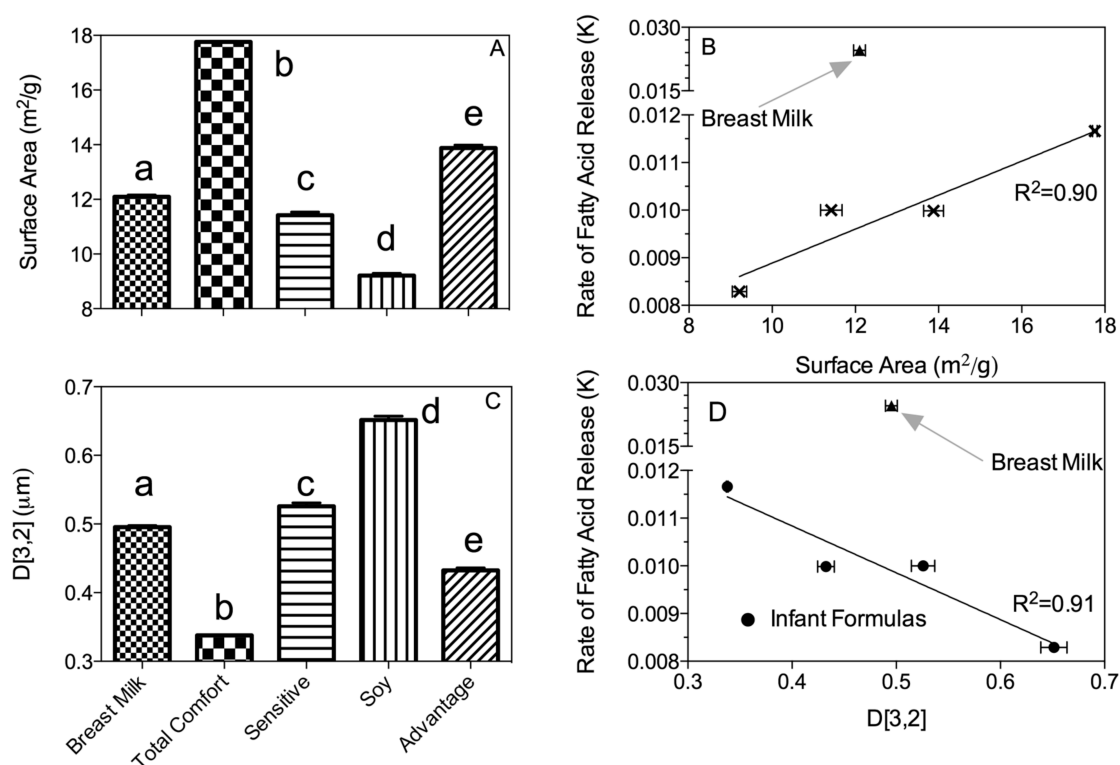
Figure 7.5: Surface area (A), and D[3,2] (C) for human breast milk and Similac[TM] infant formulas and correlations between surface area (B) and D[3,2] (D) against bioaccessibility.

Using particle size distributions (Figure 7.1), the surface area per gram (Figure 7.5A), Sauter Mean Diameter (surface weighted mean - D[3,2]) (Figure 7.5C). Total Comfort infant formula has the highest surface area followed by Advance, breast milk, Sensitive and Soy. Correlations between the rate of lipolysis and surface area (Figure 7.5B) show a very strong positive correlation (R^2=0.90) for the infant formulas, which

did not include breast milk. This highlights that the rate of lipolysis, in the infant formulas, varied based on the surface area available for lipase access. However, the difference in the rate of the reaction for breast milk suggests that it is not dictated by surface area alone; and other factors such as endogenous maternal BSSL and/or the unique interfacial properties of the milk fat globular membrane could be playing a role in the rate of lipolysis seen in breast milk.

The Sauter mean diameter (surface weighted mean - D[3,2]) (Figure 7.5C) provides information about the central point around which the surface area for each sample resides. This type of particle size measurement does not require measurement of the number of particles involved, and takes into consideration the individual value and the frequency of its presence in the distribution. D[3,2] (Figure 7.5C) values, in descending order, are Soy (~ 0.7 μm), Sensitive (~ 0.55 μm), breast milk (~0.5 μm), Advance (~ 0.45 μm), and Total Comfort (~ 0.3 μm) (Figure 7.2 A, B). A strong, negative correlation (R^2=0.91) is seen between rate of fatty acid release and D[3,2] for the infant formulas while breast milk does not follow the trend (Figure 7.5D).

7.5 Conclusion

Comparing breast milk to different Similac^{TM} infant formulas highlighted numerous differences that could result in important alterations in the biophysics of digestion. Breast milk had lower viscosities, at all pHs, than infant formulas and the highest viscosity of the breast milk was at a pH of 3 (the pH of an infants' stomach), while the highest viscosity for infant formulas were observed between 4 and 5. These changes in the viscous properties could influence gastric emptying rates and potentially satiety; however, we found no correlations between viscosity and lipid bioaccessibility.

Free fatty acid release profiles showed a lag phase during lipid digestion, exclusive to human breast milk. The droplets size and distribution varied for the different milk samples tested; similarly the calculated surface area and D[3,2] varied between different samples. It was found, for the infant formulas, that the rate of lipolysis was positively correlated with the surface area per gram. However, the rate of lipolysis, in breast milk, did not follow that trend. These biophysical aspects of breast milk versus infant formulas may alter different facets of their respective digestibility which may have unintended consequences.

7.6 Acknowledgements

8 CONCLUSIONS

TNO Intestinal Model-1 (TIM-1), spectrophotometry, and molecular rotors (MR) were integrated to generate a method capable of simultaneously measuring real-time luminal viscosity changes and *in vitro* digestion kinetics. The TIM-1 is considered the closest *in vitro* gastrointestinal (GI) simulation system to the *in vivo* human GI "gold standard" that is currently available. Numerous studies have shown good correlation between TIM-1 results and *in vivo* data, suggesting the system is reliable in predicting *in vivo* parameters [193, 195, 199]. The use of MR-based fluorescence spectroscopy as an analytical technique in food systems presents distinct advantages: it is noninvasive, site specific, rapid, sensitive, versatile, and non-complex. Therefore, we exploited the sensitivity of MRs to increased molecular crowding within the TIM-1 apparatus to achieve continuous monitoring of *in vitro* luminal chyme viscosity.

The digestate samples collected from TIM-1 facilitated estimation of digestion kinetics, which included total bioaccessibility and rate of hydrolysis (α-amylase or lipase). The investigated physico-chemical properties were determined using fluorescence spectra in addition to other techniques, and included GI viscosity, available starch and β-glucan, extent of starch gelatinization, and particle size distribution. Major findings presented in this dissertation were a product of correlations between the attained parameters of digestion kinetics and physico-chemical properties, as a function of:

    I.   Changes in amylose-to-amylopectin ratio in maize starch;

    II.   Changes in the integrity and quantity of both β-glucan and starch, due to differences in the production methods involved in oat processing;

III.   Addition of a thickening agent, milk protein concentrate (MPC) to oat-based meals.

IV.   Differences in droplet size and distribution of fat globules in Similac^{TM} infant formulas as compared to human breast milk.

Our findings suggest that the retention of meal formulation does not translate into identical physiological responses. Instead, the physico-chemical modifications associated with variable meal preparation methods, industrial processing techniques, and organoleptic considerations appear to significantly impact the biophysics of digestion. We have illustrated the role of amylopectin, in comparison to amylose and native starches, in increasing gastric viscosity in maize starch. A comparison of commercially available oat products revealed dependency of sugar bioaccessibility on available starch content. Significant differences in rate of sugar release in the oat samples were attributed to multiple factors, including, differences in β-glucan composition and physical properties associated with the different methods used in oat production. Addition of MPC to oats-based meals significantly decreased the total bioaccessible sugars and increased the rate of starch hydrolysis. Comparing breast milk to different Similac^{TM} infant formulas highlighted numerous differences that could result in important alterations in the biophysics of digestion. Free fatty acid release profiles of human breast milk showed a lag phase during lipid digestion, which was absent in the tested infant formulas. The rate of lipolysis was positively correlated with the surface area per gram in all infant formulas tested, with exclusion of human breast milk. These biophysical aspects of breast

milk versus infant formulas may alter different facets of their respective digestibility which may have unintended consequences.

The significance of this total body of work pertains to the unintentional changes in food physico-chemical properties that may influence physiological responses in an inadvertent manner; which may prove critical for production of meals specifically designated for the diabetic and/or the obese consumer. The prospective biophysical implications of our findings include manipulating food glycemic indices, controlling diabetic postprandial glycemic response, as well as weight management in cases of childhood obesity at the food production/manufacturing level. The universal interest in combatting diet-related chronic diseases has directed the food industry towards the research and development of functional foods aimed towards instigation of specific physiological responses upon digestion. For this purpose, there is a need to clearly identify the relationships between the possible mechanisms that alter food form and formulation, their role in the modification of food matrix physico-chemical properties, and the consequent changes in biophysics of digestion.

Future research interests include application of a Generally Recognized as Safe (GRAS) MR to report on changes in luminal viscosity *in vivo*. Such an application would allow correlations with accurate feedback mechanisms such as gastric emptying dependency on chyme state (solid/liquid) and temperature as well as satiety. In addition, there is insufficient knowledge about the properties and characteristics of interaction of Fast Green MR; it would be useful to understand the nature of the interaction between FG and other macronutrients and how these interactions may influence its luminescence properties. Rheological viscosity may be compared to fluorescence intensities (FI) of

samples extracted from within the TIM-1 compartments, rather than the collected digestates, to give a specific definition of the actual viscosity (mPa s) value corresponding to a certain FI measurement. Digestion kinetics and luminal viscosity parameters may also be assessed in food matrices of special health concern in TIM-1, such as high fat food and high glycemic index foods. Soluble fibers and/or other thickening agents may then be added to the same foods to determine possible alterations in digestion kinetics and luminal viscosity to attain positive physiological responses.

This body of work provided insight on the influence of physico-chemical properties on starch and lipid digestion and a better understanding of succinct physico-chemical properties that can reduce the rate and extent of bioaccessibility. We expect that the adoption of simple steps such as a homogenization process, control of β-glucan composition, or inclusion of thickening agent at the product development level can aid in achievement of desirable physiological outcomes. A better understanding of such relationships between food form and formulation may be useful in the design of food products intended for patients with specific diet-related chronic diseases, such as diabetes, with pre-determined physiological impact.

9 REFERENCES

1. Nishida, C., et al., *Diet, nutrition and the prevention of chronic diseases: report of a joint WHO/FAO expert consultation. .* Public Health and Nutrition, 2004. **7**: p. 245–250.
2. Tosh, S. and Y. Chu, *Systematic review of the effect of processing of whole-grain oat cereals on glycaemic response.* British Journal of Nutrition, 2015. **114**: p. 1256-1262.
3. Zhang, D., D. Doehlert, and W. Moore, *Rheological properties of (1-3),(1-4)-of β-D-glucan from raw, roasted, and steamed oat groats.* cereal Chemistry, 1998. **75**(4): p. 433-438.
4. Wood, P., *Physicochemical characteristics and physiological properites of oat (1-3),(1-4)-bet-D-glucan.*, in *Oat bran*, P. Wood, Editor. 1993, American Association of Cereal Chemistry: St. Paul, USA. p. 83-112.
5. Degutyte-Fomins, L., T. Sontag-Strohm, and H. Salovaara, *Oat bran fermentation by rye sourdough.* Cereal Chemistry, 2002. **79**(e): p. 345-348.
6. Decker, E., D. Rose, and D. Stewart, *Processing of oats and the impact of processing operations on nutrition and health benefits.* British Journal of Nutrition, 2014. **112**: p. S58-S64.
7. Ovando-Martinez, M., et al., *Effect of hydrothermal treatment on physicochemical and digestibility properties of oat starch.* Food Research International, 2013. **52**: p. 17-25.
8. Lookhart, G., L. Albers, and Y. Pomeranz, *The effect of commercial processing in some chemical and physical properties of oat groats.* Cereal Chemistry, 1986. **63**(3): p. 280-282.
9. Yiu, S., *Cereal structure and its relationship to nutritional quality.* Food Structure, 1989. **8**(1): p. 99-113.
10. Grandfeldt, Y., A. Eliasson, and I. Bjorck, *An examination of the possibility of lowering the glycemic index of oa and barley flakes by minimal processing.* Journal of Nutrition, 2000. **130**: p. 2207-2214.
11. Schneeman, B., *Dietary fiber and gastrointestinal function*, in *Advanced dietary fiber technology*, B. McCleary and L. Prosky, Editors. 2001, Blackwell Sciences: Ames (IA). p. 168-176.
12. Brownlee, L., *The physiological roles of dietary fibres.* Food Hydrocolloids, 2011. **25**(2): p. 238-250.
13. Wood, P., et al., *Effect of dose and modification of viscous properties of oat gum on plasma glucose and insulin following an oral glucose load.* British Journal of Nutrition, 1994. **72**: p. 731-743.
14. Whiting, D., et al., *IDF Diabetes Atlas: Global estimates of the prevalence of diabetes for 2011 and 2030.* Diabetes research and clinical practice, 2011. **94**: p. 311-321.

15. Dhital, S., et al., *Mechanisms of Starch Digestion by α-amylase–structural Basis for Kinetic Properties.* Critical Reviews in Food Science and Nutrition, 2015.

16. Englyst, H. and J. Cummings, *Digestion of the polysaccharides of some cereal foods in teh human small intesting.* The American Journal of Clinical Nutrition, 1985. **42**: p. 778-787.

17. Araya, H., et al., *A comparison between an in vitro method to determine carbohydrate digestion rate and the glycemic response in young men.* European Journal of Clinical Nutrition 2002. **56**: p. 735–739.

18. Topping, D., *Cereal complex carbohydrates and their contribution to human health.* Journal of Cereal Science, 2007. **46**: p. 220-229.

19. Prevention, C.f.D.C.a. *Adult obesity facts.* 2015 [cited 2015; Available from: http://www.cdc.gov/obesity/childhood/.

20. Fagot-Campagna, A., et al., *Type 2 diabetes among North American children and adolescents: an epidemiologic review and a public health perspective.* Journal of Pediatrics, 2000. **136**(5): p. 664-672.

21. Singhal, A. and J. Lanigan, *Breastfeeding, early growth, and later obesity.* Obesity Reviews, 2007. **8(suppl 1)**: p. 51-54.

22. Arenz, A., et al., *Breastfeeding and childhood obesity: a systematic review.* International Journal of Obesity Related Metabolic Disorders, 2004. **28**(10): p. 1247-1256.

23. Harder, T., et al., *Duration of breastfeeding and risk of overweight: a meta-analysis.* American Journal of Epidemiology, 2005. **162**(5): p. 397-403.

24. Li, R., S. Fein, and L. Grummer-Strawn, *Do Infants Fed from Bottles Lack Self-regulation of Milk Intake Compared with Directly Breastfed Infants?* Journal of Pediatrics, 2010. **125**(6): p. 1386-1393.

25. Dewey, K. and B. Lonnerdal, *Infant Self-regulation of breast milk intake.* Acta Paediatrica, 1986. **75**(6): p. 893-898.

26. Ilcol, Y., Z. Hizli, and E. Eroz, *Resistin in present in human breast milk and it correlates with materanal hormonal status and serum level of C-reactive protein.* Clinical Chemistry and Laboratory Medicine, 2008. **46**(1): p. 118-124.

27. Aydin, S., et al., *Ghrelin is present in human colostrum, transitional and mature milk.* Peptides, 2006. **27**(4): p. 878-882.

28. Aydin, S., et al., *Presence of obestatin in breast milk: relationship among obestatin, ghrelin, and leptin in lactating women.* Nutrition and Metabolism, 2008. **24**(7-8): p. 689-693.

29. Baxter, R., Z. Zaltsman, and J. Turtle, *Immunoreactive somatomedin-C/insulin-like growht factor I and its binding protein in human milk.* The journal of Clinical Endocrinology and Metabolism, 1984. **58**(6): p. 955-959.

30. Casabiell, V., et al., *Presence of leptin in colostrum and/or breast milk for lactating mothers: a potential role in the regulation of neonatal food intake.* The journal of Clinical Endocrinology and Metabolism, 1997. **82**(12): p. 4470-4273.

31. Ucar, B., et al., *Breast Milk Leptin Concentrations in Initial and Terminal Milk Samples: Relationships to Maternal and Infant Plasma Leptin Concentrations,*

Adiposity, Serum Glucose, Insulin, Lipid and Lipoprotein Levels. Journal of Pediatric Endocrinology and Metabolism, 2000. **13**: p. 149-156.

32.   Martin, L., et al., *Adiponectin is present in human milk and is associated with maternal factors,.* American Journal of Clinical Nutrition, 2006. **83**(5): p. 1106-1111.

33.   Simkovitch, R. and D. Huppert, *Optical Spectroscopy of molecular-rotor molecules adsorbed on cellulose.* Journal of Physical Chemistry, 2014. **118**: p. 8737-8744.

34.   Englyst, K. and H. Englyst, *Carbohydrate bioavailability.* British Journal of Nutrition, 2005. **94**: p. 1-11.

35.   Englyst, K., S. Liu, and H. Englyst, *Nutritional characterization and measurement of dietary carbohydrates.* European Journal of Clinical Nutrition, 2007. **61**(1): p. S19-S39.

36.   Schenk, S., et al., *Different glycemic indexes of breakfast cereals are not due to glucose entry into blood but to glucose removal by tissue.* American Journal of Clinical Nutrition, 2003. **78**: p. 742-748.

37.   Wood, P., *Cereal beta-glucans in diet and health.* Journal of Cereal Science, 2007. **46**(3): p. 230-238.

38.   Butterworth, P., F. Warren, and P. Ellis, *Human alpha-amylase and starch digestion: an intersting marriage.* Starch/ Sta"rke, 2011. **63**: p. 395-405.

39.   Yuryev, V., P. Tomasik, and E. Bertoft, *Starch: achivements in understanding structure and functionality*. 2007, New York: Nova Science Publishers.

40.   Hancock, R. and B. Tarbet, *The other double helix - The fascinating chemistry of starch.* Journal of chemical education, 2000. **77**(8): p. 988-992.

41.   Jobling, S., *Improving starch for food and industrial applications.* Current Opinion in Plant Biology, 2004. **7**: p. 210-218.

42.   O'Neil, E. and R. Field, *Mini Review: Underpinning starch biology with in vitro studies on carbohydrate- active enzymes and biosynthetic glycomaterials.* Frontiers in Bioengineering and Biotechnology, 2015. **3**(136): p. 1-6.

43.   Carvalho, P., et al., *Starch-based blends in tissue engineering*, in *Biomaterials from Nature for Advanced Devices and Therapies*, N. Neves and R. Reis, Editors. 2016, John Wiley & Sons: Hoboken, New Jersey. p. 245-247.

44.   Jane, J., *Structure of starch granules.* Journal of Applied Glycoscience, 2007. **54**(1): p. 31-36.

45.   Qi, X., et al., *Molecular basis of the gelatinisation and swelling characteristics of waxy rice starches grown in the same location during the same season.* Journal of Cereal Science, 2003. **37**: p. 363-376.

46.   Donald, A., *Understanding starch structure and functionality*, in *Starch in food: structure, function and applications*, A. Eliasson, Editor. 2004, Woodhead Publishing Limited/CRC Press LLC.: Cambridge/Boca Raton. p. 156-184.

47.   Donald, A., et al., *Scattering studies of the internal structure of starch granules.* Starch/ Sta"rke, 2001. **53**(10): p. 504-512.

48.   Pearsall, D., *Starch Analysis*, in *Paleoethnobotany: a Handbook of Procedures*. 2015, Left Coast Press, Inc.: Walnut Creek, CA. p. 342-345.

49.   Jane, J., C. Maningat, and R. Wongsagonsup, *Starch Characterization, Variety and Application*, in *Industrial Crops and Uses*, B. Singh, Editor. 2010, CAB International: London, UK. p. 216-217.

50.   Wang, T., T. Bogracheva, and C. Hedley, *Starch: as simple as A, B, and C?* Journal of Experimental Botany, 1998. **49**(320): p. 481-502.

51.   *Handbook of cereal science and technology*. 2 ed. 2000, New York, NY: CRC Press.

52.   Groot, P., et al., *The human alpha-amylase multigene family consists of haplo-types with variable numbers of genes.* Genomics, 1989. **5**(1): p. 29-42.

53.   Waugh, A. and A. Grant, *The digestive system*, in *Ross and Wilson Anatomy and Physiology in Health and Illness*. 2014, Churchill Livingstone Elsevier.

54.   Levin, R., *Digestion and absorption of carbohydrates- from molecules and membranes to humans.* American Journal of Clinical Nutrition, 1994. **59**: p. 690S-698S.

55.   Hoebler, C., et al., *Physical and chemical transformations of cereal food during oral digestion in human subjects. .* British Journal of Nutrition, 1998. **80**(5): p. 429-436.

56.   Silk, D. and A. Dawson, *Intestinal absorption of carbohydrate and protein in man*. Gastrointestinal physiology III. Vol. 19. 1979, Baltimore: University Park Press.

57.   *Carbohydrates in human nutrition*, in *FAO Food and Nutrition Paper*1997, Food and Agriculture Organization of the United Nations World Health Organization: Rome. p. 84.

58.   Colonna, P., V. Leloup, and A. Buleon, *Limiting factors of starch hydrolysis.* European Journal of Clinical Nutrition, 1992. **46**: p. S17-S32.

59.   Payan, F., et al., *3-dimensional structure of alpha-amylase from porcine pancreas at 5-A° resolution - active-site location. .* Acta Crystallographica, 1980. **36**: p. 416-421.

60.   Ramasubbu, N., et al., *Structure of human salivary alpha-amylase at 1.6 Å resolution: Implications for its role in the oral cavity.* Acta Crystallographica, 1996. **D52**: p. 435-446.

61.   Brayer, G., Y. Luo, and S. Withers, *The structure of human pancreatic alpha-amylase at 1.8 Å resolution and comparisons with related enzymes.* Protein Science, 1995. **4**: p. 1730-1742.

62.   Gilles, C., et al., *Crystal structure of pig pancreatic a-amylase isoenzyme II, in complex with the carbohydrate inhibitor, acarbose. .* European Journal of Biochemistry, 1996. **238**(2): p. 1987-1993.

63.   Brayer, G., et al., *Subsite mapping of the human pancreatic alpha-amylase active site through structural, kinetic, and mutagenesis techniques. .* Biochemistry, 2000. **39**: p. 4778-4791.

64.   Seigner, C., E. Prodanov, and G. Marchis-Mouren, *The determination of subsite binding energies of porcine pancreatic α-amylase by comparing hydrolytic activity towards substrates.* Biochimica et Biophysica Acta (BBA) - Protein Structure and Molecular Enzymology, 1987. **913**(2): p. 200-209.

65.   Braun, P., D. French, and J. Robyt, *The effect of substrate mod- ification on binding of porcine pancreatic alpha amylase: hydrolysis of modified amylose*

containing D-allose residues. Carbohydrate Research, 1985. **141**(2): p. 265-271.

66. Ganong, W., *Section V. Gastrointestinal Function*, in *Review of Medical Physiology*. 2005, LANGE Medical Publications: Los Altos, California.

67. Yook, C. and J. Robyt, *Reactions of alpha amylases with starch granules in aqueous suspensions giving products in solution and in a minimum amount of water giving products inside the granule.* Carbohydrate Research, 2002. **337**: p. 1113-1117.

68. Anderson, J., M. Root, and S. Garner, *Digestion of Foods and Absorption of Nutrients*, in *Human Nutrition: Healthy Options for Life*. 2015, Jones and Bartlett Learning: Burlington, MA.

69. Cummings , J. and A. Stephen, *Carbohydrate terminology and classification.* European Journal of Clinical Nutrition and Metabolism, 2007. **61**(1): p. S5-S18.

70. Endress, H. and J. Fisher, *Fibres and fibre blends for indivi- dual needs: a physiological and technological approach. ,* in *Advanced Dietary Fibre Technology*, B. McCleary and L. Prosky, Editors. 2001, Blackwell Science Ltd.: Oxford p. 283 – 298.

71. Montagne, L., J. Pluske, and D. Hampson, *A review of interactions between dietary fibre and the intestinal mucosa, and their consequences on digestive health in young non-ruminant animals. .* Animal Feed Science and Technology, 2003. **108**: p. 95-117.

72. Tharakan, A., et al., *Mass transfer and nutrient absorption in a simulated model of small intestine. .* Journal of Food Science, 2010. **75**: p. 339-346.

73. McKeown, N., et al., *Carbohydrate nutrition, insulin resistance, and the prevalence of the metabolic syndrome in the framingham offspring cohort.* Diabetes Care, 2004. **27**(2): p. 538–546.

74. Brennan, C., *Dietary fibre, glycaemic response, and diabetes* Molecular Nutrition and Food Research, 2005. **49**(6): p. 560–570.

75. Sahyoun, N., et al., *Whole-grain intake is inversely associated with the metabolic syndrome and mortality in older adults.* American Journal of Clinical Nutrition, 2006. **83**(1): p. 124-131.

76. Brennan, C. and L. Cleary, *Review: The potential use of cereal (1-3,1-4)-b-D-glucans as functional food ingredients.* Journal of Cereal Science 2005. **42**: p. 1-13.

77. Trepel, F., *Dietary fibre: more than a matter of dietetica. I. Compounds, properties, physiological effects.* Wiener klinische Wochenschrift 2004. **116**: p. 465–476.

78. Malkki, Y., *Trends in dietary fibre research and development.* Acta Alimentaria 2004. **33**: p. 39–62.

79. Trowell, H., *Ischemic heart disease and dietary fiber.* American Journal of Clinical Nutrition, 1972. **25**(9): p. 926-932.

80. Food and Drug Administration, U.D.o.H.a.H.S., *Food Labelling: Health Claims; Oats and Coronary Heart Disease- Final Rule.* Federal Register, 1997. **62**(15): p. 3584-3601.

81. Wood, P., et al., *Comparisons of viscous properties of oat and guar gum and effects of these and oat bran on glycemic index.* Journal of Agricultural and Food Chemistry, 1990. **38**: p. 753-757.

82. Regand, A., et al., *The molecular weight, solubility and viscosity of oat beta-glucan affect human glycemic response by modifying starch digestibility.* Food Chemistry, 2011. **129**: p. 297-304.

83. El Khoury, D., et al., *Beta glucan: health benefits in obesity and metabolic syndrome.* Journal of Nutrition and Metabolism, 2011. **2012**: p. 1-28.

84. Zekovicʹ, D., et al., *Natural and modified (1 → 3)-β-D-glu- cans in health promotion and disease alleviation.* Critical Reviews in Biotechnology, 2005. **25**(4): p. 205–230.

85. Ooi, V. and F. Liu, *Immunomodulation and anti- cancer activity of polysaccharide-protein complexes.* Current Medicinal Chemistry, 2000. **7**(7): p. 715–729.

86. Hanai, H., et al., *Long-term effects of water-soluble corn bran hemicellulose on glucose tolerance in obese and non-obese patients: improved insulin sensitivity and glucose metabolism in obese subjects. .* Bioscience, biotechnology, and biochemistry, 1997. **61**(8): p. 1358-1361.

87. Thorsdottir, I., H. Andersson, and S. Einarsson, *Sugar beet fiber in formula diet reduces postprandial blood glucose, serum insulin and serum hydroxyproline.* European Journal of Clinical Nutrition, 1998. **52**(2): p. 155–156.

88. Anderson, J., et al., *Effects of psyllium on glucose and serum lipid responses in men with type 2 diabetes and hypercholes- terolemia.* American Journal of Clinical Nutrition, 1999. **70** (4): p. 466–473.

89. Sierra, M., García, J.J., Fernández, N., Diez, M.J., Calle, Á.P., Sahagún, A.M., Prieto, C., Carriedo, D., González, A., Álvarez, J.C. and Castro, L.J.,. , *Effects of ispaghula husk and guar gum on postprandial glucose and insulin concentrations in healthy subjects.* European Journal of Clinical Nutrition, 2015. **55**(4): p. 235-243.

90. Sierra, M., et al., *Therapeutic effects of psyllium in type 2 diabetic patients .* European Journal of Clinical Nutrition, 2002. **56**(9): p. 830–842.

91. Juntunen, K., et al., *Postprandial glucose, insulin, and incretin responses to grain products in healthy subjects.* American Journal of Clinical Nutrition, 2002. **75**(2): p. 254–262.

92. Alminger, M. and C. Eklund-Jonsson, *Whole-grain cereal products based on a high-fibre barley or oat genotype lower post-prandial glucose and insulin responses in healthy humans.* European Journal of Nutrition, 2008. **47**(6): p. 294–300.

93. Skendi, A., et al., *Structure and rheological properties of water soluble b-glucans from oat cultivars of Avena sativa and Avena bysantina.* Journal of Cereal Science 2003. **38**: p. 15–31.

94. Buckeridge, M., et al., *Mixed linkage (1-3), (1-4)-b-D-glucans of grasses.* Cereal Chemistry 2004. **81**: p. 115–127.

95. Lazaridou, A., C. Biliaderis, and M. Izydorczyk, *Molecular size effects on rheological properties of oat beta-glucans in solution and gels.* Food Hydrocolloids 2003. **17**: p. 693–712.

96. Butt, M., et al., *Oat: unique among the cereals.* European Journal of Nutrition, 2008. **74**: p. 68-79.

97. Wood, P. and M. Beer, *Functional oat products*, in *Functional Foods, Biochemical and Processing Aspects*, J. Mazza, Editor. 1998, Technomic Publishing Company: Lancester, UK.

98. Ren, Y., et al., *Dilute and semi-dilute solution properties of (1-3), (1-4)-β-glucan, the endosperm cell wall polysaccharide of oats (Avena sativa L.).* Carbohydrate Polymers, 2003. **53**: p. 401-408.

99. Doublier, J. and P. Wood, *Rheological properties of aqueous solutions of (1-3), (1-4)-b-D-glucan from oats (Avena sativa L.).* Cereal Chemistry 1995. **72**: p. 335–340.

100. Lia, A., et al., *Substrates available for colonic fermentation from oat, barley and wheat bread diets. A study in ileostomy subjects.* British Journal of Nutrition, 1996. **76**: p. 797}808 (

101. Sundberg, B., et al., *Mixed-linked beta-glucan from breads of different cereals is partly degraded in human ileostomy model.* American Journal of Clinical Nutrition, 1996. **64**: p. 878-885.

102. Wood, P., M. Beer, and G. Butler, *Evaluation of role of concentration and molecular weight of oat β-glucan in determining effect of viscosity on plasma glucose and insulin following an oral glucose load.* British Journal of Nutrition, 2000. **84**(1): p. 19–23.

103. Autio, K., *Functional aspects of cell wall polysaccharides*, in *Carbohydrates in Food*, E. A.-C. Eliasson, Editor. 1996, Marcel Dekker: New York, NY, USA.

104. Braaten, J., et al., *High b-glucan oat bran and oat gum reduce postprandial blood glucose and insulin in subjects with an without type 2 diabetes.* Diabetes Medicine 1994 **11**: p. 312–318.

105. Tappy, L., E. Gugolz, and P. Wursch, *Effects of breakfast cereals containing various amounts of β-glucan fibres on plasma glucose adn isulin responses in NIDDM subjects.* Diabetes Care, 1996. **19**: p. 831-834.

106. Poyhonen, U., *Control of blood glucose through oat soluble fibre beta-glucan.* Agro-Food-Industry Hi-Tech 2004. **15**: p. 10–11.

107. Hallfrisch, J., D. Schofield, and K. Behall, *Physiological responses of men and women to barley and oat extracts (NutrimX). II. Comparison of glucose and insulin responses.* Cereal Chemistry 2003. **80**: p. 80–83.

108. Jenkins, A., et al., *Depression of the glycemic index by high levels of beta-glucan fiber in two functional foods tested in type 2 diabetes.* European Journal of Clinical Nutrition, 2002. **56**(7): p. 622-628.

109. Bio¨rklund, M., et al., *Changes in serum lipids and postprandial glucose and insulin concentrations after consumption of beverages with β-glucans from oats or barley: a randomised dose-controlled trial.* European Journal of Clinical Nutrition, 2005. **59**(11): p. 1272–1281.

110. Tapola, N., et al., *Glycemic responses of oat bran products in type 2 diabetic patients.* Nutrition, Metabolism and Cardiovascular Diseases, 2005. **15**(4): p. 255–261.

111. Cavallero, A., et al., *High (1 → 3,1 → 4)-β-glucan barley fractions in bread making and their effects on human glycemic response.* Journal of Cereal Science, 2002. **36**(1): p. 59-66.

112. Granfeldt, Y., L. Nyberg, and I. Bjo¨rck, *Muesli with 4 g oat β-glucans lowers glucose and insulin responses after a bread meal in healthy subjects.* European Journal of Clinical Nutrition, 2008. **62**(5): p. 600–607.

113. Hlebowicz, J., et al., *Effect of muesli with 4 g oat β-glucan on postprandial blood glucose, gastric emptying and satiety in healthy subjects: a randomized crossover trial.* Journal of the American College of Nutrition, 2008. **27**(4): p. 470–475.

114. Liu, H., J. Lelievre, and W. Ayoung-Chee, *A study of starch gelatinization using differential scanning calorimetry, x-ray, and birefringence measurements.* Carbohydrate Research, 1991. **210**: p. 79-87.

115. Hoover, R., *Composition, molecular structure, and physicochemical properties of tuber and root starches: a review.* Carbohydrate Polymers, 2001. **45**: p. 253-267.

116. Jenkins, P. and A. Donald, *Gelatinisation of starch: a combined SAXS/WAXS/DSC and SANS study.* Carbohydrate Research, 1998. **308** p. 133-147.

117. Parker, R. and S. Ring, *Aspects of the physical chemistry of starch.* Journal of Cereal Science, 2001. **1**: p. 1-17.

118. Ratanayake, W., C. Otani, and D. Jackson, *DSC enthalpic transitions during starch gelatnisation in excess water, dilute sodium chloride and dilute sucrose solutions.* Journal of Science, Food, and Agriculture, 2009. **89**(12): p. 2156-2164.

119. Xie, F., et al., *Rheological properties of starches with different amylose/amylopectin ratios.* Journal of Cereal Science, 2009. **49**: p. 371–377.

120. Holm, J., et al., *Degree of starch gelatinization, digestion rate of starch in vitro, and metabolic response in rats. .* American Journal of Clinical Nutrition 1988. **47**: p. 1010–1016.

121. Goni, I., A. Garcia-Alonso, and F. Saura-Calixto, *A starch hydrolysis procedure to estimate glycemic index.* Nutrition Research, 1997. **17**(3): p. 427-437.

122. Chung, H., H. Lim, and S. Lim, *Effect of partial gelatinization and retrogradation on the enzymatic digestion of waxy rice starch.* Journal of Cereal Science, 2006. **43**: p. 353-359.

123. Bravo, L., H.N. Englyst, and J.H. Hudson, *Nutritional evaluation of carbohydrates in the Spanish diet: non-starch polysaccharides and in vitro starch digestibility of breads and breakfast products. .* Food Research International, 1998. **31**: p. 129-135.

124. Englyst, K.N., et al., *Glycaemic index of cereal products explained by their content of rapidly and slowly available glucose. .* British Journal of Nutrition, 2003). **89**: p. 329-339.

125. Le Francois, P., *In vitro availability of starch in cereal products.* Journal of the Science of Food and Agriculture, 1989. **49**: p. 499-501.

126. Yiu, S., *Effects of procesing and cooking on the structure and microchemical composition of oats.* Food Structure, 1986. **5**(2): p. 219-225.

127. Capriles, V., et al., *Effect of processing methods on amaranth starch digestibility and predicted glycemic index.* Journal of Food Science, 2008. **73**(7): p. H160-H164.

128. Shannon, J. and D. Garwood, *Genetics and physiology of starch development*, in *Starch Chemistry and Technology*, R. Whistler, J. BeMiller, and E. Paschal, Editors. 1984, Academic Press: New York. p. 26-79.

129. Syahariza, Z., et al., *The importance of amylose and amylopectin fine structures for starch digestiblity in cooked rice grains.* Food Chemistry, 2013. **136**: p. 742-749.

130. Tester, R., J. Karkalas, and X. Qi, *Starch - composition, fine structure and architecture.* Journal of Cereal Science, 2004. **39**: p. 151-165.

131. Rashmi, S. and A. Urooj, *Effect of processing on nutritionally important starch fractions in rice varieties.* International Journal of Food Sciences and Nutrition, 2004. **54**(27-36).

132. Chung, H., et al., *Physicochemical properties and in vitro starch digestiblity of cooked rice from commercially available cultivars in Canada.* Cereal Chemistry, 2010. **87**(4): p. 297-304.

133. Zhang, W., et al., *In vitro measurement of resistant starch of cooked milled rice and physico-chemical characateristics affecting its formation.* Food Chemistry, 2007. **105**: p. 462-468.

134. Morita, T., et al., *In vitro and in vivo digestiblity of native maize starch grnules varying in amylose contents.* Journal of AOAC international, 2007. **90**(6): p. 1628-1634.

135. Chung, H., et al., *Physicochemical properties and in vitro starch digestibility of cooked rice from commercially available cultivars in Canada. .* Cereal Chemistry, 2010. **87**(4): p. 297–304.

136. Okuda, M., et al., *Structural characteristics, properties, and in vitro digestibility of rice. .* Cereal Chemistry
, 2005. **82**(4): p. 361–368.

137. Zhu, L., et al., *Digestibility and physicochemical properties of rice (Oryza sativa L.) flours and starches differing in amylose content. .* Carbohydrate Polymers, 2011. **86**(4): p. 1751–1759.

138. Hu, P., et al., *Starch digestibility and the estimated glycemic score of different types of rice differing in amylose contents.* Journal of Cereal Science, 2004. **40**: p. 231-237.

139. Akerberg, A., H. Liljeberg, and I. Bjo¨rck, *Effects of Amylose/Amylopectin Ratio and Baking Conditions on Resistant Starch Formation and Glycaemic Indices.* Journal of Cereal Science, 1998. **28** p. 71–80.

140. Granfeldt, Y., A. Drews, and I. Bjo¨rck, *Arepas made from high amylose corn flour produce favorably low glucose and insulin responses in healthy humans.* Journal of Nutrition 1995. **125** p. 459–465.

141. Granfeldt, Y., A. Drews, and I. Bjo¨rck, *Starch Bioavailability in Arepas Made from Ordinary or High Amylose Corn: Concentration and Gastrointestinal Fate of Resistant Starch in Rats.* The Journal of Nutrition, 1993. **123**: p. 1676-1684.

142. Mua, J. and D. Jackson, *Relationships between Functional Attributes and Molecular Structures of Amylose and Amylopectin Fractions from Corn Starch.* Journal of Agricultural and Food Chemistry, 1997. **45**: p. 3848-3854.

143. Vandeputte, G., et al., *Rice starches. I. Structural aspects provide insight into crystallinity characteristics and gelatinisation behaviour of granular starch. .* Journal of Cereal Science, 2003. **38**: p. 43–52.

144. Varavinit, S., et al., *Effect of amylose content on gelatinization, ret- rogradation and pasting properties of flours from different cultivars of thai rice. .* Starch/Stärke 2003. **55**: p. 410–415.

145. Kim, H.-S., B. Patel, and J. BeMiller, *Effects of the amylose–amylopectin ratio on starch–hydrocolloid interactions.* Carbohydrate Polymers, 2013. **98**: p. 1438-1448.

146. Park, I.-M., et al., *Gelatinization and Pasting Properties of Waxy and Non-waxy Rice Starches.* Starch/ Sta"rke, 2007. **59**: p. 388-396.

147. Matveev, Y., et al., *The relationship between thermodynamic and structural properties of low and high amylose maize starches.* Carbohydrate Polymers, 2001. **44**: p. 151–160.

148. Tester, R. and W. Morrison, *Swelling and gelatinization of cereal starches.1. Effects of amylopectin, amylose, and lipids. .* Cereal Chemistry, 1990. **67**: p. 551–557.

149. Ellis, P., F. Dawoud, and E. Morris, *Blood glucose, plasma insulin and sensory responses to guar-containing wheat breads: Effects of molecular weight and particle size of guar gum.* British Journal of Nutrition, 1991. **66**: p. 363-379.

150. Brennan, C., et al., *Effects of guar galactomannan on wheat bread microstructure and on the in vitro and in vivo digestibility of starch in bread.* Journal of Cereal Science, 1996. **24**: p. 151-160.

151. Brennan, C., et al., *Effects of guar galactomannan on wheat bread microstructure and on the in vitro and in vivo digestibility of starch in bread. .* Journal of Cereal Science, 1996 **24**: p. 151 – 160.

152. Tudorica, C., V. Kuri, and C. Brennan, *Nutritional and physicochemical characteristics of dietary fiber enriched pasta.* Journal of Agricultural and Food Chemistry, 2002. **50**(2): p. 347 – 356.

153. Symons, L. and C. Brennan, *The influence of (1-3)(1-4)-β-D-glucan-rich fraction from barley on the physicochemical properties an in vitro reducing sugar release of white wheat breads.* Journal of Food Science, 2004. **69**(6): p. C463-C467.

154. Chaisawang, M. and M. Suphantharika, *Effects of guar gum and xanthan gum additions on physical and rheological properties of cationic tapioca starch.* Carbohydrate Polymers, 2005. **61**: p. 288-295.

155. Kaur, L., et al., *Starch-cassia gum interactions: A microstructure - rheology study.* Food Chemistry, 2008. **111**: p. 1-10

.

156. Slaughter, S., et al., *The effect of guar galactomannan and water availability during hydrothermal processing on the hydrolysis of starch catalysed by pancreatic alpha–amylase. .* Biochimica et Biophysica Acta, 2002. **1571**: p. 55-63.
157. Guerra, A., et al., *Relevance and challenges in modelling human gastric and small intestinal digestion.* Trends in Biotechnology, 2012. **30**(11): p. 591-600.
158. Kong, F. and R. Singh, *Disintegration of solid foods in human stomach.* Journal of Food Science, 2008. **73**: p. R67–R80.
159. Mercuri, A., et al., *The effect of composition and gastric conditions on the self-emulsification process of ibuprofen-loaded self-emulsifying drug delivery systems: a microscopic and dynamic gastric model study.* Pharmaceutical Research, 2011. **28**: p. 1540-1551.
160. Vardakou, M., et al., *Achieving antral grinding forces in biorelevant in vitro models: comparing the USP dissolution apparatus II and the dynamic gastric model with human in vivo data.* AAPS PharmSciTech, 2011. **12**(620-626).
161. Kong, F. and R. Singh, *A human gastric simulator (HGS) to study digestion in human stomach.* Journal of Food science, 2010. **75**(9).
162. Minekus, M., et al., *A multicompartmental dynamic computer- controlled model simulating the stomach and small intestine. ATLA Altern Lab Anim.* Alternatives to laboratory animals: ATLA, 1995. **23**: p. 197-209.
163. Sherwood, L., *Introduction to Human Physiology*. 8 ed. 2013, Pacific Grove, CA: Brooks/Cole.
164. DeBruyne, L., K. Pinna, and E. Whitney, *Digestion and Absorption*, in *Nutrition and Diet Therapy*. 2015, CENGAGE learning: Boston, MA.
165. Kong, F. and R. Singh, *Disintegration of solid foods in human stomach.* Jounral of Food Science, 2008. **73**(5).
166. Golding, M. and T. Wooster, *The influence of emulsion structure and stability on lipid digestion.* Current Opinion in Colloid and Interface Science, 2010. **15**: p. 90-101.
167. Scanlon, V. and T. Sanders, *The digestive system*, in *Essentials of Anatomy and Physiology*. 2015, F.A. Davis Company: Philadelphia, PA.
168. Seeley, R., T. Stephens, and P. Tate, *Anatomy and Physiology*. 8 ed. 2008, Bostion, MA: McGraw Hill.
169. Barrett, K., *Gastrointestinal Physiology*. 2006, Lange Medical Books/ McGraw-Hill.
170. Tortora, G. and B. Derrickson, *Principles of Anatomy and Physiology: Maintenance and Continuity of the Human Body*. 12 ed. Vol. 2. 2009, Hoboken, NJ: John Wiley and Sons.
171. Seeley, R., T. Stephens, and P. Tate, *Essentials of Anatomy and Physiology*. 2007, Boston, MA: McGraw Hill.
172. Blanquet, S., et al., *A dynamic gastrointestinal system for studying the behavior of orally administered drug dosage forms under various physiological conditions* Pharmaceutical Research, 2004. **21**: p. 585-591.
173. Blanquet-Diot, S., et al., *Digestive stability of xanthophylls exceeds that of carotenes as studied in a dynamic in vitro gastrointestinal system.* The Journal of Nutrition, 2009. **139**(5): p. 876-883.

174. Dickinson, P., et al., *An Investigation into the Utility of a Multi-compartmental, Dynamic, System of the Upper Gastrointestinal Tract to Support Formulation Development and Establish Bioequivalence of Poorly Soluble Drugs.* American Association of Pharmaceutical Scienctists Journal, 2012. **14**(2): p. 196-205.

175. TA, N., et al., *Use of a gastro-intestinal model and GastroplusTM for the prediction of in vivo performance.* Journal of Applied Therapeutic Research, 2006. **6**(1): p. 15.

176. Minekus, M., *The TNO Gastro-Intestinal Model*, in *The impact of food bioactives on health*, K. Verhoeckx, et al., Editors. 2015, ProDigest: Gent, Belgium. p. 305-317.

177. Naylor, T., et al., *Use of gastro-intestinal model and gastroplus for the prediction of in vivo performance.* Industrial Pharmacy, 2006(12): p. 9-12.

178. Barker, R., B. Abrahamsson, and M. Kruusma, *Application and Validation of an Advanced Gastrointestinal In Vitro Model for the Evaluation of Drug Product Performance in Pharmaceutical Development.* Journal of Pharmaceutical Sciences, 2014. **103**: p. 3704-3712.

179. Benini, L., et al., *Gastric emptying of a solid meal is accelerated by the removal of dietary fibre naturally present in food. .* Gut 1995. **36**(6): p. 825–830.

180. HJ, E. and P.v. J, *Effect of viscosity of test meals on gastric emptying in dogs. .* Quarterly Journal of Experimental Physiology, 1982. **67**: p. 419–425.

181. Di Lorenzoa, C., et al., *Pectin delays gastric emptying and increases satiety in obese subjects.* Gastroenterology, 1988. **95**(5): p. 1211-1215.

182. Blackburn, N. and I. Johnson, *The effect of guar gum on the viscosity of the gastrointestinal contents and on glucose uptake from the perfused jejunum in the rat.* British Journal of Nutrition, 1981. **46**: p. 239–246.

183. Lecle`re, C., et al., *Role of viscous guar gums in lowering the glycemic response after a solid meal. .* American Journal of Clinical Nutrition, 1994. **59**(4): p. 914–921.

184. Marciani, L., et al., *Assessment of antral grinding of a model solid meal with echo- planar imaging. .* American Journal of Physiology, 2001. **280**: p. G844–G849.

185. Darwiche, G., O. Bjorgell, and L. Almer, *The addition of locust bean gum but not water delayed the gastric emptying rate of a nutrient semisolid meal in healthy subjects. .* BMC Gastroenterology, 2003. **3**(12): p. 1-7.

186. S, A., et al., *Floating drug delivery systems: a review.* AAPS PharmSciTech 2005. **6**(3): p. E372–E390.

187. Bjorck, I., et al., *Food properties affecting the digestion and absorption of carbohydrates.* American Journal of Clinical Nutrition, 1994. **59**(3): p. 699S-705S.

188. Pera, P., et al., *Influence of mastication on gastric emptying. .* Journal of Dental Research, 2002. **81**: p. 179–181.

189. Urbain, J., et al., *The two-component stomach: effects of meal particle size on fundal and antral emptying. .* European Journal of Nuclear Medicine, 1989. **15**: p. 254–259.

190. Stotzer, P. and H. Abrahamsson, *Human postprandial gastric emptying of indigestible solids can occur unrelated to antral phase III.* Neurogastroenterol Motility, 2000. **12**: p. 415-419.

191. Etcheverry, P., M. Grusak, and L. Fleige, *Application of in vitro bioaccessibility and bioavailability methods for calcium, carotenois, folate, iron, magnesium, polyphenols, zinc and vitamins B6, B12, D, and E.* Frontiers in Physiology, 2012. **3**: p. 1-22.

192. Marteau, P., et al., *Survival of lactic acid bacteria in a dynamic model of the stomach and small intestine: validation and the effects of the bile.* Journal of Dairy Science, 1997. **80**: p. 1031-1037.

193. Souliman, S., et al., *A level A in vitro/in vivo correlation in fasted and fed states using different methods: applied to solid immediate release oral dosage form.* European Journal of Phamaceutical Sciences, 2006. **27**: p. 72-79.

194. Larsson, M., M. Minekus, and R. Havenaar, *Estimation of the bioavailability of iron and phosphorus in cereals using a dynamic in vitro gastro-intestinal model.* Journal of the Science of Food and Agriculture, 1997. **74**: p. 99-106.

195. Verwei, M., et al., *Predicted serum folate concentrations based on in vitro studies and kinetic modeling are consistent with measured folate concentrations in humans.* The Journal of Nutrition, 2006. **136**(12): p. 3074-3078.

196. FDA., *Guidance for industry, extended release oral dosage forms: development, evaluation and application of an in vitro/in vivo correlation. .* CDER 1997., 1997.

197. Minekus, M., et al., *Effect of partially hydrolyzed guar gum (PHGG) on the bioacecessability of fat and cholesterol.* Bioscience, Biotechnology, and Biochemistry, 2005. **69**(5): p. 932-938.

198. Kondo, S., et al., *Suppressive effects of dietary fiber in yogurt on the postprandial serum lipid levels in health adult male volunteers.* Bioscience, Biotechnology, and Biochemistry, 2004. **68**: p. 1135-1138.

199. Ting, Y., et al., *Viscoelastic Emulsion Improved the Bioaccessibility and Oral Bioavailability of Crystalline Compound: A Mechanistic Study Using in Vitro and in Vivo Models.* Molecular Pharmaceutics, 2015. **12**: p. 2229-2236.

200. Verwei, M., et al., *Folic Acid and 5-Methyltetrahydrofolate in Fortified Milk Are Bioaccessible as Determined in a Dynamic In Vitro Gastrointestinal Model.* The Journal of Nutrition, 2003. **133**(7): p. 2377-2383.

201. Tamura, T. and E. Stokstad, *The availability of food folate in man.* British Journal of Nutrition, 1973. **25**: p. 513-532.

202. Abad, A. and J. Gregory, *Determination of folate bioavailabilty with rat bioassay.* The Journal of Nutrition, 1987. **117**: p. 866-873.

203. Christensen, J., et al., *Multivariate autofluorescence of intact food systems.* Chemical Reviews, 2006. **106**(6): p. 1979-1994.

204. Corradini, M.G. and R.D. Ludescher, *Making sense of luminescence from GRAS optical probes.* Current Opinion in Food Science, 2015. **4**: p. 25-31.

205. Corradini, M.G., et al., *Identifying and selecting edible luminescent probes as sensors of food quality.* AIMS Biophysics, 2016. **3**(2): p. 319-339.

206. Karoui, R. and C. Blecker, *Fluorescence spectroscopy measurement for quality assessment of food systems-a review.* Food and Bioprocess Technology, 2011. **4**(3): p. 364-386.
207. Strasburg, G.M. and R.D. Ludescher, *Theory and applications of fluorescence spectroscopy in food research.* Trends in Food Science & Technology, 1995. **6**: p. 69-75.
208. Jameson, D.M., *Introduction to Fluorescence.* 2014, Boca Raton, FL: CRC Press.
209. Turro, N.J., V. Ramamurthy, and J.C. Scaiano, *Modern Molecular Photochemistry of Organic Molecules.* 2010, Sausalito, CA: University Science Books.
210. Garcia-Canas, V., et al., *Present and future challenges in food analysis: Foodomics.* Analytical Chemistry, 2012. **84**(23): p. 10150-10159.
211. Skov, T., et al., *Chemometrics in foodomics: Handling data structures from multiple analytical platforms.* Trac-Trends in Analytical Chemistry, 2014. **60**: p. 71-79.
212. Haidekker, M.A. and E.A. Theodorakis, *Environment-sensitive behavior of fluorescent molecular rotors.* Journal of biological engineering, 2010. **4**: p. 11-11.
213. Haiddekker, M. and E. Theodorakis, *Environment-sensitive behavior of fluorescent molecular rotors.* Journal of Biological Engineering, 2010. **4**: p. 1-14.
214. Mezzenga, R., et al., *Understanding foods as soft materials.* Nature Materials, 2005. **4**(10): p. 729-740.
215. McClements, D.J., *Critical review of techniques and methodologies for characterization of emulsion stability.* Critical Reviews in Food Science and Nutrition, 2007. **47**(7): p. 611-649.
216. Haidekker, M.A., et al., *Dyes with Segmental Mobility: Molecular Rotors*, in *Advanced Flourescence Reporters in Chemistry and Biology I: Fundamentals and Molecular Design*, A.P. Demchenko, Editor. 2010. p. 267-308.
217. Loison, P., et al., *Direct investigation of viscosity of an atypical inner membrane of Bacillus spores: A molecular rotor/FLIM study.* Biochimica Et Biophysica Acta-Biomembranes, 2013. **1828**(11): p. 2436-2443.
218. Suhling, K., et al., *Fluorescence Lifetime Imaging of Molecular Rotors in Living Cells.* Jove-Journal of Visualized Experiments, 2012(60).
219. Dent, M.R., et al., *Imaging phase separation in model lipid membranes through the use of BODIPY based molecular rotors.* Physical Chemistry Chemical Physics, 2015. **17**(28): p. 18393-18402.
220. Wu, Y., et al., *Molecular rheometry: direct determination of viscosity in L-o and L-d lipid phases via fluorescence lifetime imaging.* Physical Chemistry Chemical Physics, 2013. **15**(36): p. 14986-14993.
221. Haidekker, M.A., et al., *Effects of solvent polarity and solvent viscosity on the fluorescent properties of molecular rotors and related probes.* Bioorganic Chemistry, 2005. **33**(6): p. 415-425.
222. Jee, A.-Y., E. Bae, and M. Lee, *Internal Twisting Dynamics of Dicyanovinyljulolidine in Polymers.* Journal of Physical Chemistry B, 2009. **113**(52): p. 16508-16512.

223. Jee, A.-Y., E. Bae, and M. Lee, *Internal motion of an electronically excited molecule in viscoelastic media.* Journal of Chemical Physics, 2010. **133**(1).

224. Kashi, A., et al., *Potential Use of Food Synthetic Colors as Intrinsic Luminescent Probes of the Physical State of Foods*, in *Chemical Sensory Informatics of Food: Measurement, Analysis, Integration*, B. Guthrie, et al., Editors. 2015. p. 253-267.

225. Du, H., et al., *Micro-viscosity of liquid oil confined in colloidal fat crystal networks.* Soft Matter, 2014. **10**(43): p. 8652-8658.

226. Vus, K., et al., *Thioflavin T derivatives for the characterization of insulin and lysozyme amyloid fibrils in vitro: Fluorescence and quantum-chemical studies.* Journal of Luminescence, 2015. **159**: p. 284-293.

227. Amdursky, N., Y. Erez, and D. Huppert, *Molecular Rotors: What Lies Behind the High Sensitivity of the Thioflavin-T Fluorescent Marker.* Accounts of Chemical Research, 2012. **45**(9): p. 1548-1557.

228. Grabowski, Z.R., K. Rotkiewicz, and W. Rettig, *Structural changes accompanying intramolecular electron transfer: Focus on twisted intramolecular charge-transfer states and structures.* Chemical Reviews, 2003. **103**(10): p. 3899-4031.

229. Rettig, W., *Application of a simplified microstructural solvent interaction-model to the solvatochromism of twisted intramolecular charge-transfer (TICT) states.* Journal of Molecular Structure, 1982. **84**(3-4): p. 303-327.

230. Allen, B.D., et al., *The photophysical properties of a julolidene-based molecular rotor.* Physical Chemistry Chemical Physics, 2005. **7**(16): p. 3035-3040.

231. Haidekker, M.A. and E.A. Theodorakis, *Molecular rotors - fluorescent biosensors for viscosity and flow.* Organic & biomolecular chemistry, 2007. **5**(11): p. 1669-1678.

232. Paul, A. and A. Samanta, *Free Volume Dependence of the Internal Rotation of a Molecular Rotor Probe in Room Temperature Ionic Liquids.* Journal of Physical Chemistry B, 2008. **112**(51): p. 16626-16632.

233. Doolitle, A.K., *Newtonina Flow III. The dependence of the viscosity of liquids on molecular weight and free space.* Journal of Applied Physics, 1952. **23**(236-239).

234. Sutharsan, J., et al., *Molecular rotors: synthesis and evaluation as viscosity sensors.* Tetrahedron, 2010. **66**(14): p. 2582-2588.

235. Kashi, A., et al., *Potential use of food synthetic colors as intrinsic luminescent probes of the physical state of foods*, in *Chemical Sensory Informatics of Food: Measurement, Analysis, Integration*. 2015, ACS Publications- Oxford University Press.

236. Haidekker, M.A., et al., *Hydrophilic molecular rotor derivatives - synthesis and characterization.* Bioorganic Chemistry, 2004. **32**(4): p. 274-289.

237. Sinkeldam, R.W., et al., *Emissive Nucleosides as Molecular Rotors.* Chemphyschem, 2011. **12**(3): p. 567-570.

238. Loutfy, R.O. and B.A. Arnold, *Effect of viscosity and temperature on torsional relaxation of molecular rotors. .* Journal of Physical Chemistry, 1982. **1982**(86): p. 21.

239. Loutfy, R.O. and K.Y. Law, *Electrochemistry and spectroscopy of intramolecular charge-transfer complexes. p-N,N-Dialkylaminobenzylidenemalononitriles. .* The Journal of Physical Chemistry, 1980. **84**(21): p. 2803-2808.

240. Howell, S., et al., *Intrinsic and Extrinsic Temperature-Dependency of Viscosity-Sensitive Fluorescent Molecular Rotors.* Journal of Fluorescence, 2012. **22**(1): p. 457-465.

241. Brummond, K.M. and L.S. Kocsis, *Intramolecular Didehydro-Diels-Alder Reaction and Its Impact on the Structure-Function Properties of Environmentally Sensitive Fluorophores.* Accounts of Chemical Research, 2015. **48**(8): p. 2320-2329.

242. Bahaidarah, E., et al., *Fluorescent molecular rotors based on the BODIPY motif: effect of remote substituents.* Photochemical & Photobiological Sciences, 2014. **13**(10): p. 1397-1401.

243. Kocsis, L.S., et al., *Cyclopenta b naphthalene cyanoacrylate dyes: synthesis and evaluation as fluorescent molecular rotors.* Organic & biomolecular chemistry, 2015. **13**(10): p. 2965-73.

244. Shao, J., et al., *Thiophene-Inserted Aryl-Dicyanovinyl Compounds: The Second Generation of Fluorescent Molecular Rotors with Significantly Redshifted Emission and Large Stokes Shift.* European Journal of Organic Chemistry, 2011(30): p. 6100-6109.

245. Dakanali, M., et al., *Self-calibrating viscosity probes: Design and subcellular localization.* Bioorganic & Medicinal Chemistry, 2012. **20**(14): p. 4443-4450.

246. Nipper, M.E., et al., *Detection of liposome membrane viscosity perturbations with ratiometric molecular rotors.* Biochimie, 2011. **93**(6): p. 988-994.

247. Haidekker, M.A., et al., *A ratiometric fluorescent viscosity sensor.* Journal of the American Chemical Society, 2006. **128**(2): p. 398-399.

248. Kuimova, M.K., *Mapping viscosity in cells using molecular rotors.* Physical Chemistry Chemical Physics, 2012. **14**(37): p. 12671-12686.

249. Peng, X., et al., *Fluorescence Ratiometry and Fluorescence Lifetime Imaging: Using a Single Molecular Sensor for Dual Mode Imaging of Cellular Viscosity.* Journal of the American Chemical Society, 2011. **133**(17): p. 6626-6635.

250. Uzhinov, B.M., V.L. Ivanov, and M.Y. Melnikov, *Molecular rotors as luminescence sensors of local viscosity and viscous flow in solutions and organized systems.* Russian Chemical Reviews, 2011. **80**(12): p. 1179-1190.

251. Kuimova, M.K., *Molecular Rotors Image Intracellular Viscosity.* Chimia, 2012. **66**(4): p. 159-165.

252. Wang, K. and H. Ma, *Biologically Environment-Sensitive Fluorescent Probes.* Progress in Chemistry, 2010. **22**(8): p. 1633-1640.

253. Kuimova, M.K., et al., *Imaging intracellular viscosity of a single cell during photoinduced cell death.* Nature Chemistry, 2009. **1**(1): p. 69-73.

254. Battisti, A., et al., *Imaging intracellular viscosity by a new molecular rotor suitable for phasor analysis of fluorescence lifetime.* Analytical and Bioanalytical Chemistry, 2013. **405**(19): p. 6223-6233.

255. Levitt, J.A., et al., *Fluorescence Anisotropy of Molecular Rotors.* Chemphyschem, 2011. **12**(3): p. 662-672.

256. Lopez-Duarte, I., et al., *A molecular rotor for measuring viscosity in plasma membranes of live cells.* Chemical Communications, 2014. **50**(40): p. 5282-5284.

257. Baskurt, O.K. and H.J. Meiselman, *Blood rheology and hemodynamics.* Seminars in Thrombosis and Hemostasis, 2003. **29**(5): p. 435-450.

258. Haidekker, M.A., et al., *Phospholipid-bound molecular rotors: Synthesis and characterization.* Bioorganic & Medicinal Chemistry, 2002. **10**(11): p. 3627-3636.

259. Akers, W.J., J.M. Cupps, and M.A. Haidekker, *Interaction of fluorescent molecular rotors with blood plasma proteins.* Biorheology, 2005. **42**(5): p. 335-344.

260. Hall, D. and A.P. Minton, *Macromolecular crowding: qualitative and semiquantitative successes, quantitative challenges.* Biochimica Et Biophysica Acta-Proteins and Proteomics, 2003. **1649**(2): p. 127-139.

261. Ellis, R.J., *Macromolecular crowding: obvious but underappreciated.* Trends in Biochemical Sciences, 2001. **26**(10): p. 597-604.

262. Festy, F., et al., *Imaging proteins in vivo using fluorescence lifetime microscopy.* Molecular Biosystems, 2007. **3**(6): p. 381-391.

263. Thompson, A.J., et al., *Molecular Rotors Provide Insights into Microscopic Structural Changes During Protein Aggregation.* Journal of Physical Chemistry B, 2015. **119**(32): p. 10170-10179.

264. Thompson, A.J., et al., *Quantitative sensing of microviscosity in protocells and amyloid materials using fluorescence lifetime imaging of molecular rotors*, in *Imaging, Manipulation, and Analysis of Biomolecules, Cells, and Tissues*, D.L. Farkas, D.V. Nicolau, and R.C. Leif, Editors. 2014, Proceedings of SPIE.

265. Ferri, G., et al., *Organization of inner cellular components as reported by a viscosity-sensitive fluorescent Bodipy probe suitable for phasor approach to FLIM.* Biophysical Chemistry, 2016. **208**: p. 17-25.

266. Levitt, J.A., et al., *Membrane-Bound Molecular Rotors Measure Viscosity in Live Cells via Fluorescence Lifetime Imaging. .* Journal of Physical Chemistry C, 2009. **113**(27): p. 11634-11642.

267. van der Meer, W., *Physiology of membrane fluidity*. 1984, Boca Raton, FL: CRC Press.

268. Dunham, W.R., et al., *EPR measurements showing that plasma membrane viscosity can vary from 30 to 100 cP in human epidermal cell strains.* Spectrochimica Acta Part A: Molecular and Biomolecular Spectroscopy, 1996. **52**(10): p. 1357-1368.

269. Kung, C.E. and J.K. Reed, *Microviscosity measurements of phospholipid bilayers using fluorescent dyes that undergo torsional relaxation.* Biochemistry, 1986. **25**(20): p. 6114-6121.

270. Rohrbach, D. and R. Timpl, *Molecular and cellular aspects of basement membranes*. 1993, San Diego, CA: Academic Press.

271. Luneva, O.G., et al., *Ion transport, membrane fluidity and haemoglobin conformation in erythrocyte from patients with cardiovascular diseases: Role of augmented plasma cholesterol.* Pathophysiology : the Official Journal of the International Society for Pathophysiology / ISP 2007. **14**(1): p. 41-46.

272. Shinitzky, M., *Membrane fluidity in malignancy. Adversative and recuperative.* Biochimica et biophysica acta, 1984. **738**(4): p. 251-261.

273. Kearney-Schwartz, A., et al., *Haemorheological disturbances in hypertensive type 2 diabetic patients – influence of antihypertensive therapy.* Fundamental & Clinical Pharmacology, 2007. **21**(4): p. 387-396.

274. Deliconstantinos, G., V. Villiotou, and J.C. Stavrides, *Modulation of particulate nitric oxide synthase activity and peroxynitrite synthesis in cholesterol enriched endothelial cell membranes.* Biochemical pharmacology, 1995. **49**(11): p. 1589-1600.

275. Salazar Vázquez, B.Y., et al., *Increased hematocrit and reduced blood pressure following control of glycemia in diabetes. .* Clinical hemorheology and microcirculation, 2008. **38**(1): p. 57-64.

276. Hou, X., et al., *Binding of Amyloidogenic Transthyretin to the Plasma Membrane Alters Membrane Fluidity and Induces Neurotoxicity.* Biochemistry, 2005. **44**(34): p. 11618-11627.

277. Nipper, M.E., et al., *Characterization of changes in the viscosity of lipid membranes with the molecular rotor FCVJ.* Biochimica Et Biophysica Acta-Biomembranes, 2008. **1778**(4): p. 1148-1153.

278. Lentz, B.R., Y. Barenholz, and T.E. Thompson, *Fluorescence depolarization studies of phase transitions and fluidity in phospholipid bilayers. 2. Two-component phosphatidylcholine liposomes.* Biochemistry, 1976. **15**(20): p. 4529-4537.

279. Anderson, R.G.W. and K. Jacobson, *Cell biology - A role for lipid shells in targeting proteins to caveolae, rafts, and other lipid domains.* Science, 2002. **296**(5574): p. 1821-1825.

280. Simons, K. and R. Ehehalt, *Cholesterol, lipid rafts, and disease.* The Journal of Clinical Investigation, 2002. **110**(5): p. 597-603.

281. Yasuhara, K., Y. Sasaki, and J.I. Kikuchi, *Fluorescent sensor responsive to local viscosity and its application to the imaging of liquid-ordered domain in lipid membranes.* Colloids and Surfaces B-Biointerfaces, 2008. **67**(1): p. 145-149.

282. Ramírez-Alvarado, M., J.S. Merkel, and L. Regan, *A systematic exploration of the influence of the protein stability on amyloid fibril formation in vitro.* Proceedings of the National Academy of Sciences, 2000. **97**(16): p. 8979-8984.

283. Pulawski, W., et al., *Ubiquitous Amyloids.* Applied Biochemistry and Biotechnology, 2012. **166**(7): p. 1626-1643.

284. Sutharsan, J., et al., *Rational Design of Amyloid Binding Agents Based on the Molecular Rotor Motif.* Chemmedchem, 2010. **5**(1): p. 56-60.

285. Yu, W.-T., et al., *Protein sensing in living cells by molecular rotor-based fluorescence-switchable chemical probes.* Chemical Science, 2016. **7**(1): p. 301-307.

286. Hosny, N.A., et al., *Fluorescent lifetime imaging of atmospheric aerosols: a direct probe of aerosol viscosity.* Faraday Discussions, 2013. **165**: p. 343-356.

287. Hosny, N.A., et al., *Mapping microbubble viscosity using fluorescence lifetime imaging of molecular rotors.* Proceedings of the National Academy of Sciences of the United States of America, 2013. **110**(23): p. 9225-9230.

288. Roche, C.J., F. Guo, and J.M. Friedman, *Molecular level probing of preferential hydration and its modulation by osmolytes through the use of pyranine complexed to hemoglobin.* Journal of Biological Chemistry, 2006. **281**(50): p. 38757-38768.

289. Akers, W. and M.A. Haidekker, *A molecular rotor as viscosity sensor in aqueous colloid solutions.* Journal of Biomechanical Engineering-Transactions of the Asme, 2004. **126**(3): p. 340-345.

290. Dragan, A., A.E. Graham, and C.D. Geddes, *Fluorescence-based Broad Dynamic Range Viscosity Probes.* Journal of Fluorescence, 2014. **24**(2): p. 397-402.

291. Tang, D. and A.G. Marangoni, *Quantitative study on the microstructure of colloidal fat crystal networks and fractal dimensions.* Advances in Colloid and Interface Science, 2006. **128–130**: p. 257-265.

292. Kumar, S., et al., *Thioflavin T Displays Enhanced Fluorescence Selectively Inside Anionic Micelles and Mammalian Cells.* Journal of Fluorescence, 2008. **18**(6): p. 1199-1205.

293. Vaccaro, G., et al., *Direct monitoring of self-assembly of copolymeric micelles by a luminescent molecular rotor.* Chemical Communications, 2013. **49**(76): p. 8474-8476.

294. Nazar, M.F. and S. Murtaza, *Physicochemical investigation and spectral properties of Sunset Yellow dye in cetyltrimethylammonium bromide micellar solution under different pH conditions.* Coloration Technology, 2014. **130**(3): p. 191-199.

295. Raeburn, J., et al., *Using molecular rotors to probe gelation.* Soft Matter, 2015. **11**(18): p. 3706-3713.

296. Miguel, D., et al., *Development of a New Dual Polarity and Viscosity Probe Based on the Foldamer Concept.* Organic Letters, 2015. **17**(11): p. 2844-2847.

297. Frochot, C., et al., *Fluorescence Spectroscopy as a Non Invasive Tool to Follow In Situ the Polymerization in Miniemulsion.* Journal of Applied Polymer Science, 2011. **119**(1): p. 219-224.

298. Ismail, L.F.M., *Photophysical properties of a surfactive long-chain styryl merocyanine dye as fluorescent probe.* Journal of Luminescence, 2012. **132**(9): p. 2512-2520.

299. Hawe, A., V. Filipe, and W. Jiskoot, *Fluorescent Molecular Rotors as Dyes to Characterize Polysorbate-Containing IgG Formulations.* Pharmaceutical Research, 2010. **27**(2): p. 314-326.

300. Ablinger, E., S. Leitgeb, and A. Zimmer, *Differential scanning fluorescence approach using a fluorescent molecular rotor to detect thermostability of proteins in surfactant-containing formulations.* International Journal of Pharmaceutics, 2013. **441**(1-2): p. 255-260.

301. Iio, T., S. Takahashi, and S. Sawada, *Fluorescent Molecular Rotor Binding to Actin. .* Journal of Biochemistry, 1993. **113**(2): p. 196-199.

302. Jin, Y.-J., et al., *Fluorescent Molecular Rotor-in-Paraffin Waxes for Thermometry and Biometric Identification.* Acs Applied Materials & Interfaces, 2015. **7**(26): p. 14485-14492.

303. Alamiry, M.A.H., et al., *Freezing and glass transition phenomena for 1,2-dichloroethane under high pressure as revealed by fluorescence spectroscopy.* Rsc Advances, 2012. **2**(5): p. 1936-1941.

304. Martini, G., et al., *Julolidine fluorescent molecular rotors as vapour sensing probes in polystyrene films.* Dyes and Pigments, 2015. **113**: p. 47-54.

305. Minei, P., et al., *Reversible vapochromic response of polymer films doped with a highly emissive molecular rotor.* Journal of Materials Chemistry C, 2014. **2**(43): p. 9224-9232.

306. Holdsworth, S.D., *Applicability of rheological models to the interpretation of flow and processing behaviour of fluid food products. .* Journal of Texture Studies, 1971. **2**(4): p. 393-418.

307. Mustafic, A., et al., *Imaging of Flow Patterns with Fluorescent Molecular Rotors.* Journal of Fluorescence, 2010. **20**(5): p. 1087-1098.

308. Dilorenzo, C., et al., *Pectin delalys gastri-emptying and increases satiety in obese subjects.* Gastro-enterology, 1988. **95**: p. 1211-1215.

309. Bergmann, J.F., et al., *Correlation between echographic gastric emptying and appetite- influence of psyllium.* Gut, 1922. **33**: p. 1042-1043.

310. Marciani, L., et al., *Gastric response to increased meal viscosity assessed by echo-planar magnetic resonance imaging in humans.* Journal of Nutrition, 2000. **130**: p. 122-127.

311. Mattes, R.D. and D. Rothacker, *Beverage viscosity in inversely related to postrandial hunger in humans.* Physiology behavior, 2001. **74**: p. 551-557.

312. Marciani, L., et al., *Effect of meal viscosity and nutrients on satiety, intragastric dilution, and emptying assessed by MRI.* American Journal of Physiology, 2001. **280**(6): p. G1227-G1233.

313. Norton, I., P. Fyer, and S. Moore, *Product/Process Integration in Food Manufacture: Engineering Sustained Health.* American Institute of Chemical Engineers, 2006. **52**(5): p. 1632-1640.

314. Dikeman, C., M. Murphy, and G. Fahey, *Dietary fibers affect viscosity of solutions and simulated human gastric and small intestinal digesta.* The Journal of Nutrition, 2006. **136**(4): p. 913-919.

315. Steffe, J., *Rheological methods in food precess engineering.* 2nd ed. 1996, MI, East Lansing: Freeman Press.

316. Lentle, R., et al., *High definition mapping of circular and longitudinal motility in the terminal ileum of the brushtail possum Trichosurus vulpecula with watery and viscous perfusates.* Journal of Comparative Physiology B, 2007. **177**: p. 543-556.

317. Alhassawi, F., et al., *Potential Applications of Luminescent Molecular Rotors in Food Science and Engineering. .* Critical Reviews in Food Science and Nutrition, 2017. **in press**.

318. Villemejane, C., et al., *In vitro digestion of short-dough biscuits enriched in proteins and/or fibes, using a mulit-compartmental and dynamic system (1): Viscosity measurment and prediction.* Food Chemistry, 2015. **182**: p. 55-63.

319. *poly(vinyl chloride).* [cited 2013 09/27/2013]; Available from: http://www.polymerprocessing.com/polymers/PVC.html.

320. Loutfy, R. and B. Arnold, *Effect of viscosity and temperature on torsional relaxation of molecular rotors.* Journal of Physical Chemistry, 1982. **86**: p. 4205-4211.

321. Law, K., *Fluorescence probe for microenvironments: anamolous viscosity dependence of the fluorescence quantum yield of p-N,N-dialkyl-amino-benzylidene-malonitirile in 1-alkanols.* Chemical Physics Letters, 1980. **75**: p. 545-549.

322. Turro, N., V. Ramamurthy, and J. Scaiano, *Modern molecular photochemistry of organic molecules.* 2010, Herndon, VA, USA: University Science Books.

323. Blazek, J. and L. Copeland, *Pasting and swelling properties of wheat flour and starch in relation to amylose content.* Carbohydrate Polymers, 2008. **71**: p. 380-387.

324. Copeland, L., et al., *Form and functionality of starch.* Food Hydrocolloids, 2009. **23**: p. 1527-1534.

325. Maurer, H. and R. Kearney, *Opportunities and challenges for starch in the paper industry.* Starch/Stärke 1998. **50**: p. 396–402.

326. Case, S., et al., *Physical properties and gelation behavior of Low-amylopectin maize starch and other high-amylose maize starches.* journal of cereal science, 1998. **27**: p. 301-314.

327. Jane, J., et al., *Effects of amylopectin branch chain length and amylose content on the gelatinization and pasting properties of starch. .* Cereal Chemistry, 1999. **76**: p. 629–637.

328. Morrison, W. and M. Azudin, *Variation in the amylose and lipid contents and some physical properties of rice starches. .* Journal of Cereal Science, 1987. **5**(1): p. 35-44.

329. Singh, N., et al., *Morphological, thermal and rheological properties of starches from different botanical sources.* Food Chemistry, 2003. **81**(2): p. 219-231.

330. Haidekker, A. and E. Theodorakis, *Environment-sensitive behavior of fluorescent molecular rotors.* Journal of Biological Engineering, 2010. **4**: p. 1-14.

331. Collado, L., R. Mabesa, and H. Corke, *Genetic variation in the physical properties of sweet potato starch.* Journal of Agricultural and Food Chemistry, 1999. **47**: p. 4195–4201.

332. Zeng, M., et al., *Sources of variation for starch gelatinization, pasting, and gelation properties in wheat.* Cereal Chem, 1997. **74**: p. 63–71.

333. Hunga, P., T. Maedac, and N. Moritaa, *Study on Physicochemical Characteristics of Waxy and High-amylose Wheat Starches in Comparison with Normal Wheat Starch.* Starch/ Sta"rke, 2007. **59**: p. 125-131.

334. Schirmer, M., et al., *Physicochemical and morphological characterization of different starches with variable amylose/amylopectin ratio.* Food Hydrocolloids, 2013. **32**: p. 52-63.

335. Sarker, M., et al., *Rheological behavior of starch‐based biopolymer mixtures in selected processed foods.* Starch/Stärke, 2013. **65** (1-2): p. 73-81.

336. Conde-Petit, B., et al., *Perspectives of starch in food science.* Chimia, 2001). . **55**(3): p. 201-205.

337. Fortuna, T., et al., *The influence of starch pore characteristics on pasting behaviour.* International Journal of Food Science & Technology, 2000. **35**: p. 285-291.

338. Colonna, P. and C. Mercier, *Gelatinization and melting of maize and pea starches with normal and high-amylose genotypes.* Phytochemistry, 1985. **24**: p. 1667-1674.

339. BeMiller, J. and R. Whistler, *Starch: chemistry and technology.* 2009, Oxford: Academic Press.

340. Marciani, L., et al., *Gastric response to increased meal viscosity assessed by echo-planar magnetic resonance imaging in humans.* The Journal of Nutrition, 2000. **130**(1): p. 122-127.

341. Panahi, S., et al., *Beta-glucan from two sources of oat concentrates affect postprandial glycemia in relation to the level of viscosity.* American College of Nutrition, 2007. **26**(6): p. 639-644.

342. wood, P., *Relationships between solution properties of cereal beta-glucans and physiological effects: a review.* Trends in Food Science and Technology, 2004. **15**(6).

343. Makelainen, H., et al., *The effect of beta-glucan on the glycemic and insulin index.* European Journal of Clinical Nutrition, 2007. **61**(6): p. 779-785.

344. Onning, G., *The use of cereal beta-glucans to control diabetes and cardiovascular disease* in *Functional Foods, Cardiovascular Disease, and Diabetes*, A. Arnoldi, Editor. 2004, Woodhead Publishing Ltd: Cambridge, England. p. 402-421.

345. Dikeman, C. and G. Fahey, *Viscosity as related to dietary fiber: a review.* Critical Reviews of Food Science and Nutrition, 2006. **46**(8): p. 649-663.

346. Battilana, P., et al., *Mechanisms of action of beta-glucan in postprandial glucose metabolism in healthy men.* European Journal of Clinical Nutrition, 2001. **55**: p. 327-333.

347. Miller, S. and R. Fulcher, *Microstructure and chemistry of the oat kernel.*, in *Oats: Chemistry and Technology*, F. Webster and P. Wood, Editors. 2011, American Association of Cereal Chemists: St Paul, MN. p. 77-94.

348. Wang, Q. and P. Ellis, *Oat β-glucan: physico-chemical characteristics in relation to its blood-glucose and cholesterol-lowering properties.* British Journal of Nutrition, 2014. **112**: p. S4-S13.

349. Fabek, H., et al., *The effect of in vitro digestive processes on the viscosity of dietary fibres and their influence on glucose diffusion.* Food Hydrocolloids, 2014. **35**: p. 718-726.

350. Sasaki, T. and K. Kohyama, *Influence of non-starch polysaccharides on the in vitro digestibility and viscosity of starch suspensions.* Food Chemistry, 2012. **133**: p. 1420-1426.

351. Englyst, K., et al., *Rapidly available glucose in foods: an in vitro measurement that reflects the glycemic response.* American Journal of Clinical Nutrition, 1999. **69**: p. 448-454.

352. Giradet, N. and F. Webster, *Oat milling: specifications, storage and processsing*, in *Oats: Chemistry and Technology*, F. Webster and P. Wood, Editors. 2011, American Association of Cereal Chemists: St. Paul, MN. p. 301-302.

353. Speranza, A., et al., *Influence of Emulsifier Structure on Lipid Bioaccessability in Oil-Water Nanoemulsions.* Journal of Agricultural and Food Chemistry, 2013. **61**: p. 6505-6515.

354. Troncoso, E., J. Aguilera, and D. McClements, *Fabrication, characterization and lipase digestibility of food-grade nanoemulsions.* Food Hydrocolloids, 2012. **27**: p. 355-363.

355. Li, Y. and D. McClements, *Inhibition of lipase-catalyzed hydrolysis of emulsified triglyceride oils by low-molecular weight surfactants under simulated gastrointestinal conditions.* European Journal of Pharmaceutics and Biopharmaceutics, 2011. **79**: p. 423-431.

356. Jenkins, D., et al., *Glycemic index of foods: a physiological basis for carbohydrate exchange.* American Journal of Clinical Nutrition, 1981. **34**: p. 362-366.

357. Gannon, M., et al., *Effects of dose of ingested glucose on plasma metabolite and hormone response in type II diabetic subjects.* Diabetes Care, 1989. **12**: p. 544-552.

358. Brand, J., et al., *Food processing and the glycemic index.* American Journal of Clinical Nutrition, 1985. **42**: p. 1192-1196.

359. Sheard, N., et al., *Dietary carbohydrate (Amount and Type) in the prevention and management of diabetes.* Diabetes Care, 2004. **27**(9): p. 2266-2271.

360. Englyst, H., J. Veenstra, and J. Geoffrey, *Measurement of rapidly available glucose (RAG) in plant foods: A potential in vitro predictor of the glycaemic response.* British Journal of Nutrition, 1996. **75**: p. 327-337.

361. Bornet, F., et al., *Insulin and glycemi responses in healthy humans to native starches processed in different ways: correlation with in vitro alpha-amylase hydrolysis.* The American Journal of Clinical Nutrition, 1989. **50**(2): p. 315-323.

362. Hu, X., X. Xing, and C. Ren, *The effects of steaming and roasting treatments on beta-glucan, lipid and starch in the kernels of nake oat (Avena nuda).* Journal of Science, Food, and Agriculture, 2010. **90**: p. 690-695.

363. Englyst, K., et al., *Glycaemic index of cereal products explained by their content of rapidly and slowly available glucose.* Journal of Nutrition, 2003. **89**: p. 329-339.

364. Jones, C., *The production of mechanically damaged starch in milling is a governing factor in the diastatic activity of flour.* Cereal Chemistry, 1940. **17**: p. 133-164.

365. Knudsen, K., B. Jensen, and I. Hansen, *Digestion of polysaccharides and other major components in the small and large intestine of pigs fed on diets consisting of oat fractions rich in beta-D-glucan.* British Journal of Nutrition, 1993. **70**: p. 537-556.

366. Ezeogu, L., et al., *Influence of cooking conditions on the protein matrix of sorghum and maize endosperm flours.* Cereal Chemistry, 2008. **85**: p. 397-402.

367. Kim, E., et al., *Effect of structural and physicochemical characteristics of the protein matrix in pasta on in vitro starch digestibility.* Food Biophysics, 2008. **3**: p. 229-234.

368. Rainbird, A. and A. Low, *Effect of guar gum on gastric emptying in growing pigs.* British Journal of Nutrition, 1986. **55**: p. 87-98.

369. Cherburt, C., *Role of gastrointestinal motility in the delay of absorption of dietary fiber.* European Journal of Clinical Nutrition, 1995. **49**: p. S74-S80.

370. Anttila, H., T. Sontag-Strohm, and H. Salovaara, *Viscosity of beta-glucan in oat products.* Agricultural and Food Science, 2004. **13**: p. 80-87.

371. Johansen, H., et al., *Physico-chemical properties and the digestibility of polysaccharides from oats in teh gastrointestinal tract of pigs.* Journal of Science, Food, and Agriculture, 1997. **73**: p. 81-92.

372. Johansen, H., et al., *Effects of varying content of soluble dietary fibre from wheat flour and oat milling fractions on gastric emptying in pigs.* British Journal of Nutrition, 1996. **75**: p. 339-351.

373. Fulcher, R. and P. Wood, *Interaction of some dyes with cereal beta-glucans.* Cereal Chemistry, 1978. **55**: p. 952-966.

374. Johansen, H., *Dietary fibre from oats: Physico-chemical properties and physiological function in the stomach adn small intestine of pigs.*, 1993, The Royal Veterinary and Agricultural University: Copenhagen.

375. Ames, N., J. Storsley, and S. Tosh, *Effects of processing on physicochemical properties adn efficacy of beta-glucan from oat and barley.* Cereal Foods World, 2015. **60**(1): p. 4-8.

376. Kim, H. and P. White, *Impact of molecular weight, viscosity and solubility of beta-glucan on in vitro oat starch digestibility.* Journal of Agricultural and Food Chemistry, 2013. **61**: p. 3270-3277.

377. Wolever, T., et al., *Physicochemical properties of oat beta-glucan influence its ability to reduce serum LDL cholesterol in humans: A randomized clinical trial.* American Journal of Clinical Nutrition, 2010. **92**: p. 723-732.

378. Wood, P., J. Weisz, and W. Mahn, *Molecular characterisation of cereal beta-glucan. II. Size-exclusion chromatography for comparison of molecular weight.* Cereal Chemistry, 1991. **86**: p. 530-536.

379. Wang, X., *The effects of processing on the nutritional characteristics of oat fibre*, in *Department of Human Nutritional Science*2014, University of Manitoba: Winnipeg.

380. Kim, H. and P. White, *Interactional effects of beta-glucan, starch and protein in heated oat slurries on viscosity and in vitro bile acid binding.* Journal of Agricultural and Food Chemistry, 2012. **60**: p. 6217-6222.

381. Guerin, S., et al., *Changes in intragastric meal distribution are better predictors of gastric emptying rate in conscious pigs than are meal viscosity or dietary fibre concentration.* British Journal of Nutrition, 2001. **85**(3): p. 343-350.

382. Foster-Powell, K., S.H.A. Holt, and J.C. Brand-Miller, *International table of glycemic index and glycemic load values: 2002.* American Society for Clinical Nutrition, 2002. **76**: p. 5-56.

383. Tecante, A. and J. Doublier, *Steady flow and viscoelastic behavior of crosslinked waxy cornstarch-k-carrageenan pastes and gels.* Carbohydrate Polymers, 1999. **40**(221-231).

384. Gidley, M., *Hydrocolloids in the digestive tract and related health implications.* Current Opinion in Colloid & Interface Science, 2013. **18**: p. 371-378.

385. Martin, G., R. Williams, and D. Dunstan, *Effect of manufacture and reconstitution of milk protein concentrate powder on the size and rennet gelation behaviour of casein micelle.* International Dairy Journal, 2010. **20**: p. 128-131.

386. Abu-Jdayil, B., M. Mohameed, and A. Eassa, *Rheology of wheat starch–milk–sugar systems: effect of starch concentration, sugar type and concentration, and milk fat content.* Journal of Food Engineering, 2004. **64**: p. 207-212.

387. Bradley, G., *Starch performance in UHT systems.* Dairy Industries International, 1993(58): p. 43.

388. Tarrega, A., J. Velez-Ruiz, and E. Costell, *Influence of milk on the rheological behaviour of cross-linked waxy maize and tapioca starch dispersions.* Food Research International, 2005. **38**: p. 759–768.

389. AlHasawi, F., et al., *In vitro measurements of luminal viscosity and glucose/maltose bioaccessibility for oat bran, instant oats, and steel cut oats.* Food Hydrocolloids, 2017. **70**: p. 293-303.

390. Kottas, G., et al., *Artificial Molecular Rotors.* Chemical Reviews, 2005. **105**(4): p. 1281-1376.

391. Nilsson, M., J. Holst, and I. Björck, *Metabolic effects of amino acid mixtures and whey protein in healthy subjects: studies using glucose-equivalent drinks. .* American Journal of Clinical Nutrition, 2007. **85**(4): p. 996–1004.

392. Akhavan, T., et al., *Effect of premeal consumption of whey protein and its hydrolysate on food intake and postmeal glycemia and insulin responses in young adults. .* American Journal of Clinical Nutrition, 2010. **91**(4): p. 966–975.

393. Claessens, M., et al., *The effect of different protein hydrolysate/carbohydrate mixtures on postprandial glucagon and insulin responses in healthy subjects. .* European Journal of Clinical Nutrition, 2009. **63**(1): p. 48–56.

394. Jakubowicza, D. and O. Froy, *Biochemical and metabolic mechanisms by which dietary whey protein may combat obesity and Type 2 diabetes.* Journal of Nutritional Biochemistry, 2013. **24**: p. 1-5.

395. Villemejane, C., et al., *In vitro digestion of short-dough biscuits enriched in proteins and/or fibres using a multi-compartmental and dynamic system (2): Protein and starch hydrolyses.* Food Chemistry, 2016. **190**: p. 164-172.

396. Corradini, M. and M. Peleg, *Linear and non-linear kinetics in the synthesis and degradation of acrylamide in foods and model systems.* Critical Reviews in Food Science and Nutrition, 2006. **46**: p. 489-517.

397. Descamps, O., P. Langevin, and D. Combs, *Physical effect of starch/carrageenan interactions in water and milk.* Food Technology, 1986. **40**: p. 81-88.

398. Velez-Ruiz, J. and G. Barbosa-Canovas, *Rheological properties of selected dairy products.* Critical Reviews of Food Science and Nutrition, 1997. **37**: p. 311–359.

399. Matser, A. and P. Steeneken, *Rheological properties of highly cross-linked waxy maize starch in aqueous suspensions of skim milk components. Effects of the concentration of starch and skim milk components.* Carbohydrate Polymers, 1996. **32**: p. 297-305.

400. Ling, L.H., *Effect of heat denaturation of whey proteins on the rheological properties of corn starch-milk systems.* Dessertation Abstracts International, 1984. **B44**(12): p. 131.

401. Spies, R. and R. Hoseney, *Effect of sugars on starch gelatinization. .* Cereal Chemistry, 1982. **59**(2): p. 128-131.

402. Boirie, Y., et al., *Slow and fast dietary proteins differently modulate postprandial protein accretion. Proc Natl Acad Sci U S A ;94:14930–5.* PRoceedings of the National Academy of Sciences, 1997. **94**: p. 1430-1435.

403. Chin, S. and R. Rona, *Prevalence and trends in overweight and obesity in three cross-sectional studies of British Children, 1974-94.* BMJ, 2001. **322**: p. 24-26.

404. Statistics, N.C.f.H. *Prevalence of overweight among children and adolescents: United States.* 1999 [cited 2014; Available from: http://www.cdc.gov/nchs/products/pubs/pubd/hestats/ overwght99.htm

405. Wang, Y., C. Monteiro, and B. Popkin, *Trends of obesity and underweight in older children and adolescentes in the United States, Brazil, China, and Russia.* American Journal of Clinical Nutrition, 2002. **75**: p. 971-977.

406. Murata, M., *Secular trends in growth and changes in eating patterns of Japanese children.* American Journal of Clinical Nutrition, 2000. **72**: p. 1379S-1383S.

407. deOnis, M. and M. Blossner, *Prevalence and trends of overweight among preschool children in developing countries.* American Journal of Clinical Nutrition, 2000. **72**: p. 1032-1039.

408. Filozof, C., et al., *Obesity prevalance and trends in Latin-American countries.* Obesity Reviews, 2001. **2**: p. 99-106.

409. Magarey, A., L. Daniels, and T. Boulton, *Prevalence of overweight and obesity in Australian children and adolescents: reassessment of 1985-1995 data against new standard international definitions.* Medical Journal of Australia, 2001. **174**: p. 561-564.

410. Ogden, C., et al., *Prevalence of overweight and obesity in the United States, 1999-2004.* JAMA, 2006. **295**(13): p. 1549-1555.

411. Ogden, C., et al., *Prevalence and trends in overweight among US children and adolescents, 1999-2000.* JAMA, 2002. **288**(14): p. 1728-1732.

412. Ogden, C., M. Carrol, and K. Flegal, *High body mass index for age among US children and adolescents.* JAMA, 2008. **299**(20): p. 2401-2405.

413. Horowitz, M., et al., *Abnormalities of gastric emptying in obese patients.* International Journal of Obesity 1983. **7**: p. 415-421.

414. Tosetti, C., et al., *Gastric emptying of solids in morbid obesity.* International Journal of Obesity and Related Metabolic Disorders : Journal of the International Association for the Study of Obesity, 1996. **20**: p. 200-205.

415.   Keogh, J.B., et al., The Journal of Nutrition, 2011. **141**: p. 809-815.
416.   Lindquist, S. and O. Hernell, *Lipid digestion and absorption in early life: an update.* Current Opinion in Clinical Nutrition and Metabolic Care, 2010. **13**: p. 314-320.
417.   Wilde, P.J. and B.S. Chu, *Interfacial & colloidal aspects of lipid digestion.* Advances in Colloid and Interface Science, 2011. **165**: p. 14-21.
418.   Patton, J. and C. M., *Watching fat digestion.* Science, 1979. **2014**: p. 145-148.
419.   Hayes, J.R., et al., *Review of Triacylglycerol Digestion, Absorption, and Metabolism with Respect to Salatrim Triacylglycerols.* Journal of Agriculture and Food Chemistry, 1994. **42**(474-483): p. 474.
420.   Hamosh, M., *Textbook of Gastroenterology and Nutrition in Infants*, ed. E. Lebenthal. 1981, New York, NY: Raven Press.
421.   Jensen, R., et al., *Sterospecificity of Premature Human Infant Lingual Lipase.* Lipids, 1982. **17**(8).
422.   Plucinski, M. Hamosh, and P. Hamosh, *Fat digestion in rat: role of lingual lipase.* American Journal of Physiology, 1979. **237**(6): p. G541-G547.
423.   *Handbook of Milk Composition*, ed. R. Jensen. 1995, San Diego, California: Academic Press, Inc. .
424.   Blackberg, L., K.-A. Angquist, and O. Hernell, *Bile salt stimulated lipase in human milk: Evidence for its synthesis in the lactating mammary gland.* FEBS letters, 1987. **217**: p. 37-42.
425.   Ellis, L. and M. Hamosh, *Bile salt stimulated lipase: Comparative studies in ferret milk and lactating mammary gland.* LIpids, 1992. **27**: p. 917-922.
426.   Hernell, O. and L. Blackberg, *Human milk bile salt-stimulated lipase: Functional and molecular aspects.* Journal of Pediatrics, 1994. **125**(5): p. S56-S61.
427.   Bernback, S., L. Blackberg, and O. Hernell, *The complete digestion of human milk triacylglycerol in birto requires gastric lipase, pancreatic colipase-dependent lipase and bile salt stimulatedl lipase.* Journal of Clinical Investigation, 1989. **85**(4): p. 1221-1226.
428.   Brown, G., et al., *Faecal chymotrypsin: a reliable index of exocrine pancreatic function.* Archives of Disease in Childhood BMJ Journals, 1988. **63**(7): p. 785-789.
429.   Hamosh, M., *Lingual and breat milk lipases.* Advances in Pediatrics, 1982. **Lingual and breast milk lipases**(29): p. 33-67.
430.   Alemi, B., et al., *Fat digestion in low birth weight infants: Effect of addition of human milk to low birth weight formula.* Pediatrics, 1981. **68**: p. 484-488.
431.   Wang, C., et al., *Bile-salt-activated lipase: Effect on kitten growth rate.* American Journal of Clinical Nutrition, 1989. **49**(3): p. 457-463.
432.   Stromqvist, M., et al., *Recombinant human bile salt-stimulated lipase: An example of defective O-glycosylation of a protein produced in milk of transgenic mice.* Transgenic Research, 1996. **5**(6): p. 475-485.
433.   Howles, P., et al., *Cholesterol ester lipase activity in milk prevents fat-derived intestinal injury in neonatal mice.* American Journal of Gatroenterology, 1999. **40**(3): p. G653-G661.

434. Maljaars, P.W.J., et al., *Effect of ileal fat perfusion on satiety and hormone release in healthy volunteers.* International Journal of Obesity, 2008. **32**: p. 1633-1639.

435. Michalski, M., et al., *Size Distribution of Fat Globules in Human Colostrum, Breast Milk, and Infant Formula.* Journal of Dairy Science, 2005. **88**: p. 1927-1940.

436. Jesen, R., et al., *LIpids of bovine and human milks: A Comparison.* Journal of Dairy Science, 1990. **73**: p. 223-240.

437. Armand, M., et al., *Effect of Human Milk or Formula on Gastric Function and Fat digestion in Premature Infant.* Pediatric Research, 1996. **40**: p. 429-437.

438. Grosvenor, M. and L. Smolin, *The digestive system: from meals to molecules.* Nutrition everyday choices. 2006, Hoboken: NJ: John Wiley & Sons.

439. M, M., et al., *Effect of Partially Hydrolyzed Guar Gum (PHGG) on the Bioaccessibility of Fat and Cholesterol.* Bioscience, Biotechnology, and Biochemistry, 2005. **69**(5): p. 932-938.

440. Edmondson, L., et al., *Feeding Encapsulated Oils to Increase the Polyunsaturation in Milk and Meat Fat.* Journal of American Oil Chemists Society, 1974. **51**(3): p. 72-76.

441. Bode, S., M. Dreyer, and G. Greisen, *Gastric emptying and small intestinal transit time in preterm infants: a schintigraphic method.* Journal of pediatric gastroenterology and nutrition, 2004. **39**: p. 378-382.

442. Michalski, M.C., et al., *Size Distribution of Fat Globules in Human Colostrum, Breast Milk, and Infant Formula.* Journal of Dairy Science, 2005. **88**: p. 1927-1940.

443. Mason, S., *Some Aspects of Gastric Function in The Newborn.* Archives of Disease in Childhood BMJ Journals, 1962: p. 387- 391.

444. Zhu, Y., W.H. Hsu, and J.H. Hollis, *The Impact of Food Viscosity on Eating Rate, Subjective Appetite, Glycemic Response and Gastric Emptying Rate.* PLoS One, 2013. **8**: p. 1-6.

445. Berton, A., et al., *Individual and combined action of pancreatic lipase and pancreatic lipase-related proteins 1 and 2 on native versus homogenized milk fat globules.* Molecular Nutrition and Food Research, 2009. **53**(2009): p. 1592-1602.

446. Hamosh, M., et al., *Protective function of human milk: The milk fat globule.* Seminars in Perinatology, 1999. **23**(3): p. 242-249.

447. Lindstrom, M., B. Sternby, and B. Borgstrom, *Concerted action of human carboxyl ester lipase and pancreatic lipase during lipid digestion in vitro: importance of the physicochemical state of the substrate.* Biochimica et Biophysica Acta (BBA) - Lipids and Lipid Metabolism, 1988. **959**: p. 178-184.

448. LIndstrom, M., et al., *Effect of pancreatic phospolipase A2 and gastric lipase on the action of pancreatic carboxylester lipase against lipid substrates in vitro.* Biochimica et Biophysica Acta (BBA) - Lipids and Lipid Metabolism, 1991. **1084**: p. 194-197.

449. Cohen, M., G. Morgan, and A. Hoffman, *Lipolytic activity of human gastric and duodenal juice against medium- and long-chain triglycerides.* Gastroenterology, 1971. **60**: p. 1-15.

450.   Brockman, H., *Kinetic behavior of the pancreatic lipase-colipase-lipid system.* Biochimie, 2000. **82**: p. 987-995.

451.   Ye., A., J. Cui, and H. Singh, *Effect of the fat globule membrane on in vitro digestion of milk fat globules with pancreatic lipase.* International Dairy Journal, 2010. **20**: p. 822-829.